KU LEUVEN

FACULTY OF SCIENCE

Cavity optomechanics in a millikelvin environment

Yasmine SFENDLA

Supervisor: Prof. D. Bouwmeester
Leiden University

Co-supervisor: *Prof. J. Van de Vondel*
KU Leuven

Mentor: *F. M. Buters*

Thesis presented in
fulfillment of the requirements
for the degree of Master of Science
in Physics

Academic year 2016-2017

© Copyright by KU Leuven

Without written permission of the promotors and the authors it is forbidden to reproduce or adapt in any form or by any means any part of this publication. Requests for obtaining the right to reproduce or utilize parts of this publication should be addressed to KU Leuven, Faculteit Wetenschappen, Geel Huis, Kasteelpark Arenberg 11 bus 2100, 3001 Leuven (Heverlee), Telephone +32 16 32 14 01.

A written permission of the promotor is also required to use the methods, products, schematics and programs described in this work for industrial or commercial use, and for submitting this publication in scientific contests.

Abstract

Cavity Optomechanics in a Millikelvin Environment
by
Yasmine Laura Sfendla
KU Leuven

Under supervision of Prof. Dirk Bouwmeester
Leiden Institute of Physics

Mechanical resonators that are cooled close to their quantum mechanical ground state are promising candidates for the realization and observation of non-classical states of motion, and macroscopic quantum superpositions. We demonstrate optical cooling and thermometry of a nested trampoline resonator that constitutes one end-mirror of a Fabry-Pérot type cavity, although the presented discussions are equally relevant for similar optomechanical systems. Light from two lasers circulates in the cavity: a locking laser, tuned to the cavity resonance, and a red-detuned cooling laser. In a 200mK environment, we present a comparative demonstration of three thermometry schemes. The first entails read-out of the Pound-Drever-Hall error signal locking the lasers to the cavity, the second monitors the mechanical sidebands on the locking beam, the third the mechanical sidebands on the cooling beam. In addition, we discuss their application to sideband asymmetry thermometry in the near-ground state regime. Furthermore, laser noise heating and heating by optical absorption of the resonator are observed. These findings are incorporated in the comparison of the read-out methods, and we find that optomechanical systems that endure a limited amount of circulation power, benefit greatly from the utilization of sideband-thermometry over Pound-Drever-Hall thermometry. These are for example systems prone to heating of the mechanical mode caused by optical absorption, or optomechanical interaction with the locking beam. Finally, we review practical compensations for the reported challenges, that hold promise for cavity-optical cooling of a high-quality mechanical resonator near the quantum-mechanical ground state.

Let us go then, you and I,
When the evening is spread out against the sky
Like a patient etherized upon a table;
Let us go, through certain half-deserted streets,
The muttering retreats
Of restless nights in one-night cheap hotels
And sawdust restaurants with oyster-shells:
Streets that follow like a tedious argument
Of insidious intent
To lead you to an overwhelming question...
Oh, do not ask, "What is it?"
Let us go and make our visit.

– T.S. Eliot, *The Love Song of J. Alfred Prufrock*

Prologue
On quantum superpositions of a mirror and doubting Thomases

Something with a mirror that is "in two places at the same time"
- Anonymous friend, describing my daily duties.

Attempting to make my friends lose the finger quotes as they describe my occupancy, has become a continuous and unfruitful struggle of mine, yet one that I'm desperate to win. They have adopted the idea that either *two places*, or *at the same time*, mustn't be taken literally, and quite probably is either a figure of speech, or a blatant lie. They are not in bad company. Both Erwin Schrödinger and Albert Einstein were, at least at some point, skeptical [1] towards some uncomfortable philosophical implications of the theory of quantum mechanics, notably their own brainchild. Schrödinger is known for his slightly lugubrious thought experiment, involving a cat, a box, and an atom. The following is a translated [2] excerpt from his 1935 paper: Die gegenwärtige Situation in der Quantenmechanik. [3]

"One can even set up quite ridiculous cases. A cat is penned up in a steel chamber, along with the following device (which must be secured against direct interference by the cat): in a Geiger counter, there is a tiny bit of radioactive substance, so small, that perhaps in the course of the hour one of the atoms decays, but also, with equal probability, perhaps none; if it happens, the counter tube discharges and through a relay releases a hammer that shatters a small flask of hydrocyanic acid. If one has left this entire system to itself for an hour, one would say that the cat still lives if meanwhile no atom has decayed. The first atomic decay would have poisoned it. The ψ-function of the entire system would express this by having in it the living and dead cat (pardon the expression) mixed or smeared out in equal parts."

Prior to its publication, the idea was part of a letter exchange with Einstein himself, outshining a more modest thought experiment by the latter involving a keg of simultaneously exploded and unexploded gunpowder. The aim of these thought experiments was in part to ridicule the idea of a macroscopic superposition state, yet, as these things often go, the term macroscopic Schrödinger cat is now used to describe just that.

Let us go back to the skepticism of my "friends". My first attempt at convincing them that a spatial superposition is a real thing, rather than just opium of the mathematicians, consisted of talking about scanning tunneling microscopes [4]: real machines, used in real laboratories, making real images, only being able to operate because of electrons that are *in places where they cannot be*. The problem with this is, that electrons are not an object you can see anyway. So, in all fairness, if someone claims an electron is in two places at the same time, well, I can't see it anyway, so "sure". (This time it's me, doing the air quotes.) With a cat, it's different. So here is what has been bugging my friends, myself, and physicists all around: what is the frontier separating them?

Electrons and atoms can be put in a superposition state. A person, a cat, car keys:[1] they are apparently too big. So let me rephrase: where lies the frontier separating them? How large can one make an object, before it slips away from the world dictated by quantum-law, into the chaotic, macroscopic world governed by everyday banalities? We believe we can make it about 10^{14} atoms big. They make up a disk-shaped mirror, about 70μm in diameter, suspended on four arms to make it a trampoline resonator. A picture is shown in the center of Fig. 3.14 of this thesis. It's not big - but it's there. You can unpack it from the little plastic box it comes in, hold it in your hand, make sure you don't drop it - it is *very real*.[2]

In Schödingers original experiment, the microscopic object (the atom) transfers a quantum superposition state to a macroscopic object (the cat) by interacting with it (the interaction is mediated via the Geiger tube and the hammer). Our resonator is brought into a superposition state in much the same way. The idea, laid out by Marshall, Simon, Penrose and Bouwmeester in their 2003 paper [8], is that a single photon in a superposition state, interacts with the mechanical resonator, thereby bringing the latter in a superposition state. Of course, the experimental implementation of this scheme comes with a few conditions. These will be the focus of this thesis. I came into touch with this experiment for the first time exactly two years ago, during a lecture by Dirk Bouwmeester. I found it wonderful. Ten months ago, I came back, this time to work on it myself. With this thesis, I hope to convey at least a glimpse of the wonder of this project. In the next section, I will try to express my immense gratitude for being able to take part in this work, and my thanks to the remarkable scientists and human beings[3] in the Kamerlingh Onnes Laboratory at Leiden University, who took away the chaos, and/or the banality of the macroscopic world.

[1] Even though the latter, like electrons, have been repeatedly reported to occur in places they cannot be. Despite years of research efforts, the physical laws governing this phenomenon have remained unresolved up to this day.

[2] Seriously, don't drop it. It took a whole lot of work [5–7] to make it.

[3] One not excluding the other.

Acknowledgement

First and foremost, I am indebted to my supervisor, Dirk Bouwmeester, who first invented, then told me about, and finally gave me a place in, an experiment that touched my physicist's heart, thereby inviting me in the field of optomechanics as a whole. I owe thanks to Martin van Exter, who took care of my application a year ago, and without whom I wouldn't have been here.

I thank Daniël Geelen and Chris Smiet, for taking me up in the group, and in their home, and making me leave Leiden with pain in my heart. Flavio Mariani, for unlimited comfort food and words. Oliver Ostojic, for obligating me to take breaks and making me laugh while at it. Gesa Welker, for late-night lab sessions and knödels. Kaveh Lahabi, for even-later-night lab sessions, and the best lamb chops I ever had (sorry, Chris). Michiel de Dood, for teaching me Quantum Optics with remarkable patience and empathy. Hedwig Eerkens, for kind words and solid optomechanical advise. Tobias de Jong, for good times all year round. Many thanks to Sven de Man, for answering with respect and patience any question - whether optomechanical, professional, statistical, financial, abstruse or silly. Furthermore, for mentoring me, for input in all chapters, especially in chapter 7, for encouragement when I thought I was after something - albeit the littlest thing - and for motivating me and reviewing my work in the months leading up to the finish line. I'm grateful towards Matthew Weaver, Fernando Jose Luna, and Wolfgang Löffler, for helpful discussions. Many thanks to Kier Heeck, who is a permanent ray of sunshine in the corner of our ever so isolated lab. Essential to the contents of this thesis was the work of Frank Buters, who set up the basis on which this thesis was built, showed me all tricks of the trade, brought structure in my work and thesis, aligned my AOM when I couldn't, locked my lasers when they wouldn't, and found a lost sideband when I needed it most. Never will I forget the most effective remedy in case of non-responsive electronics: turn them on!

Growing is difficult without good roots, and mine are and remain in Leuven. I am endlessly grateful to my professors at the KU Leuven, who have set an example for me both in life and in science. In my five years in Leuven, I was met with flexibility, humanity and encouragement, in a climate accommodating and catalyzing academic, personal and scientific progress. Someone who specifically

contributed to that in the context of this thesis is of course my co-supervisor, Joris van de Vondel, without whose trust and generosity (in terms of time and efforts) this thesis wouldn't have been.

Above all, I am massively indebted to four people who have put up with me (and my physics) for years and years. My mother, Marina Boermans, who is my greatest example of how a teacher should be, and whose compassion, insightfulness and rationality I one day hope to level. Hannah Penders, who is my red-headed sister in mind, whom I share my youth and adolescence with, and who listened to my stories on physics to the point that she fell asleep on the tram. It must be said, we ate a lot of Chinese food right before - so I guess the cause of that incident will never unambiguously be disclosed. Alas! Finally, Olivia Verstrepen and Mariam Eshaghzey, who moved in next to me in my first year in Leuven and soon left the building, but never my side.

Less colloquial, I must acknowledge P. McMahon, whose "Hints and Tips on (Science and Engineering) Bachelor's and Master's thesis writing" [9] I used to give my thesis its current form and style, and S.J. Aaronson, S.J. Johnson and D.M. Bacon [10–12], whose theses I used as a model for my own. I must remention Gesa Welker, together with Martin de Wit, for operating the cryostat with relentless devotion, also Kier Heeck again, and Harmen van der Meer, for building up the experiment to what it is today.

All optical layouts were drawn using the ComponentLibrary by Alexander Franzen, retrievable at `http://www.gwoptics.org/ComponentLibrary/`

Dedicated to the memory of my grandfather, Frans Boermans - smuggler-catcher, writer and storyteller - who was the first to trick me with mathemagical riddles.

Contents

List of Figures

Chapter 1

Introduction

I imagine experimental physicists must often look with envy at men like Kamerlingh Onnes, who discovered a field like low temperature, which seems to be bottomless and in which one can go down and down.

– Richard Feynman, *There's Plenty of Room at the Bottom*

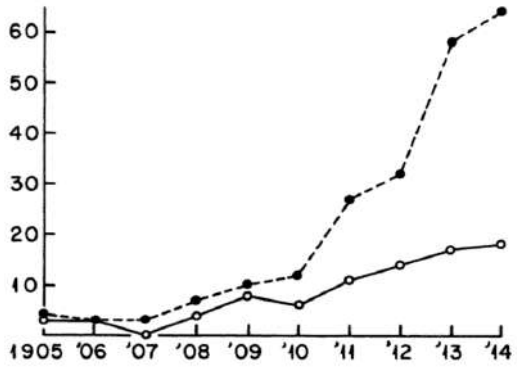

Figure 1.1: The slow rise of quantum theory. The solid circles indicate the number of authors who published on quantum topics. The open circles refer to the number of authors who dealt with blackbody theory, a subset of early quantum physics. In 1905, Albert Einstein was the first and only one to realize the nonclassical nature of Planck's theory. From [1].

In the first days of the 20th century, Max Planck found an expression for the entropy of an ensemble of oscillators, that involved 'quantization' of their total energy. [13] This was part of a years-long attempt to theoretically derive the empirical laws that describe the spectral density of black body radiation. For most of the decade, Planck believed that his radiation law could be reconciled with classical mechanics and electrodynamics. [1] We now know this is not the case. The microscopic and the macroscopic world are two worlds, divided. In recent years, approximately a century later, new technologies have emerged that

make it possible to probe and push the frontier between them, in - sometimes tabletop [8] - experiments. The field of optomechanics specifically, is regarded as particularly suitable to accommodate these kinds of experiments, because it comprises components from both worlds: photons (optics), and micro- to macroscopic mechanical objects (mechanics). Both can be described as resonators: in case of the optical element because they can resonantly trap and enhance light, and in case of the mechanical element because all objects at finite temperatures vibrate and therefore exhibit resonances. Also, as is known particularly in the field of atomic force microscopy, frequency shifts of oscillatory motion are generally easier to measure than minuscule displacements.
Optomechanical systems are systems that combine those components and lets them interact. They come in all sizes and shapes. The optical resonators include, but are not limited to, whispering gallery-type resonators [14], spheres [15], superconducting microwave circuits [16], and photonic crystal defects [17]. The mechanical resonators can be membranes [18–20], micro-pillars [21], strings [15], disks [22], rods [23], spheres [24], rings [25], and even cold atoms [26] and superfluid helium films [27]. This thesis focusses on what is maybe the most conceivable of all of those: a Fabry-Pérot cavity, of which one of the mirrors is a trampoline resonator [6, 7, 28].

While the field of quantum mechanics slowly rose over the course of the twentieth century, another, much more heated competition emerged: the cryogenic quest to the absolute zero. One of the three main players[1] in the contest was Heike Kamerlingh Onnes, and with him the Leiden Laboratory. At the beginning of this century it was realized, that the two fields together provided the means to reach a common goal: creating a macroscopic Schrödinger cat.

In Schödingers famous thought experiment, a microscopic object (an atom) transfers a quantum superposition state to a macroscopic object (a cat) by interacting with it. The interaction is mediated via a Geiger tube, detecting the decay of the atom, and a hammer, smashing a cyanide-filled flask upon detection. In a less sinister version of this experiment, one could replace the atom with a photon, and the cat with a small mechanical resonator: a movable mirror, supported by 'springs' like a trampoline. This is the core of the idea laid out by Marshall, Simon, Penrose and Bouwmeester, in their 2003 paper [8]. By bringing a photon into a spatial superposition state, and letting it interact with the movable mirror, the latter can be brought into a spatial superposition state itself. The mediator of this optomechanical interaction, is the radiation pressure force: a photon, much like any other particle, can exert a pressure or force on an object when bouncing off it. It turned out that creating a macroscopic superposition state is not the biggest challenge; observing it is. In the experiment described above, the most fundamental prerequisite is that the temperature of the mirror

[1] The other two were Britain's James Dewar and Poland's Karol Olszewski.

must be as close to the absolute zero as possible. Equivalently, one can say that its phonon occupancy must be nearly zero, or that its fundamental mechanical mode must be near the ground state. [8, 29]

In practice, cooling towards the ground state proceeds in two stages. First, the environment is cryogenically brought to sub-kelvin temperatures. From there, lasers take over: photons [2] interacting with the mirror can damp, and therefore effectively cool, its motion. This thesis deals with precisely that. The objective of this thesis is twofold. We want to optimize the experimental methods responsible for optical cooling and thermometry (read-out of the mirror's motion and subsequent determination of the phonon occupancy) so that:

(I) the ground state regime can be reached.

(II) once the ground state regime is reached, reliable detection and analysis of the strongly damped signals resulting from drastically low phonon occupancy and strong damping, is ensured.

To that extent, we implement two read-out schemes that could potentially carry out thermometry with higher precision than the method currently in use. We immediately put them to the test in a millikelvin environment, probing the motion of a nested trampoline resonator.

[2] Copious amounts of them, not single photons.

Chapter 2

The optomechanic's guide to the ground state

This section offers a guide through this thesis. In what is to come, we will walk through the cooldown process of a microscopic trampoline resonator. Each chapter describes a different stage of the process, starting with the methods (if applicable), followed by experimental results. More often than not, these results will impose a challenge. Small or big, each chapter will be concluded with a solution, or a plan to change course.

In **chapter 3, part 1**, we will take our first steps in the field of optomechanics. The theory will lead us to the experimental preparations of the system, and via the cryogenics we will descend from room temperature to the Kelvin regime in **chapter 3, part 2**. We will take a break at a stable temperature stage in **chapter 4**, and verify if all is in place for the final descent, in **chapter 5**. Once we have reached the millikelvin base, we will further explore the optomechanical system, in preparation of optical cooling to even lower temperatures. In doing so, we'll encounter an obstacle, marking the end of **chapter 5**. In **chapter 6**, we will explore two methods that severely lower the hindrance, and allow us to continue *to* our final destiny, the zero-point. Even more, they will ensure we are optimally prepared for measurements *at* our final destiny, the zero-point. In **chapter 7**, we demonstrate an optical cooling run, and we try and get down as far as we can. Our path ends in **chapter 8**, where we'll look back, and ahead, and draw a map for who comes after us.

Chapter 3

Theory & experiments in optomechanics

Nothing happens until something moves.
– Albert Einstein

3.1 Theory of cavity-optomechanics

Fig. 3.1 shows the core of our system. It is a Fabry-Pérot cavity, of which one of the mirrors can move. This section summarizes the different parameters that come into play, and the equations governing them. First, we will introduce the optics (that is, the cavity), then the mechanics (the resonator), and finally the optomechanics (the optics and mechanics, interacting). The following is based on the review paper by Aspelmeyer et al. [30], containing a more extensive mathematical background.

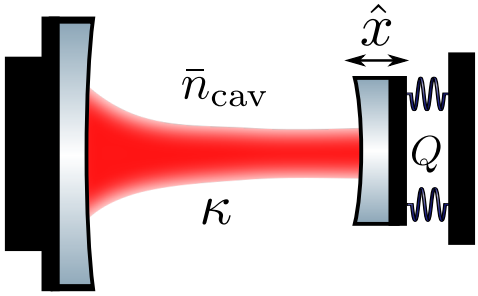

Figure 3.1: The optomechanical system, comprising a Fabry-Pérot cavity characterized by the linewidth κ, and a movable mirror characterized by the quality factor Q. There are $\bar{n}_{\mathrm{cav}}$ photons circulating in the cavity. They interact with the mirror, whose motion is described by the displacement $\hat{x}$.

3.1.1 The optics

A cavity of length L has resonances at frequencies that are integer multiples of $\pi\frac{c}{L} = \omega_{\mathrm{FSR}}$, the free spectral range (FSR).[1] As only one of the resonances is used, the relevant one will be called the cavity resonance:

$$\omega_{\mathrm{cav}} = N\frac{\pi c}{L} \qquad N \in \mathbb{N} \tag{3.1}$$

The light intensity (that is, the photons) in the cavity has a finite decay rate κ, covering 'extrinsic' losses associated with the input coupling κ_{ex}, and remaining losses κ_0 so $\kappa = \kappa_{\mathrm{ex}} + \kappa_0$. The quality of the cavity is then contained in the finesse, $\mathcal{F} = \frac{\omega_{\mathrm{FSR}}}{\kappa}$.
The optical resonator is described by the bare Hamiltonian

$$\hat{H}_{\mathrm{opt}} = \hbar\omega_{\mathrm{l}}\hat{a}^\dagger\hat{a} \tag{3.2}$$

with $\hat{a}^\dagger$ the photon creation operator, $\hat{a}$ the photon annihilation operator, and ω_{l} the frequency of the (laser)light. If light of a laser with detuning $\Delta = \omega_{\mathrm{l}} - \omega_{\mathrm{cav}}$ is incident on the cavity, the average cavity amplitude is, from Aspelmeyer et al. [30]:

$$\langle\hat{a}\rangle = \frac{\sqrt{\kappa_{\mathrm{ex}}}\langle\hat{a}_{\mathrm{in}}\rangle}{\frac{\kappa}{2} - i\Delta}. \tag{3.3}$$

where $\hat{a}_{\mathrm{in}}$ is the incoming field amplitude. The response of the cavity to incoming light of power $P_{\mathrm{in}} = \hbar\omega_{\mathrm{cav}}|\langle\hat{a}_{\mathrm{in}}\rangle|^2$ is described by the susceptibility $\chi_{\mathrm{opt}}[\omega] = \frac{1}{\frac{\kappa}{2} - i(\omega+\Delta)}$. This gives rise to the cavity profile:

$$\bar{n}_{\mathrm{cav}} = |\langle\hat{a}\rangle|^2 = \frac{\kappa_{\mathrm{ex}}}{\Delta^2 + (\frac{\kappa}{2})^2}\frac{P_{\mathrm{in}}}{\hbar\omega_{\mathrm{l}}}. \tag{3.4}$$

where $\bar{n}_{\mathrm{cav}}$ is the number of photons circulating in the cavity. The spectrum, which is a Lorentzian profile, is depicted in Fig. 3.2. Qualitatively, if one scans the frequency of incoming light over the cavity resonance, more and more light builds up in the cavity as the resonance frequency is approached. Meanwhile, a fraction of that light leaks out via both sides of the cavity. If one were to measure the intensity circulating in the cavity during that process[2], this is the profile one would obtain. Far from the cavity resonance, almost all light is reflected from the cavity. Therefore, the reflected spectrum[3] would be exactly the opposite of the profile in Fig. 3.2: a Lorentzian upside-down, with a minimal reflected intensity

[1] The reader new to the field may note here that when the length of the cavity changes, the cavity resonance frequency changes as well. That reader already got to the heart of cavity-optomechanics.

[2] Which would correspond to hypothetically placing a photodetector in the middle of Fig. 3.1, in between the mirrors.

[3] Corresponding to placing a photodetector outside of the cavity, on the left side of Fig. 3.1.

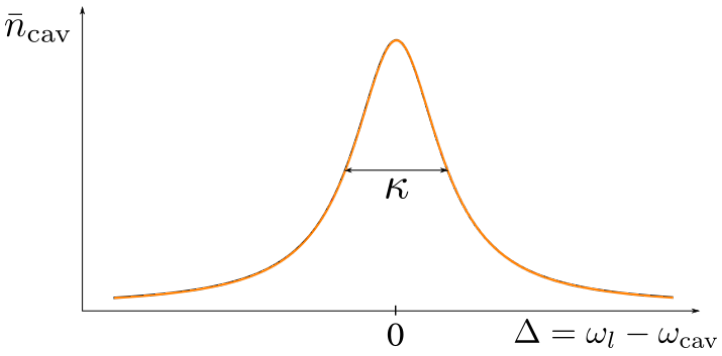

Figure 3.2: Cavity profile. The circulating photon number is maximal if the frequency of the incoming light ω_{l} is equal to the resonance frequency of the cavity ω_{cav}.

(or a minimal number of reflected photons) if the frequency of the laser equals the cavity resonance. The transmitted intensity profile[4] however, is of the same form as the circulating intensity in Fig. 3.2, because it concerns a fraction of the circulating intensity.

3.1.2 The mechanics

The bare Hamiltonian for the mechanical resonator is

$$\hat{H}_{\mathrm{m}} = \hbar\Omega_m \hat{b}^\dagger \hat{b} \tag{3.5}$$

with $\hat{b}^\dagger$ the phonon creation operator, and $\hat{b}$ the phonon annihilation operator. For the sake of simplicity, we discarded the contribution of the zero-point energy $\frac{1}{2}\hbar\Omega_m$ to the total energy. The zero-point fluctuation will be denoted $x_{\mathrm{ZPF}} = \sqrt{\frac{\hbar}{2m\Omega_m}}$ and m is the effective mass of the resonator.
The equation of motion for a damped harmonic oscillator driven by an external force $F(t)$ is

$$\ddot{x} + \Gamma_m \dot{x} + \Omega_m^2 x = \frac{F(t)}{m} \tag{3.6}$$

with Γ_m the effective damping, Ω_m the mechanical resonance and quality factor $Q = \frac{\Omega_m}{\Gamma_m}$. The mechanical susceptibility $\chi_m[\omega] = \left(m(\Omega_m^2 - \omega^2) - im\Gamma_m\omega\right)^{-1}$ reduces to

$$\chi_m[\omega] = \frac{1}{m\Omega_m}\frac{1}{2(\Omega_m - \omega) - i\Gamma_m} \tag{3.7}$$

for frequencies close to the resonance frequency. When the oscillator is coupled to or interacting with an environment, the true mechanical damping Γ_{eff} will differ from the intrinsic mechanical damping Γ_m. In the following, we will already replace the intrinsic damping with the effective damping. The same argument applies to the intrinsic resonance Ω_m, and the effective mechanical resonance frequency Ω_{eff}.

[4]Corresponding to placing a photodetector outside of the cavity, on the right in Fig. 3.1.

Applying the fluctuation-dissipation theorem[5] to the mechanical oscillator, one obtains its motional spectrum [30]:

$$S_{xx}[\omega] = \frac{2k_B T_{\text{eff}}}{\Omega_m} \Im(\chi_m[\omega]) \tag{3.8}$$

where the effective temperature of the mechanical motion T_{eff} has entered. This expression is valid in the weak damping regime, which is appropriate for the entirety of this thesis.
Using

$$\Im\big(\chi_m[\omega]\big) = \frac{1}{2m\Omega_m} \frac{\Gamma_{\text{eff}}/2}{(\Omega_{\text{eff}} - \omega)^2 + (\Gamma_{\text{eff}}/2)^2}$$

we obtain the mechanical noise spectrum

$$S_{xx}[\omega] = \frac{k_B T_{\text{eff}}}{m\Omega_m^2} \frac{\Gamma_{\text{eff}}/2}{(\Omega_{\text{eff}} - \omega)^2 + (\Gamma_{\text{eff}}/2)^2}, \tag{3.9}$$

which is again a Lorentzian profile. The relevant parameters that characterize the profile, and therefore the motion of the mirror, are the linewidth Γ_{eff}, the central frequency Ω_{eff} and the area under the spectrum. The latter is the root mean square (RMS) displacement of the mirror[6]:

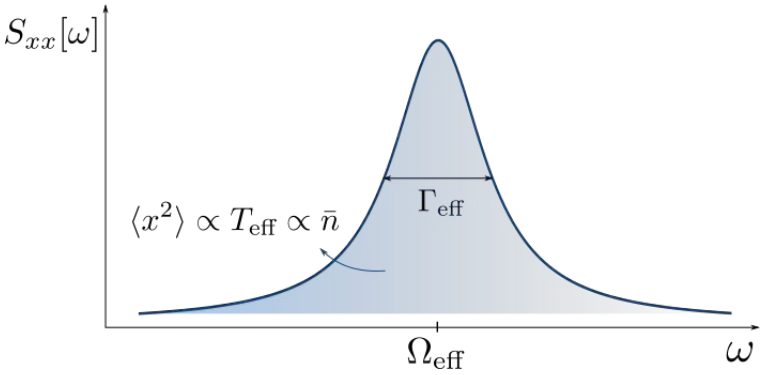

Figure 3.3: Mechanical noise spectrum

$$\begin{aligned} \langle x^2 \rangle &= 2 \times \int_{-\infty}^{\infty} S_{xx}(\omega) \frac{d\omega}{2\pi} && (3.10) \\ &= \int_{-\infty}^{\infty} \frac{1}{\pi} \frac{k_B T_{\text{eff}}}{m\Omega_m^2} \frac{\Gamma_{\text{eff}}/2}{(\Omega_m - \omega)^2 + (\Gamma_{\text{eff}}/2)^2} d\omega \\ &= \frac{k_B T_{\text{eff}}}{m\Omega_m^2} \underbrace{\int_{-\infty}^{\infty} \frac{1}{\pi} \frac{\Gamma_{\text{eff}}/2}{(\Omega_m - \omega)^2 + (\Gamma_{\text{eff}}/2)^2} d\omega}_{1} && (3.11) \end{aligned}$$

[5]The theorem relates the *fluctuation* S_{xx} to the *dissipational* (imaginary) part of the response function χ_m.

[6]The factor 2 accounts for the mechanical noise spectrum being symmetric for $\omega \to -\omega$.

Therefore, the area under the mechanical power spectrum $\mathcal{A}$, is proportional to the effective temperature T_{eff} of the motion, to the phonon occupation number $\bar{n} = k_B T_{\text{eff}}/\hbar\Omega_m$, and to the mirror's RMS displacement $\langle x^2 \rangle$.

3.1.3 The interaction: radiation pressure

When the length of the cavity changes, the cavity resonance frequency changes, which changes the radiation pressure, which changes the length of the cavity. This feedback loop is the core of optomechanics, that we already touched upon in the footnote in section 3.1.1.

When the mirror moves, the length of the cavity changes

When the mirror moves, the length of the cavity changes, which in turn changes the resonance frequency of the cavity. In Eq. (3.1) we set $L = L_0 + x(t)$ so $\omega_{\text{cav}}(t) = N\pi c/[L_0 + x(t)]$. As a result, the detuning is effectively varied over time synchronous with the oscillation of the mirror. One essentially moves along the cavity profile, and the circulation photon number changes accordingly:

$$\bar{n}_{\text{cav}}(t) = \frac{\kappa_{\text{ex}}}{\Delta(t)^2 + (\frac{\kappa}{2})^2} \frac{P_{\text{in}}}{\hbar\omega_{\text{l}}}.$$

When the length of the cavity changes, the mirror moves

The photons exert a pressure on the mirror: radiation pressure. If the amount of photons $\bar{n}_{\text{cav}}$ exerting pressure on the mirror varies, the force $F(t)$ on the mirror varies as well. Therefore, the motion of the mirror is altered. As the photon number varies with precisely the mechanical frequency, the force created is resonant with the mechanical motion. Its form can be easily derived if we consider a photon of momentum $p = h/\lambda = \hbar\omega_{\text{l}}/c$, circulating in the cavity. In each round-trip, the photon bounces off the movable mirror once. Thereby its momentum changes by an amount $\Delta p = 2\hbar\omega_{\text{l}}/c$, so the force applied to the mirror is $\Delta F = \Delta p/\Delta t = \hbar\omega_{\text{l}}/L$ where we used the travel time $\Delta t = 2L/c$. Thus, the total force applied to the mechanical resonator by $\bar{n}_{\text{cav}} = \langle \hat{a}\dagger\hat{a} \rangle$ photons is $F(t) = \bar{n}_{\text{cav}}(t)\hbar\omega_{\text{l}}/L$.

The interaction Hamiltonian

The external force $\hat{F}$ driving the mirror is the radiation pressure force. The new Hamiltonian, including the interaction between the optical and mechanical

resonator, is [30]

$$\hat{H} = \hat{H}_{\rm opt} + \hat{H}_{\rm m} + \hat{H}_{\rm int} \tag{3.12}$$

$$= \hbar\omega_{\rm l}\hat{a}^\dagger\hat{a} + \hbar\Omega_m\hat{b}^\dagger\hat{b} - \underbrace{\hbar G\hat{a}^\dagger\hat{a}}_{\hat{F}}\,\underbrace{x_{\rm ZPF}(\hat{b}+\hat{b}^\dagger)}_{\hat{x}} \tag{3.13}$$

with $\hat{x} = x_{\rm ZPF}(\hat{b}+\hat{b}^\dagger)$, the radiation pressure force $\hat{F} = \frac{\partial\hat{H}_{\rm int}}{\partial\hat{x}}$, and approximating $\omega_{\rm cav}(t) \approx \omega_{\rm cav} + \frac{\omega_{\rm cav}}{L_0}\hat{x}(t)$ with $G = -\frac{\partial\omega_{\rm cav}}{\partial\hat{x}} = \frac{\omega_{\rm cav}}{L_0} \approx \frac{\omega_{\rm l}}{L_0}$.
In what follows, we will dig deeper into the interaction, its effects, and the ways in which we can use these effects in practice, to extract dynamical information from the system.

3.1.4 Visualizing the mechanical spectrum

In this section, we describe methods to read out the motion of the mirror, without altering the motion. The mirror acts on the laser light, and its imprint on the latter is observed.

Mechanical sidebands on the optical field

A mirror moving with a frequency Ω_m modulates the phase of the light field in the cavity.[7] Light of frequency $\omega_{\rm l}$ that is phase-modulated with frequency Ω_m develops optical field components or 'sidebands' at two additional frequencies, $\omega_{\rm l} \pm \Omega_m$. This can be seen from the following simplified argument.

In the absence of the mechanical oscillator, the light field in the cavity is $E_0\cos(\omega_{\rm l}t)$. The moving mirror modulates the phase, so the modified field is:

$$E = E_0\cos(\omega_{\rm l}t + \phi(t)) \tag{3.14}$$

where $\phi(t) = \mathcal{M}\cos(\Omega_m t + \phi_0)$ with $\mathcal{M}$ the modulation amplitude. Then

$$E = E_0\Big\{\cos(\omega_{\rm l}t + \mathcal{M}\cos(\Omega_m t + \phi_0))\Big\} \tag{3.15}$$

$$= E_0\Big\{\cos(\omega_{\rm l}t)\cos(\mathcal{M}\cos(\Omega_m t + \phi_0)) + \sin(\omega_{\rm l}t)\sin(\mathcal{M}\cos(\Omega_m t + \phi_0))\Big\}$$

[7] To simplify notation, in the following we will assume the resonance frequency of the mirror motion is the intrinsic frequency Ω_m. It can be replaced by $\Omega_{\rm eff}$ if applicable.

For small $\mathcal{M}$, small angle approximations are justified[8]:

$$\begin{aligned} E &\approx E_0 \left\{ \cos\omega_\mathrm{l} t(1-(\mathcal{M}\cos(\Omega_m t+\phi_0))^2) + \mathcal{M}\sin(\omega_\mathrm{l} t)\cos(\Omega_m t+\phi_0) \right\} \\ &\approx E_0 \left\{ \cos(\omega_\mathrm{l} t) + \mathcal{M}\frac{1}{2}\sin((\omega_\mathrm{l}+\Omega_m)t+\phi_0) + \mathcal{M}\frac{1}{2}\sin((\omega_\mathrm{l}-\Omega_m)t-\phi_0) \right\} \end{aligned}$$

There are now field components at ω_l, $\omega_\mathrm{l}+\Omega_m$ and $\omega_\mathrm{l}-\Omega_m$.

Recording the mechanical spectrum

After having interacted with the mirror, light leaks out via the front and the back of the cavity. Depending on where one places a photodetector, transmitted or reflected light can be detected.
A photodetector measures the intensity of the light, that is, the square of the field amplitude. This means that when the field amplitude is a sum of components at different frequencies, the beating signal of these components will be registered.

$$I = |E|^2 \tag{3.16}$$

$$= E_0^2 \left| \cos(\omega_\mathrm{l} t) + \mathcal{M}\frac{1}{2}\sin((\omega_\mathrm{l}+\Omega_m)t) + \mathcal{M}\frac{1}{2}\sin((\omega_\mathrm{l}-\Omega_m)t) \right|^2 \tag{3.17}$$

where we set $\phi_0 := 0$ for the sake of the simplicity of this argument. After expansion, one obtains:

$$\begin{aligned} I &= E_0^2 \left\{ \frac{3}{2} + \frac{\mathcal{M}^2}{4}\cos(2\Omega_m t) \underbrace{-\frac{\mathcal{M}}{2}\sin(-\Omega_m t) - \frac{\mathcal{M}}{2}\sin(\Omega_m t)}_{0} + ... \right\} \\ &= E_0^2 \left\{ \frac{3}{2} + \frac{\mathcal{M}^2}{4}\cos(2\Omega_m t) + ... \right\}, \end{aligned} \tag{3.18}$$

omitting components at optical frequencies $2\omega_\mathrm{l}, 2(\omega_\mathrm{l}\pm\Omega_m), 2\omega_\mathrm{l}\pm\Omega_m$ and $2\omega_\mathrm{l}$. These intensity fluctuation frequencies are much too high for the photodetector to record ($\omega_\mathrm{l}/2\pi \sim 100\mathrm{THz}$, while $\Omega_m/2\pi \sim 100\mathrm{kHz}$), so the measurement process time-averages the signal. The detected intensity is:

$$\begin{aligned} \langle I\rangle_t &= E_0^2 \left\langle \frac{3}{2} + \frac{\mathcal{M}^2}{4}\cos(2\Omega_m t) + ... \right\rangle_t \\ &= E_0^2 \left\{ \frac{3}{2} + \frac{\mathcal{M}^2}{4}\cos(2\Omega_m t) \right\} \end{aligned} \tag{3.19}$$

Only one spectral component is left, at twice the mechanical frequency.

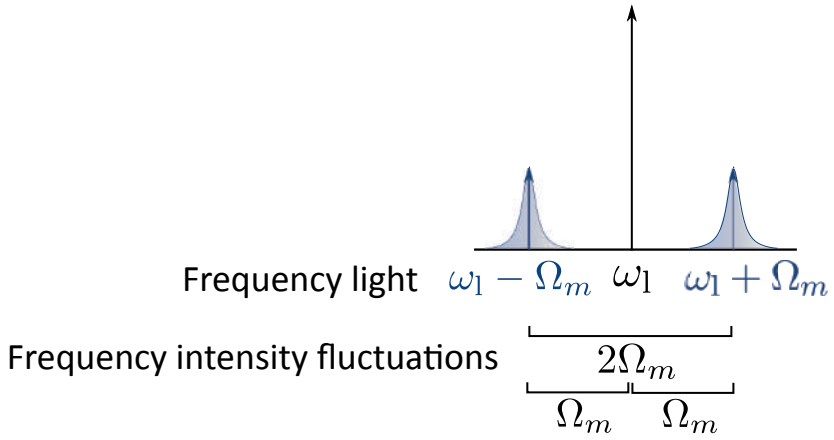

Figure 3.4: Mechanical sidebands on the optical field. Light entering with frequency ω_l develops sidebands at frequency $\omega_l \pm \Omega_m$ as a result of phase modulation by the moving mirror. The photodetector registers an intensity fluctuating at the beating frequency $2\Omega_m$ and, if $\Delta \neq 0$, Ω_m.

Two things are noteworthy here:

I. In Eq. (3.18), the opposite signs of the terms oscillating at exactly the mechanical frequency Ω_m cause them to cancel each other and leave only the component at $2\Omega_m$. The signs depend however critically on the phase relation between the sidebands and the carrier, so on the value of ϕ_0. By assuming $\phi_0 = 0$, we implicitly assumed that the frequency of the incoming light was equal to the cavity resonance frequency (i.e. $\Delta = 0$). If $\omega_l \neq \omega_{cav}$, the components at Ω_m do not cancel and the final detected intensity (3.19) contains components at $2\Omega_m$ and Ω_m. This is depicted on Fig. 3.4 and 3.5. Intuitively, this can be seen from the cavity profile in Fig. 3.6. Because the intensity is symmetric around zero detuning, the observed signal fluctuates with twice the frequency of that of the mechanical motion.The component of the intensity fluctuating with the mechanical frequency itself appears when the laser is set at a non-zero detuning, but: using detuned laser light is undesirable for reasons that will be explained in section 3.1.5.

II. The resulting signal (3.19) carries the imprint of *both* sidebands. We measure both sidebands 'folded' on top of each other. This is not a problem an sich, but: there are reasons for which one might want to measure the sidebands individually.

[8]The same result can be obtained using Bessel functions: $\cos(\omega_l t + \mathcal{M}\sin(\Omega_m t)) = \sum_{k=0}^{\infty} J_k(\mathcal{M})\cos((\omega_l + k\Omega_m)t) + \sum_{k=1}^{\infty}(-1)^k J_k(\mathcal{M})\cos((\omega_l - \Omega_m)t)$. This gives rise to an infinite amount of sidebands of decreasing amplitude, because each is proportional to $J_k(\mathcal{M})$. If $\mathcal{M} \to 0$, all but the first sidebands can be discarded.

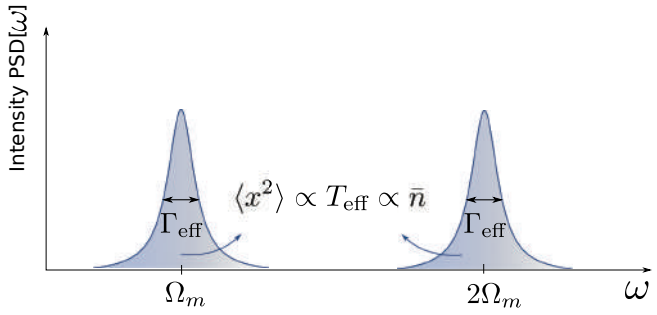

Figure 3.5: Intensity spectrum at the beating frequencies $2\Omega_m$ and, if $\Delta \neq 0$, Ω_m. Each spectral feature, at Ω_m or $2\Omega_m$, carries the imprint of both sidebands at $\omega_{\rm l} + \Omega_m$ and $\omega_{\rm l} - \Omega_m$. Note how the spectrum essentially shifted from frequencies in the optical domain ($\sim$ 100THz), to mechanical frequencies ($\sim$ 100kHz).

In the next two paragraphs, we will describe two different read-out methods for the mechanical motion. The first, Pound-Drever-Hall read-out, deals with comment (I). The second, sideband read-out, deals with comment (II).

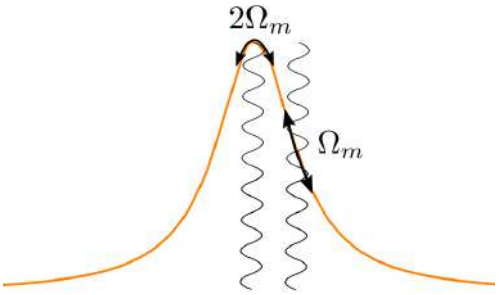

Figure 3.6: Components of the detected intensity fluctuation. For a laser set at zero detuning, the circulating intensity [orange] $\bar{n}_{\rm cav}(t)$ varies with a frequency twice that of $x(t)$ and $\omega_{\rm cav}(t)$ [grey].

PDH read-out of the mechanical motion

We would like to display the signal at Ω_m, but at the same time, we want to keep the laser frequency $\omega_{\rm l}$ equal to the cavity resonance frequency $\omega_{\rm cav}$. A solution is provided by a method initially developed to stabilize the frequency of a noisy laser, by Pound, Drever and Hall [31]. At the start of this section, we stated that laser light, when phase modulated, develops sidebands. In the Pound-Drever-Hall (PDH) method, sidebands are created by actively phase modulating the laser light *before* it enters the cavity. Using for example a Pockels cell

or an electro-optical modulator (EOM) driven by a local oscillator at a frequency ω_{PDH}, sidebands at $\omega_{\mathrm{l}} \pm \omega_{\mathrm{PDH}}$ are generated. ω_{PDH} is high enough such that the sidebands do not enter the cavity; they will be promptly reflected and add to the rest of the reflected signal only [19]. Fig. 3.7 gives an overview of the tones that are incident on, inside, and reflected from the cavity.

The fields reflected from the cavity are again squared and time averaged upon

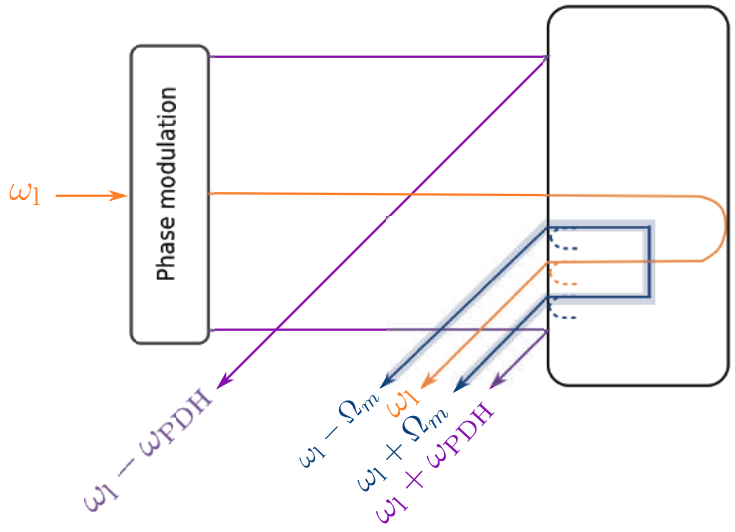

Figure 3.7: Reflected fields after external sideband generation for the PDH read-out method.

detection by the photodetector. The resulting signal is of the form

$$I(t) = I_0 + \epsilon(\omega_{\mathrm{cav}}) \sin(\omega_{\mathrm{PDH}} t + \psi) \tag{3.20}$$

The amplitude of this AC signal is generally called the PDH-error signal, and approximately $\epsilon(\omega_{\mathrm{cav}}) \propto \omega_{\mathrm{cav}}$ [32]. Now recall that $\omega_{\mathrm{cav}}(t)$ fluctuates around the mechanical frequency Ω_m like $\hat{x}(t)$. The spectrum of the PDH-error signal $\epsilon(\omega_{\mathrm{cav}}) \propto \omega_{\mathrm{cav}}(t) \propto \hat{x}(t)$ *is* (up to a scaling factor) $S_{xx}[\omega]$, the mechanical noise spectrum.

Sideband read-out of the mechanical motion

In the previous paragraph, we described a protocol for displaying the noise spectrum that results from beating between zero-detuned laser light (and its externally imposed sidebands) and the mechanical sidebands. There is however another protocol, that allows us to display each sideband individually.

Here, instead of generating two sidebands on the laser signal prior to entering

the cavity, only one extra tone will be generated. Suppose part of the laser light is down-shifted by a frequency ω_{LO}, so that two fields are incident on the cavity; one at ω_{l} and one at $\omega_{\mathrm{l}} - \omega_{\mathrm{LO}}$.

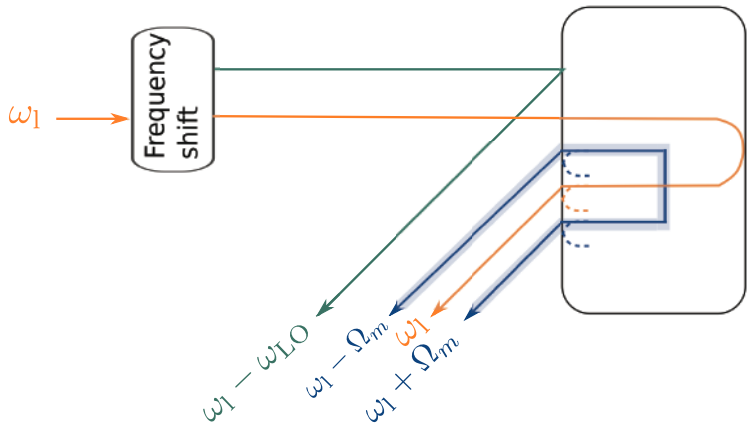

Figure 3.8: Reflected fields after frequency shifting for the sideband read-out method.

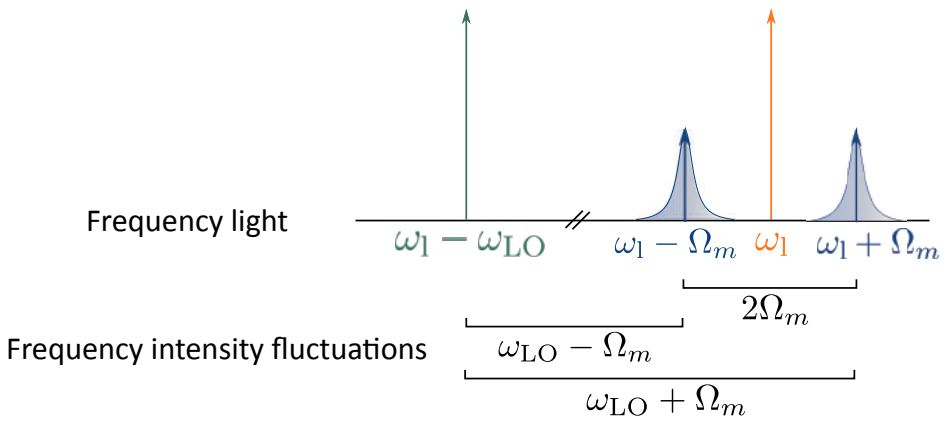

Figure 3.9: Beating between the local oscillator and the individual mechanical sidebands.

Again, the frequency of the new tone must be far enough from the original laser frequency (and, therefore from the cavity resonance) such that it does not enter the cavity and only recombines on the photodetector with the original field and the mechanical sidebands. This is depicted in Fig. 3.8 and 3.9. As a result, the final intensity spectrum comprises a Lorentzian feature around $\omega_{\mathrm{LO}} - \Omega_m$ and one around $\omega_{\mathrm{LO}} + \Omega_m$. The first is an image of the sideband at $\omega_{\mathrm{l}} - \Omega_m$, the latter

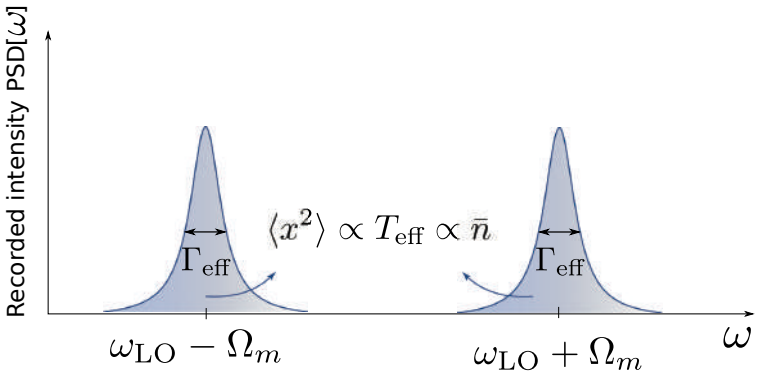

Figure 3.10: Spectrum registered by the photodetector in the sideband read-out method. The features at $\omega_{\rm LO} \mp \Omega_m$ are proportional to the mechanical sidebands at $\omega_{\rm l} \mp \Omega_m$, who in turn are (approximately) proportional to the mechanical noise spectrum $S_{xx}[\omega]$.

of the sideband at $\omega_{\rm l} + \Omega_m$. The sidebands are denoted the red and blue sideband respectively. Each spectral feature on Fig. 3.10 is approximately proportional to the mechanical noise spectrum $S_{xx}[\omega]$. The exact relation between the two will be obtained in the next section.

3.1.5 Detuning, damping and amplification

In the previous section, we have described how we can monitor the motion of the mirror, without interfering with the system's dynamics. We will now overthrow this fly-on-the-wall approach, and see how we can do just the opposite: actively alter the motion of the mirror, using laser light. First, we will explain how light can control the motion of the mirror, and what effect that has on the mechanical spectrum and the mechanical sidebands of the optical spectrum. Then, we will focus on damping of the motion.

We need to talk about the detuning

Up to now we haven't paid much attention to the detuning of the laser - or rather, we have swept it under the rug - but it plays the lead role in this section. From Fig. 3.2 it is clear that if you want any light circulating in the cavity at all, the frequency of the light sent into the cavity should be within a distance κ from the cavity resonance frequency. Up to now we assumed that $\omega_{\rm l} = \omega_{\rm cav}$ because at exactly zero detuning, the light does not alter the motion of the mirror. In the frequency regime around the cavity resonance, the circulating power is still strongly enhanced. What we will explain now is that due to the detuning, the circulating light will be coupled to, and act on, the mirror. It can damp or

amplify its motion.

Let us look again at the interaction Hamiltonian in Eq. (3.12):

$$\hat{H}_{\rm int} = -\hbar G x_{\rm ZPF} \hat{a}^\dagger \hat{a} (\hat{b} + \hat{b}^\dagger)$$

The detuning hides in the photon number operator: $\hat{a}^\dagger \hat{a} = \bar{n}_{\rm cav}(\Delta)$. Therefore, the detuning determines how strong the optomechanical coupling is.
The effect of the optomechanical coupling is to modify the mechanical susceptibility. In other words, the susceptibility of the mirror to external forces is altered in the presence of the optomechanical coupling, and, slightly Escherian, the external forces are the radiation pressure forces. The modified mechanical susceptibility $\chi[\omega]$ can be found by solving the linearized classical or quantum mechanical equations of motion for the system. [30] The new susceptibility can be written in the form

$$\chi[\omega]^{-1} = \chi_m[\omega]^{-1} + \delta\chi[\omega]^{-1} \tag{3.21}$$

with $\chi_m[\omega]$ the 'bare' susceptibility as given in Eq. (3.7) and the modification

$$\frac{1}{\delta\chi[\omega]} = 2\Omega_m m g_0^2 \bar{n}_{\rm cav}(\Delta) \left(\frac{1}{(\Delta+\omega) + i\frac{\kappa}{2}} + \frac{1}{(\Delta-\omega) - i\frac{\kappa}{2}} \right) \tag{3.22}$$

where $g_0 = G x_{\rm ZPF}$ is the single-photon coupling constant.
With the mechanical susceptibility, also the resonance frequency and damping of the motion are altered:

$$\Omega_m \to \Omega_{\rm eff} = \Omega_m + \delta\Omega_m \text{ and } \Gamma_m \to \Gamma_{\rm eff} = \Gamma_m + \Gamma_{opt} \tag{3.23}$$

By writing the susceptibility modification at $\omega = \Omega_m$ as

$$\delta\chi[\Omega_m]^{-1} = m\Omega_m(2\delta\Omega_m - i\Gamma_{opt}),$$

the shift and broadening of the resonance are obtained:

$$\begin{aligned} \delta\Omega_m &= \frac{\Re(\delta\chi[\Omega_m]^{-1})}{2\Omega_m m} \\ &= g_0^2 \bar{n}_{\rm cav}(\Delta) \left(\frac{\Delta+\Omega_m}{(\Delta+\Omega_m)^2 + (\frac{\kappa}{2})^2} + \frac{\Delta-\Omega_m}{(\Delta-\Omega_m)^2 + (\frac{\kappa}{2})^2} \right) \end{aligned} \tag{3.24}$$

also called the optical spring term, and

$$\begin{aligned} \Gamma_{opt} &= \frac{-\Im(\delta\chi[\Omega_m]^{-1})}{\Omega_m m} \\ &= g_0^2 \bar{n}_{\rm cav}(\Delta) \kappa \left(\frac{1}{(\Delta+\Omega_m)^2 + (\frac{\kappa}{2})^2} - \frac{1}{(\Delta-\Omega_m)^2 + (\frac{\kappa}{2})^2} \right) \end{aligned} \tag{3.25}$$

the optical damping. Note that the damping is positive for $\Delta < 0$, i.e. red detuning of the laser, and it is maximal for $\Delta = -\Omega_m$.

We will explain the physical origin of these effects in a scattering picture borrowed from atomic physics, Raman scattering. Simultaneously, we will give physical meaning to the concept of mechanical sidebands on the optical field. Fig. 3.11 shows how the scattering picture ties the amplification and damping of the mechanics to the optical sidebands.

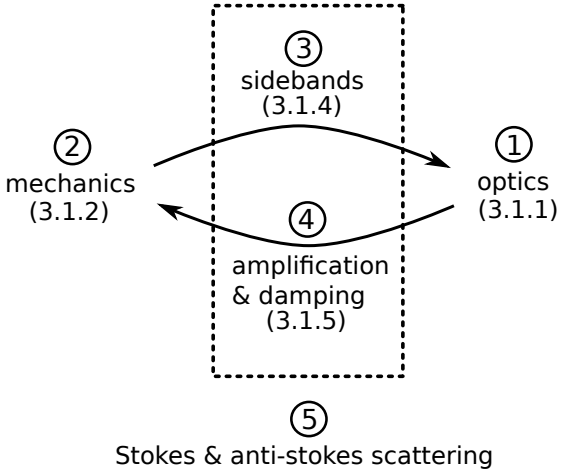

Figure 3.11: Overview of the optomechanical interaction. The mechanics impose sidebands on the optical fields, the optical fields impose damping and amplification on the mechanics. The scattering picture ties both actions together. Numbered steps represent the road taken in this chapter.

Stokes & anti-stokes scattering: a motion picture featuring the sidebands

The generation of sidebands in the cavity at frequencies $\omega_\mathrm{l} \pm \Omega_m$ implies that photons are created at energies lower and higher than the 'original' photon energy $\hbar\omega_\mathrm{l}$. So, if the rate of upscattering (scattering of photons to the blue sideband) exactly compensates the rate of downscattering (scattering of photons to the red sideband), nothing happens. However, if more photons go into the blue (red) sideband, energy is effectively added to (extracted from) the optical field, and extracted from (added to) the mechanical oscillator: T_eff decreases (increases) and the mirror's motion is damped (amplified). Now we can add what we know from the previous paragraph. Damping occurs when the laser is detuned with respect to the cavity resonance, so, *the rate of scattering of photons into the sideband at* $\omega_l - \Omega_m$ *versus* $\omega_l + \Omega_m$ *is not symmetric if* $\Delta \neq 0$. This is depicted in Fig. 3.12, in the case of maximal cooling with $\Delta = -\Omega_m$.

Let us look back at the power spectral density (PSD) of the sidebands, in Fig. 3.10. The features shown there are (imprints of) the mechanical noise spectrum $S_{xx}[\omega]$. So, the area under each sideband is proportional to the area under the

mechanical noise spectrum, which is proportional to the effective temperature of the mirror. But, as we just argued, the area under the sideband must also reflect the amount of photons scattered into that sideband. From that we can guess that the spectra of the red and blue sideband in Fig. 3.9 must be of the form:

$$\mathrm{PSD}^{r,b}[\omega] = f^{r,b}(\Delta) S_{xx}^{r,b}[\omega] \tag{3.26}$$

$$= f^{r,b}(\Delta) \frac{k_B T_{\mathrm{eff}}}{m\Omega_m^2} \frac{\Gamma_{\mathrm{eff}}/2}{(\omega_{r,b} - \omega)^2 + (\Gamma_{\mathrm{eff}}/2)^2} \tag{3.27}$$

with $\omega_r = \omega_\mathrm{l} - \Omega_m$ and $\omega_b = \omega_\mathrm{l} + \Omega_m$ the central frequencies of the sidebands, and $f^{r,b}(\Delta)$ a function such that

$$f^r(\Delta = 0) \to f^b(\Delta = 0), \text{ and } f^r(\Delta \gg \kappa) = f^b(\Delta \gg \kappa) \to 0. \tag{3.28}$$

Before we are going to look for an expression that fits these constraints, let us

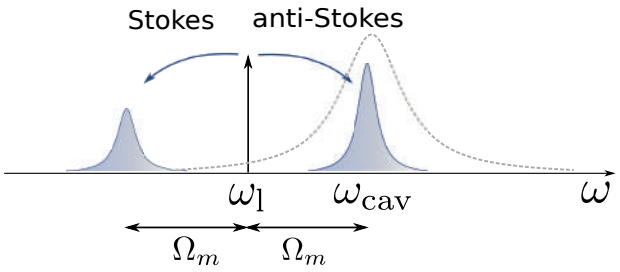

Figure 3.12: Scattering picture of optical cooling. Cooling of the mechanical motion proceeds when the laser is red-detuned with respect to the cavity resonance. The rate of photon upscattering (anti-Stokes scattering) is greater than photon downscattering (Stokes scattering), resulting in sideband asymmetry. At $\Delta = -\Omega_m$, the cooling is maximal. The cavity profile $\bar{n}_\mathrm{cav}$ [grey] is shown on the background for reference.

reexamine equations (3.24) and (3.25) for the optical damping and optical spring effect. If $\Gamma_{opt} > 0$, Eq. (3.23) implies $\Gamma_{\mathrm{eff}} > \Gamma_m$ so the motion is damped, and the rate of photon upscattering > downscattering. Hence, the sign of Γ_{opt} determines which sideband grows most. It represents a net scattering rate. Defining the detuning of the sidebands as $\Delta_{r,b} = \omega_{r,b} - \omega_\mathrm{cav}$, so $\Delta_r = \omega_\mathrm{l} - \Omega_m - \omega_\mathrm{cav} = \Delta - \Omega_m$ and $\Delta_b = \omega_\mathrm{l} + \Omega_m - \omega_\mathrm{cav} = \Delta + \Omega_m$, the first term in Eq. (3.25) appears to be suspiciously similar to the cavity profile, Eq. (3.4), evaluated at Δ_b, and the second term to the cavity profile, evaluated at Δ_r. In other words, the optical damping is proportional to the difference between the strength of the blue and the red sideband.

Now, back to where we left off. We were looking for a function, proportional to the amplitude of the sidebands (3.26), that fulfills the conditions (3.28). But, this is precisely what we just deduced.

$$f^{r,b}(\Delta) \propto \bar{n}_{\mathrm{cav}}(\Delta)\bar{n}_{\mathrm{cav}}(\Delta_{r,b}) \propto \bar{n}_{\mathrm{cav}}(\Delta)\kappa\frac{1}{(\Delta_{r,b})^2+(\frac{\kappa}{2})^2} \tag{3.29}$$

And in fact, with Eq. (3.4),

$$\mathrm{PSD}^{r,b}[\omega] \approx \pi^{-1}\frac{k_B}{\hbar\Omega_m}g_0^2T_{\mathrm{eff}}\frac{P_{\mathrm{in}}\kappa_{\mathrm{ex}}/\hbar\omega_{\mathrm{l}}}{(\frac{\kappa}{2})^2+\Delta^2}\frac{\kappa}{(\Delta_{r,b})^2+(\frac{\kappa}{2})^2}\frac{\Gamma_{\mathrm{eff}}/2}{(\omega_{r,b}-\omega)^2+(\Gamma_{\mathrm{eff}}/2)^2} \tag{3.30}$$

Thus, the areas under the sideband spectra are

$$\mathcal{A}_{r,b} \approx \frac{k_B}{\hbar\Omega_m}g_0^2\frac{\kappa_{\mathrm{ex}}\kappa P_{\mathrm{in}}}{\hbar\omega_{\mathrm{l}}}\frac{1}{(\frac{\kappa}{2})^2+\Delta^2}\frac{T_{\mathrm{eff}}}{(\frac{\kappa}{2})^2+(\Delta_{r,b})^2} \tag{3.31}$$

The effective temperature is then approximately

$$T_{\mathrm{eff}} = \frac{m\Omega_m^2}{k_B}\frac{2\hbar L_0^2}{\omega_{\mathrm{cav}}\kappa_{\mathrm{ex}}\kappa}\frac{1}{P_{\mathrm{in}}}\left(\left(\frac{\kappa}{2}\right)^2+\Delta^2\right)\left(\left(\frac{\kappa}{2}\right)^2+(\Delta_{r,b})^2\right)\mathcal{A}_{r,b} \tag{3.32}$$

where we substituted $g_0^2 = \frac{\omega_{\mathrm{cav}}^2\hbar}{L_0^2 2m\Omega_m}$. This also relates the area under the mechanical noise spectrum to the area under each sideband:

$$\mathcal{A} = \frac{2\hbar L_0^2}{\omega_{\mathrm{cav}}\kappa_{\mathrm{ex}}\kappa}\frac{1}{P_{\mathrm{in}}}\left(\left(\frac{\kappa}{2}\right)^2+\Delta^2\right)\left(\left(\frac{\kappa}{2}\right)^2+(\Delta_{r,b})^2\right)\mathcal{A}_{r,b}. \tag{3.33}$$

Effective temperatures and damping

Of course, the effective temperature and the cooling of the resonator is intimately connected to the damping. They are in fact so connected, that often the words cooling and damping are used interchangeably, while technically only the first implies a decrease in effective temperature.

In Fig. 3.13, the interactions between the mechanical oscillator and the different thermal baths are depicted. In the first place, the mirror is coupled with coupling rate Γ_m to the environment, which is at a temperature T_{mat} ('mat' from 'material' immediately surrounding and holding the mirror). Secondly, there is the optomechanical interaction that couples the mirror to the optical field via the optical damping Γ_{opt}.
Fig. 3.13 looks a bit like tug of war, and this comparison is spot-on. In order to efficiently optically cool the mechanical oscillator, the coupling to the thermal bath should be weak. This explains the care taken in the development of mechanical resonators with a Q-factor as high as possible.

The laser itself is in principle a thermal bath with an effective bath temperature T_l, because both classical and quantum laser noise components act as thermal baths that couple with the mechanical oscillator. It follows that:

$$T_\mathrm{eff} = \frac{\Gamma_m T_\mathrm{mat} + \Gamma_\mathrm{opt} T_\mathrm{l}}{\Gamma_\mathrm{eff}} \tag{3.34}$$

with $\Gamma_\mathrm{eff} = \Gamma_m + \Gamma_{opt}$ according to Eq. (3.23). In the absence of the optomechanical interaction, this reduces to $T_\mathrm{eff} = T_\mathrm{mat}$, meaning the mirror is completely thermalized with the environment.
If classical laser noise is negligible, the effective temperature of the laser vanishes. One gets the equally simple and powerful result:

$$T_\mathrm{eff} = \frac{\Gamma_m}{\Gamma_\mathrm{eff}} T_\mathrm{mat}. \tag{3.35}$$

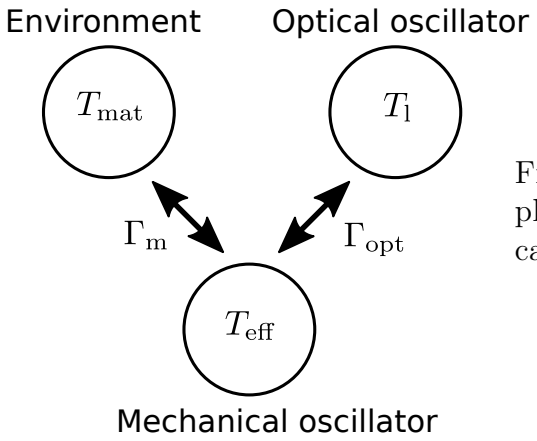

Figure 3.13: Thermodynamically coupled environments of an optomechanical system

Ground-state sideband asymmetry

We have two pressing questions still hanging over our heads: "Why are the sidebands *approximately* proportional to the motion spectrum?", and, "When are we going to do something quantum?" After all, we did start off with Hamiltonians and operators! First, let us start thinking in terms of oscillator quanta, so we switch from effective temperatures T_eff to phonon occupation numbers $\bar{n} = k_B T_\mathrm{eff}/\hbar\Omega_m$.
The rate at which Stokes and anti-Stokes scattering proceeds is inherently asymmetric, regardless of the detuning of the laser.

If the oscillator is in the ground state $\bar{n} = 0$, no further cooling is possible: the anti-Stokes process must vanish, but the the Stokes process must not. In extension to all temperatures and detunings, the red sideband grows with $\bar{n}+1$, while the blue sideband grows only with $\bar{n}$. Like in atomic physics, this is a consequence of the final density of available phonon states. Thus, the true sideband spectra and respective areas are:

$$\mathrm{PSD}^{r,b}[\omega] = (\bar{n} + \delta_r^{r,b})\pi^{-1}\bar{n}_{\mathrm{cav}}(\Delta)\frac{\kappa}{(\Delta_{r,b})^2 + (\frac{\kappa}{2})^2}\frac{\Gamma_{\mathrm{eff}}/2}{(\omega_{r,b} - \omega)^2 + (\Gamma_{\mathrm{eff}}/2)^2} \tag{3.36}$$

$$\mathcal{A}_{r,b} = \bar{n}_{\mathrm{cav}}(\Delta)\kappa\frac{\bar{n} + \delta_r^{r,b}}{(\frac{\kappa}{2})^2 + (\Delta_{r,b})^2} \tag{3.37}$$

For $\bar{n} \gg 1$, these equations reduce to Eq. (3.30) and (3.31), becoming equal for $\Delta = 0$.

The inherent scattering asymmetry implies that close to the ground state, in the countable phonon regime (say $\bar{n} < 100$, depending on the sensitivity and noise floor of the measurement) there is an alternative method for thermometry of the mirror:

$$\frac{\mathcal{A}_b}{\mathcal{A}_r} = \frac{\bar{n}}{\bar{n}+1}\frac{(\frac{\kappa}{2})^2 + (\Delta - \Omega_m)^2}{(\frac{\kappa}{2})^2 + (\Delta + \Omega_m)^2} \tag{3.38}$$

That is, the phonon occupation number follows from the ratio of the sidebands. At exactly zero detuning, the result becomes strikingly simple:

$$\frac{\mathcal{A}_b}{\mathcal{A}_r} = \frac{\bar{n}}{\bar{n}+1} \tag{3.39}$$

The mechanical occupation number can be determined by merely comparing the areas under the sideband spectra, and no knowledge about any system parameter is required.

Damping and amplification: an intuitive picture

To help digest all the formulas and Lorentzians, we will conclude this section with a more conceivable picture of optical cooling and amplification. In the second paragraph of 3.1.3, we explained that the photons can alter the motion of the mirror because they exert pressure on it. In fact, there is something more to this. Because the photons circulating in the cavity have a finite decay rate κ, $\bar{n}_{\mathrm{cav}}$ does not instantaneously react to a change of the resonance frequency ω_{cav}. Some time is necessary for the photons to leak out or to build up again after the detuning is increased or decreased. As a result of this retardation [30], the driving radiation force can be out of phase with the mechanical motion. It's like trying to drive a kid on a swing by pushing it with a frequency or phase different than that of the swing; you might end up doing nothing, or slowing it down, or getting hit in the face. The out-of-phase part of the force is responsible for cooling or heating.

3.2 Experimental methods

The first three subsections of this section describe the fundaments of the experiment that was set up by F.M. Buters et al. from the Bouwmeester Quantum Optics group at Leiden University. It has been used for optical cooling and thermometry of various samples (the sample utilized in this thesis, as well as precursors) at room temperature and cryogenic temperatures [6, 28, 33, 34]. Relatively small modifications to the set-up (i.e., the optical table) have allowed the demonstrations of a vast range of optomechanical experiments, including OMIT (optomechanically induced transparency) [35] and mechanical state transfer in a membrane-in-the-mirror sample [20]. The fourth subsection describes the preparations for an experimental run at milliKelvin temperatures, following protocols developed in the same group.

3.2.1 The mechanics

The mechanical resonator is a high-quality ($Q \sim 10^6$) nested trampoline resonator, produced and developed in the UCSB Bouwmeester Group by M.J. Weaver et al. [5–7]. Here, we will stick to the absolute basics necessary to understand the dynamics.[9] Fig. 3.14 shows an optical microscope image of the

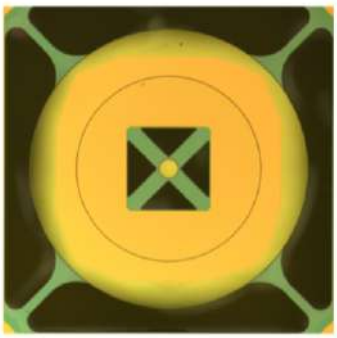

Figure 3.14: Optical microscope image of the nested trampoline resonator. The central mirror is a distributed Bragg reflector (DBR) made up of alternating layers of Ta_2O_5 and SiO_2. Courtesy of M.J. Weaver.

resonator. It is 'nested', because the full sample comprises a central mirror (the mass) about 70μm in diameter, attached via four 200μm long silicon nitride arms (the springs) to what could be called a second resonator, because this surrounding structure is suspended as well. The purpose of the outer resonator, designed by K. Heeck, is to filter out low frequency noise, making the measured spectra extraordinary clean [35]. The central small mirror has an effective mass of $140 \cdot 10^{-12}$kg and a resonance frequency of $\sim$ 300kHz. The intrinsic mechanical damping at room temperature is of the order 1Hz. The high mechanical reso-

[9] Chapter 2 and 9 in Ref. [35] are especially recommended for a concise version of the nested resonator's backstory.

nance, together with low intrinsic damping (manifested as a ultra high Q) is an essential prerequisite of reaching the ground state.

3.2.2 The optics

The small moving mirror, and a stationary mirror fixed at a 5cm distance from it, form a Fabry-Pérot cavity, with a FSR of 3GHz and $\lambda = 2\pi c/\omega_{\mathrm{cav}} \approx 1064$nm. Accordingly, two infrared lasers are used. One, a Coherent Mephisto S Nd:YAG-laser, will be in charge of reading out the motion via the PDH method and will be denoted probe laser, locking laser or read-out laser. The second, a Coherent Mephisto with higher power output, carries the responsibility of cooling down the mirror and will therefore be denoted the cooling laser, or pump laser. Fig. 3.15 shows the nested resonator in the sample holder on the right, and the stationary mirror in the middle. The light of both lasers enters the cavity via the same single mode fiber, and is subsequently coupled into the cavity using a lens and periscope mirrors. The reflected light follows the same route. Transmitted light, that is, light leaking through the moving mirror, exits the cavity and is then captured in a multimode fiber.

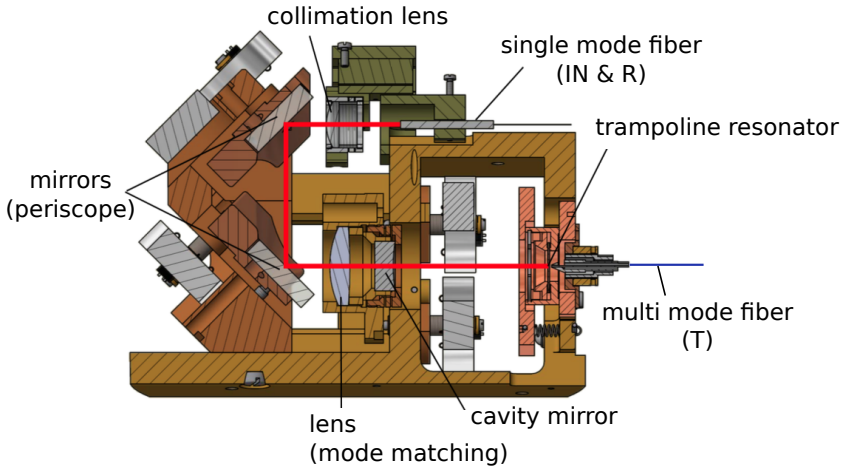

Figure 3.15: The 5cm long Fabry-Perot cavity. The path followed by the light is marked in red. IN: incoming light, R: reflected light, T: transmitted light. Courtesy of F.M. Buters.

3.2.3 The set-up

Fig. 3.16 shows an overview of the fundamental experiment for optical cooling and PDH thermometry (measurement of the effective temperature of the motion

by analysis of the mechanical spectrum obtained via the PDH read-out method). Let us follow the path of the light, starting from the probe laser, whose frequency must match the cavity resonance frequency. We already explained that the cavity length and resonance change as a result of the motion of the mirror, but in practice there are also fluctuations resulting from environmental noise that are not filtered out by the vibration isolation mentioned in section 3.2.1. These low frequency noise components, together with thermal drift of the frequency of the laser, make that the laser's frequency must be continually adjusted so that it stays locked to the cavity resonance. The optical and electrical components that accomplish this are grouped together in the lower half of Fig. 3.16. They serve a dual purpose: cavity fluctuations around the mechanical frequency are extracted and read out for thermometry, and the noisy low frequency components are extracted and sent to the PID (proportional-integral-derivative) controlling the laser frequency.

In section 3.1.4, we described how sidebands at $\omega_{\mathrm{LI}} \pm \omega_{\mathrm{PDH}}$ must be gener-

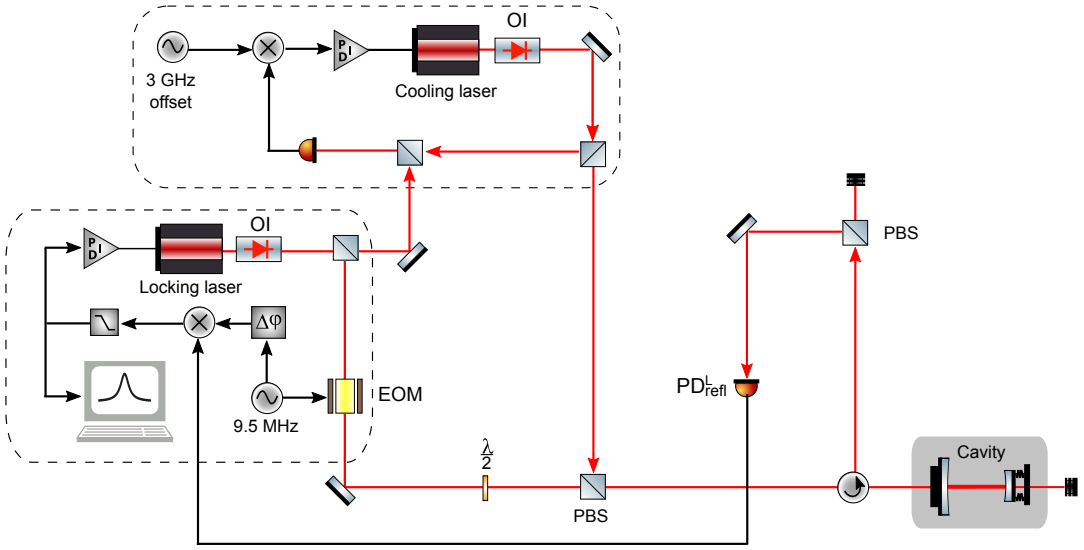

Figure 3.16: The optical set-up. The components displayed are: $\lambda/2$: waveguide, BS: beam splitter, PBS: polarizing beam splitter, EOM: electro-optical modulator, OI: optical isolator and PI: proportional-integral feedback controller.

ated externally, prior to entrance in the cavity. This is accomplished by sending the light from the locking laser through an EOM, driven at $\omega_{\mathrm{PDH}} = 2\pi \times 9.5\mathrm{MHz}$. The resulting fields, displayed in orange and purple on Fig. 3.7, pass through a waveguide and a polarizing beamsplitter and a circulator, and end on the stationary mirror of the cavity. The PDH sidebands are reflected, the probe field enters the cavity, and the reflected signal exits the cavity via the same fiber. Sub-

sequently, the circulator guides it to the photodetector $\mathrm{PD}^{\mathrm{L}}_{\mathrm{refl}}$. The PDH error signal is obtained by mixing the signal registered on the photodetector with the same local oscillator at $\omega_{\mathrm{PDH}} = 2\pi \times 9.5\mathrm{MHz}$ that drives the EOM and sending it through a low-pass filter. We only need the amplitude ϵ of the AC signal given by Eq. (3.20) because this amplitude fluctuates synchronous with the mirror. The PID (proportional-integral-derivative controller) keeps the probe laser locked to the cavity resonance frequency.

The second laser at play, is the pump laser. It is meant to be red-detuned

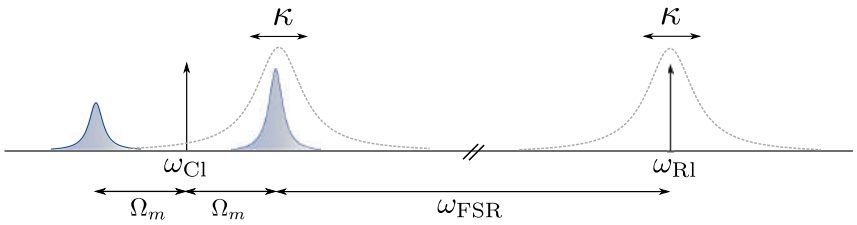

Figure 3.17: Positions of the lasers in the frequency domain for an optical cooling set-up. In the case depicted, the cooling laser is set at $\Delta = -\Omega_m$. The system is sideband-resolved ($\kappa < \Omega_m$). The cavity profile $\bar{n}_{\mathrm{cav}}$ [grey, dotted] is shown on the background for reference.

with respect to the cavity resonance, in order to pump the blue sideband.[10] In practice, the pump laser operates near a cavity resonance that is a free spectral range separated from the cavity resonance to which the probe laser is locked. This way, we do not have to worry about beating between the two beams, which would show up at exactly the frequencies we are interested in. This is depicted in Fig. 3.17. Thus, the frequency of the pump laser must be $\omega_{\mathrm{Cl}} = \omega_{\mathrm{Ll}} - \omega_{\mathrm{FSR}} + \Delta_{\mathrm{Cl}} \approx \omega_{\mathrm{Ll}} - 2\pi \cdot 3\mathrm{GHz} + \Delta_{\mathrm{Cl}}$. The right frequency is obtained by picking off some of the read-out laser light, and mixing it with a $3\mathrm{GHz} - \frac{\Delta_{\mathrm{Cl}}}{2\pi}$ signal from the R&S (Rohde and Schwarz SMA100A) signal generator. The loop keeping the frequency of the cooling laser at a relative distance to the probe laser, is termed a phase locked loop and depicted on the upper half of Fig. 3.16. The pump laser light is then combined with the probe laser light in the PBS, and also enters the cavity. The reflected pump laser light passes through the circulator as well. Subsequently, it is separated from the reflected probe laser light by the polarizing beamsplitter, because they have orthogonal polarizations.

[10] If we talk about sidebands, from here on we always mean the mechanical sidebands on the probe beam that result from phase modulation by the mirror, never the PDH sidebands at ±10 Mhz

The photodetector PD^{L}_{refl} therefore detects only the reflected locking laser light. Orthogonal polarization of probe and pump laser light is achieved by controlling the waveguide in the path of the probe laser light.

The diagram of the set-up shows two beam dumps: one for the transmitted light, and one for the reflected pump laser light. In practice, both can be replaced by additional photodetectors. The transmission signal is of importance in the system preparation stage, and is then detected by a photodetector placed behind the trampoline resonator. The reflected pump laser light will be of importance in chapter 6 of this thesis.

3.2.4 The road to mK temperatures

The following section is a brief summary of the methods developed in the Kamerlingh Onnes Laboratory at Leiden University.

System preparation at room temperature

A new experimental run generally means that a new sample (the trampoline resonator, or something more exotic such as a double membrane resonator) must be placed in the cavity. So, after all other optical and electronic components are installed on the optical table, as in Fig. 3.16, the first step is the cavity alignment. In order to fit the rigorous definition of a cavity, the distance between the two mirrors must exactly match the frequency of the laser light that we intend to shine on it. At this point the mirrors are not yet perfectly 'aligned', so the configuration of the mirrors is adjusted, and the process is monitored with the help of a 1064nm Toptica DL Pro laser and a CCD.

Once the cavity is made resonant with the laser light, the finesse $\mathcal{F}$ is determined via a ringdown measurement [36, 37]. The Toptica laser is scanned over the cavity resonance frequency, and as soon as the frequency of the laser matches the resonance frequency of the cavity, light builds up in the cavity, and a corresponding transmission signal is generated. If the circulating intensity is maximal, the transmission signal triggers a voltage controller that shuts down the laser and the decaying transmitted intensity is measured by the photodetector behind the sample.

At this point in the process, the transmission signal still goes to the photodetector through air, so the transmission fiber and its holder need to be installed. Once the single mode fiber for the reflected signal and the multimode fiber for the transmitted signal are in their proper positions, the cavity can be placed in a vacuum chamber. The cavity environment is then brought to $\sim 10^{-3}$mbar, necessary to exclude effects of gas damping on the movable mirror.

The last step prior to the cooling stage is the determination of the quality factor [38] of the resonator $Q = \frac{\Omega_m}{\Gamma_m}$. It is of utmost importance that the intrinsic, not the effective, values for the mechanical resonance and linewidth are determined, so optomechanical interactions must be avoided. To that extent, the Toptica laser is used, operating at 980nm. The cavity mirrors reflect poorly in this frequency regime, and as a result the photons will leak our the cavity very fast. This is precisely what we need, because we do *not* want the photons to keep bouncing between the mirrors, hitting the movable mirror each time. A very low finesse cavity is created in this way. [39] The mechanical noise spectrum is then measured by locking the laser to a slope of the resonance in the transmission signal, as in Fig. 3.4. The central frequency and linewidth of the spectrum are then the intrinsic mechanical resonance frequency Ω_m and damping Γ_m.

System preparation at cryogenic temperatures

This thesis presents the first experiments with the double nested trampoline resonator conducted in a millikelvin environment. The cryogenic environment is a cryogen free dilution refrigerator (Leiden Cryogenics CF-CS81-1400). A cool-down process proceeds in two stages. First, a pulse tube cryocooler is used to reach a cryostat temperature of 5.7K. Vibration isolation for the vibrations of the pulse tube is implemented in both the cryostat itself [40] and the optomechanical system [41]. Secondly, the dilution refrigeration unit is activated. Taking advantage of the fact that mixing two helium isotopes costs enthalpy, it cools the cryostat further to a base temperature of 200mK, by diluting ^{3}He in ^{4}He.
Such drastic changes in the environment have an impact on the optomechanical system. [18, 42] Most importantly, the temperature drop causes the materials to contract or expand. These are the materials of the nested resonator (like the Si_3N_4 mirror suspensions and the Si wafer) but also the optical bench itself. Because of the latter, during the cool down process, the cavity length needs to be continuously adjusted in order retain the best possible cavity finesse $\mathcal{F}$. This is done by electronically remotely controlling the motors steering the cavity mirror. The impact on the mechanical resonator is a lowering of the intrinsic mechanical resonance frequency Ω_m due to reduced tension in the Si_3N_4 arms. Furthermore, the intrinsic mechanical damping Γ_m can decrease if the vacuum improves due to reduced gas damping. As a result, the values for κ, Ω_m and Γ_m will differ from those at room temperature. [38, 43]

As the temperature is lowered, more and more subtleties come into play. For example, the use of high laser powers can cause fluctuations of the environment temperature. Thus, before completely cooling down the system from room temperature to sub-Kelvin temperatures, it is good practice to pause at an in-between stage, and try out the envisaged experiments. An ideal moment for this

second system check is the stable temperature stage at 5.7K. Between 5.7K and the millikelvin regime, the cavity linewidth κ and the mechanical quality factor Q are not expected to change anymore. This is mostly for the simple reason that expansion coefficients of the materials involved vanish, or that the temperature change is small enough for the length contractions or extensions to be negligible. System check-ups at 293K and 5.7K are described in the next chapter, after which we will get down to millikelvin business, in chapter 5.

Chapter 4

System characterization

> *Milo tried very hard to understand all the things he'd been told, and all the things he'd seen, and, as he spoke, one curious thing still bothered him.*
> *"Why is it," he said quietly, "that quite often even the things which are correct just don't seem to be right?"*
>
> – Norton Juster, *The Phantom Tollbooth*

We hope to obtain some characteristic parameters of the system, and test whether the system behaves like it should. Therefore, we vary the detuning of the pump laser, and compare the response of the mirror to theory. We find that our system is doing fine. So fine, we noticed the modeling theory could be refined!

4.1 Varying the pump laser detuning

The two objectives through this thesis are always the same: thermometry and cooling of the resonator. The resonance frequency shift, Eq. (3.24), and spectral broadening, Eq. (3.25), carry the effects of damping, so together with Eq. (3.35) connecting the temperature to the damping in the absence of laser noise, they serve as the basis for all analyses of the system. Combining them with Eq. (3.4)

and (3.23), we obtain:

$$\Omega_{\text{eff}} = \Omega_m + \delta\Omega_m^{\text{Cl}} \tag{4.1}$$

$$\delta\Omega_m^{\text{Cl}} = \frac{g_0^2\kappa_{\text{ex}}}{\Delta_{\text{Cl}}^2 + (\frac{\kappa}{2})^2}\frac{C_{\text{mm}}P_{\text{Cl}}}{\hbar\omega_{\text{l}}}\left(\frac{\Delta_{\text{Cl}} + \Omega_m}{(\Delta_{\text{Cl}} + \Omega_m)^2 + (\frac{\kappa}{2})^2} + \frac{\Delta_{\text{Cl}} - \Omega_m}{(\Delta_{\text{Cl}} - \Omega_m)^2 + (\frac{\kappa}{2})^2}\right)$$

$$\Gamma_{\text{eff}} = \Gamma_m + \Gamma_{opt}^{\text{Cl}} \tag{4.2}$$

$$\Gamma_{opt}^{\text{Cl}} = \frac{g_0^2\kappa_{\text{ex}}}{\Delta_{\text{Cl}}^2 + (\frac{\kappa}{2})^2}\frac{C_{\text{mm}}P_{\text{Cl}}}{\hbar\omega_{\text{l}}}\left(\frac{\kappa}{(\Delta_{\text{Cl}} + \Omega_m)^2 + (\frac{\kappa}{2})^2} - \frac{\kappa}{(\Delta_{\text{Cl}} - \Omega_m)^2 + (\frac{\kappa}{2})^2}\right)$$

$$T_{\text{eff}} = \frac{m\Omega_m^2}{k_B}\mathcal{A} \tag{4.3}$$

$$\overset{T_{\text{l}}\approx 0}{=} T_{\text{mat}}\frac{\Gamma_m}{\Gamma_{\text{eff}}} \tag{4.4}$$

where we substituted $P_{\text{in}} = P_{\text{Cl}}C_{\text{mm}}$. Here, P_{Cl} is the pump laser power launched into the cavity (displayed on the power meter), but not all of it effectively enters the cavity. The power truly entering the cavity is smaller by a 'mode matching' factor C_{mm}, depending on the coupling into the fiber and the alignment of the cavity. We assume that our system is critically coupled, i.e. $\kappa_{\text{ex}} = \kappa/2$.[1]

What are we looking for?

The parameters unknown at the start of an experimental run are the mode matching factor C_{mm}, the cavity linewidth κ, and a fixed offset for the pump laser detuning Δ_0. The detuning is adjustable by tuning the frequency of the R&S signal generator, but the starting frequency is not known a priori, so strictly we have $\Delta_{\text{Cl}} = \omega_{\text{Cl}} - \omega_{\text{cav}} = \Delta_{\text{R\&S}} + \Delta_0$, with $\Delta_{\text{R\&S}}$ the tunable parameter and Δ_0 unknown.

The effective temperature can be obtained from the Lorentzian mechanical spectrum in two ways. The most fundamental way is rescaling the area under the mechanical spectrum $\mathcal{A}$, because the effective temperature is related to the area under the spectrum via Eq. (3.11). If we assume that the laser has an effective temperature $T_{\text{l}} \approx 0$, then Eq. (3.35) is valid and *damping the motion is cooling the motion*. In that case, T_{eff} can equally well be determined from the spectral linewidth Γ_{eff} using Eq. (3.35). Both ways to determine T_{eff} are described in Eq. (4.3) and (4.4).

[1] If the true coupling would be different, this would not influence the analysis of the experiment, as any deviation from $\kappa_{\text{ex}} = \kappa/2$ is absorbed into the mode matching factor C_{mm}.

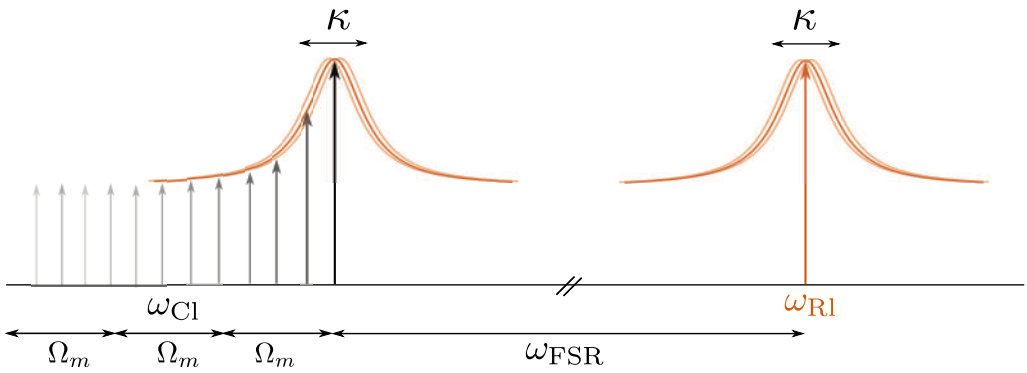

Figure 4.1: Variation of the pump laser detuning. The closer to the cavity resonance the pump laser frequency is set, the more light circulates in the cavity. This follows from the cavity profile $\bar{n}_{\text{cav}}(\Delta_{\text{Cl}})$ [orange]. The probe laser remains locked to the cavity resonance. The cavity resonance frequency (and therefore the cavity profile) fluctuates with respect to the probe laser frequency, allowing PDH read-out of the motion.

Don't stay tuned, for more information

As described in section 3.2.4, before starting an experiment, we want to obtain as much information as possible about the system. To that end, a detuning sweep is performed. We scan the frequency of the cooling laser Δ_{Cl} and check how equations (4.1-4.4) evolve. This is schematically depicted in Fig. 4.1. For each value of the detuning, a mechanical spectrum is recorded via the PDH read-out method. The power spectrum PSD$[\frac{\omega}{2\pi}]$ is originally expressed in $\text{V}^2_{\text{rms}}/\text{Hz}$, and is rescaled to m^2/Hz after calibration. A Lorentzian profile $\frac{\mathcal{A}}{\pi}\frac{\Gamma_{\text{eff}}/2}{(\Omega_{\text{eff}}-\omega)^2+(\Gamma_{\text{eff}}/2)^2}+\mathcal{N}$ is fitted to each spectrum, which returns four properties: central frequency Ω_{eff}, linewidth Γ_{eff}, area $\mathcal{A}$, noise floor $\mathcal{N}$. Hence, each value of the detuning Δ_{Cl} corresponds with four measured values: $\Omega_{\text{eff}}(\Delta_{\text{Cl}}), \Gamma_{\text{eff}}(\Delta_{\text{Cl}}), \mathcal{A}(\Delta_{\text{Cl}})$ and $\mathcal{N}$.

In Fig. 4.2, a sequence of mechanical noise spectra is plotted, measured during a detuning sweep at 293K. The intrinsic resonance frequency and damping were predetermined during the system preparation, as described in section 3.2.4: $\Omega_m/2\pi = 308\text{kHz}$ and $\Gamma_m/2\pi = 1.05 \pm 0.05\text{Hz}$. When the pump laser frequency is tuned closer and closer to the cavity resonance, the amplitude of the Lorentzian spectum decreases, and increases again after passing through a minimum at $\Delta_{\text{Cl}} = -\Omega_m$. Fig. 4.3 displays the same spectra, from a different perspective, to showcase the optical spring effect and optical damping. The linewidths, central frequencies and areas under these spectra are then fitted to

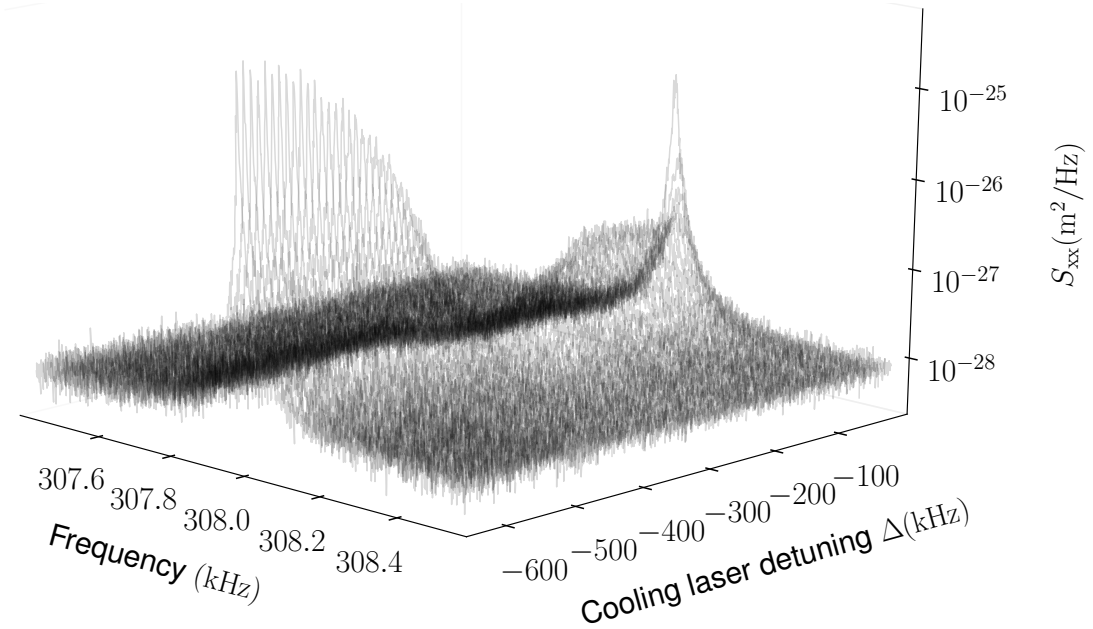

Figure 4.2: Evolution of the mechanical noise spectrum through variation of the pump laser detuning. Measurement at room temperature.

equations (4.1) - (4.4). The result of the analysis is shown in Fig. 4.4. Green, blue and yellow points represent respectively the measured quantities $\Gamma_{\mathrm{eff}}(\Delta_{\mathrm{Cl}})$, $T_{\mathrm{eff}}(\Delta_{\mathrm{Cl}}) = \frac{m\Omega_m^2}{k_B}\mathcal{A}(\Delta_{\mathrm{Cl}})$ and $\delta\Omega_m(\Delta_{\mathrm{Cl}}) = \Omega_{\mathrm{eff}}(\Delta_{\mathrm{Cl}}) - \Omega_m$. The optimization algorithm fits the spectral linewidths (green) and resonance frequencies (yellow) to the optomechanical theory Eq. (4.1) and (4.2) with κ, C_{mm} and Δ_0 as free parameters. The fit returns a cavity linewidth $\kappa/2\pi = 110.7 \pm 0.6$kHz and a mode matching factor $C_{\mathrm{mm}} = 0.018$, which means that for the launched cooling power $P_{\mathrm{Cl}} = 83 \pm 2\mu$W, the net cooling laser power incident on the cavity was $P_{\mathrm{in}} = 0.018 \times (83 \pm 2\mu\mathrm{W}) = 1.50 \pm 0.04\mu$W.

Red curves for Γ_{eff} and $\delta\Omega_m$ represent the optomechanical theory, Eq. (4.1) and (4.2), for the fitted system parameters. The areas under the noise spectra (blue) are not used in any fitting procedure. The theoretical curve for T_{eff} uses the fitted linewidth according to Eq. (4.4), while the blue datapoints are the rescaled areas in Eq. (4.3). From Fig. 4.4, we conclude there is a satisfying agreement between theory and experiment.

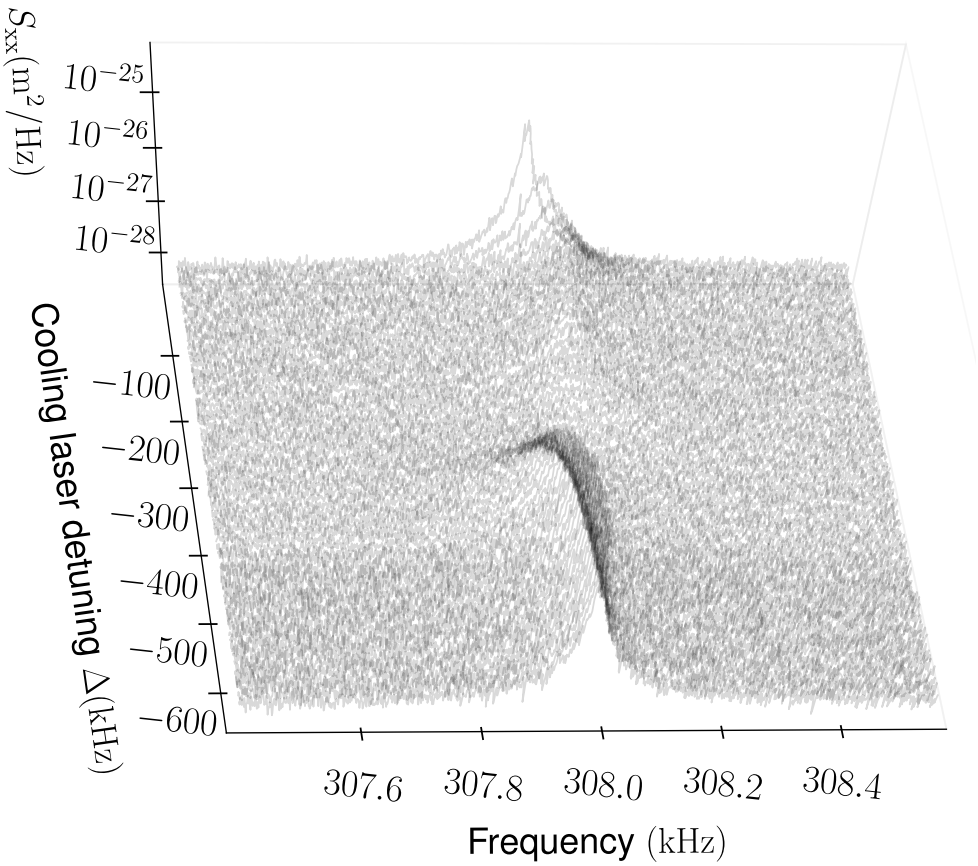

Figure 4.3: Optical spring effect. Detuning sweep at room temperature.

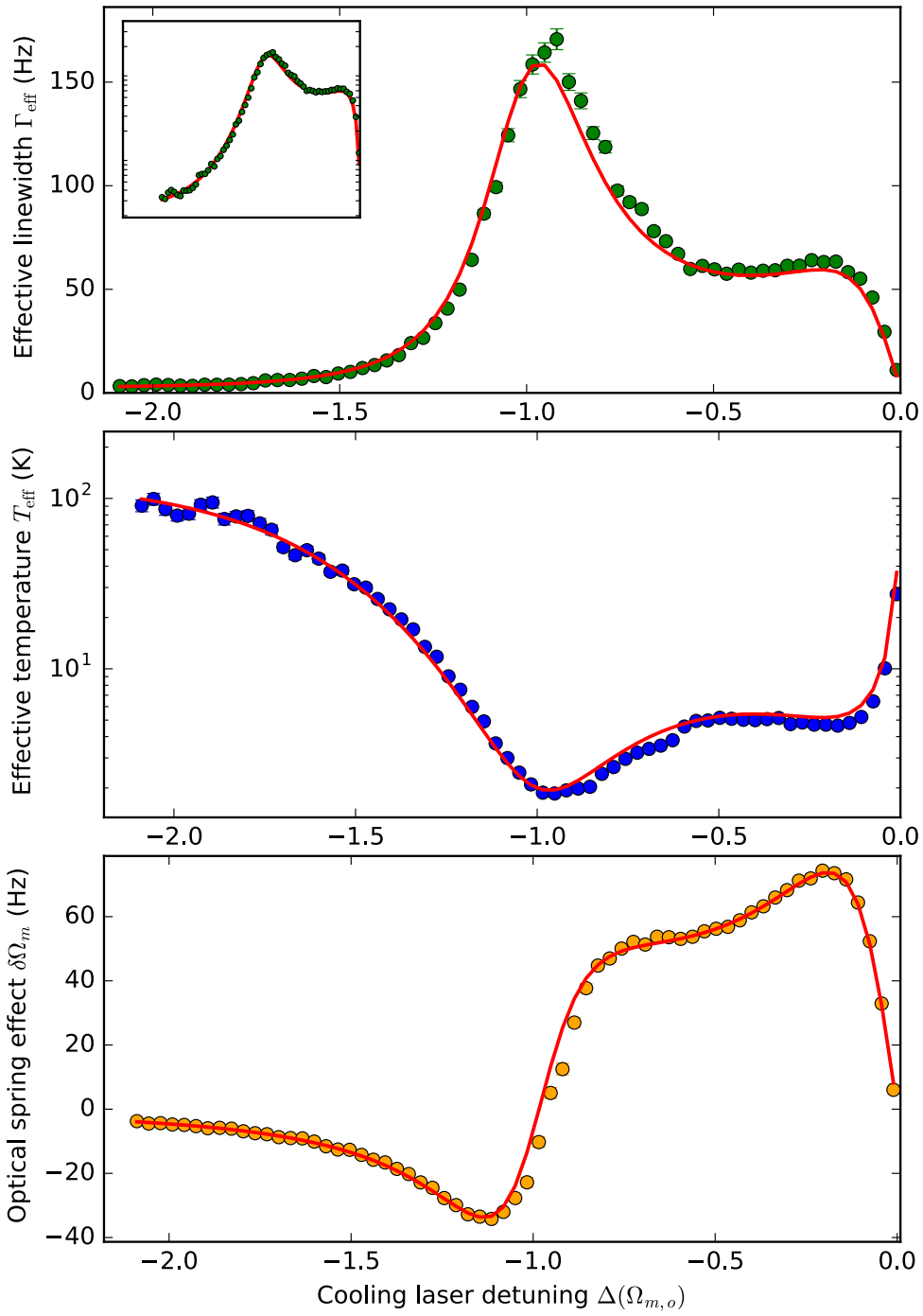

Figure 4.4: Detuning sweep at 293K. Red curves represent the fit to optomechanical theory.

4.2 Optimization, optimized

Fig. 4.5 shows the results of a detuning sweep at 5.7K. The intrinsic mechanical resonance frequency and damping were redetermined at this stage, because they are affected by the changed environmental conditions. Using the protocols laid out in section 3.2.4, the intrinsic parameters $\Gamma_m/2\pi = 0.67 \pm 0.03$Hz and $\Omega_m/2\pi = 302$kHz were obtained. The in-fiber pump laser power was $P_{\mathrm{Cl}} = 15\mu$W, and a power $P_{\mathrm{Ll}} = 10\mu$W was used to read out the motion.
The dotted red lines are the fits that result from the optimization algorithm described in the previous section. Two aspects are notable here. Firstly, when approaching the cavity resonance, the system becomes unstable. As a result, one cannot cover the full frequency range up to $\Delta_{\mathrm{Cl}} = 0$. Secondly, the measured data deviates from the theory far from resonance and around $\Delta_{\mathrm{Cl}} = -\Omega_m$. Both observations can be explained if the read-out laser is not locked exactly to the cavity resonance, but is slightly blue-detuned.

In fact, this is not a new finding. The frequency of the probe laser is manually set using a PID controller that maintains the Pound-Drever-Hall lock, and setting it exactly on resonance is difficult. Like the pump laser frequency, the probe laser frequency can be increased or decreased, but the starting point is unknown. Furthermore, at cryogenic temperatures the probe laser a priori cannot be red-detuned during measurements, because this gives rise to non-equilibrium effects, explained and described by Buters et al. in Ref. [33]. However, the presence of a laser that is blue-detuned with respect to the cavity resonance brings about amplification of the mirror's motion, and this effect has been unaccounted for - until now.

In order to accomodate the amplification by the probe laser, Eq. (3.23) is modified to include an optical spring and optical damping term from the probe laser:

$$\Omega_{\mathrm{eff}} = \Omega_m + \delta\Omega_m^{\mathrm{Cl}}(\Delta_{\mathrm{Cl}}, P_{\mathrm{Cl}}) + \delta\Omega_m^{\mathrm{Ll}}(\Delta_{\mathrm{Ll}}, P_{\mathrm{Ll}}) \tag{4.5}$$

$$\Gamma_{\mathrm{eff}} = \Gamma_m + \Gamma_{opt}^{\mathrm{Cl}}(\Delta_{\mathrm{Cl}}, P_{\mathrm{Cl}}) + \Gamma_{opt}^{\mathrm{Ll}}(\Delta_{\mathrm{Ll}}, P_{\mathrm{Ll}}) \tag{4.6}$$

with $\delta\Omega_m^{\mathrm{Ll}}$ and $\Gamma_{opt}^{\mathrm{Ll}}$ given by Eq. (3.24) and Eq. (3.25), with $P_{\mathrm{in}} = C_{\mathrm{mm}}P_{\mathrm{Ll}}$ and $\Delta = \Delta_{\mathrm{Ll}}$. Because the probe laser detuning Δ_{Ll} and power P_{Ll} are constant, $\delta\Omega_m^{\mathrm{Ll}}$ and $\Gamma_{opt}^{\mathrm{Ll}}$ are constant. So, including the effects of the probe laser in the fitting algorithm is as simple as adding two free offsets: one for the mechanical resonance and one for the linewidth. The resulting fit is displayed in solid red in Fig. 4.5. Excellent agreement between theory and experiment is now seen over the full detuning range.

The prime purpose of the detuning sweep is determination of the cavity linewidth κ. The unadapted and adapted fitting methods return a cavity linewidth of respectively 78.4 ± 0.3kHz and 85.4 ± 0.5kHz. The latter is in perfect accordance with the value found in an independent measurement of the cavity linewidth

via OMIT (F.M. Buters, [35]) returning $\kappa/2\pi = 87 \pm 3$kHz. In conclusion, incorporating the antidamping by the probe laser in the optomechanical theory significantly improves the quality of the fit and the reliability of the fitted system parameters for the nested resonator.
The other fitted parameters were $C_{\mathrm{mm}} = 0.12$ for the mode matching factor, and $\delta\Omega_m^{\mathrm{Ll}}/2\pi = 4 \pm 1$Hz and $\Gamma_{opt}^{\mathrm{Ll}}/2\pi = -3.3 \pm 0.2$Hz for the optical spring effect and antidamping from the probe laser. The negative optical damping confirms the probe laser is blue detuned, and the values indicate a detuning of approximately 10kHz. As stated at the beginning of this section, detuning of the probe laser also justifies the observed instability for $\Delta_{\mathrm{Cl}} \to 0$. If the damping by the cooling laser would become less than the amplification by the read-out laser, the total linewidth Γ_{eff} would become negative. The mirror then departs from thermal equilibrium. This precisely takes place when $\Delta_{\mathrm{Cl}} \to 0$.
At last, one could ask: "The amplification, is that bad?" or "Shouldn't we do something about it, rather than tucking it into the theory?" After all, our final purpose will be to laser-cool the motion of the mirror, so it might seem silly to have a read-out laser simultaneously amplifying the motion, partially undoing the work of the cooling laser. The answer is no, provided there is no harm in using that extra bit of cooling laser power compensating for the anti-damping.

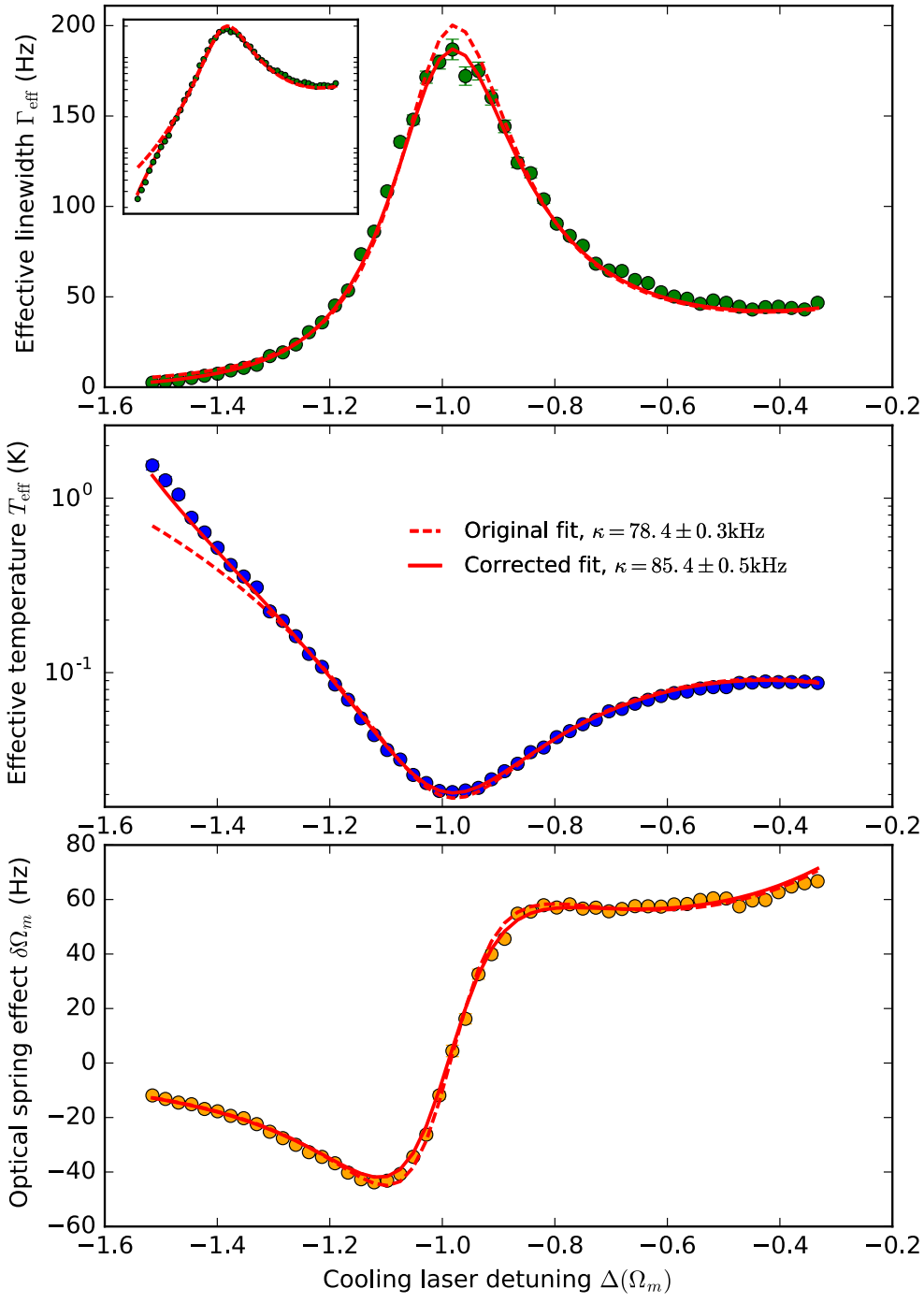

Figure 4.5: Detuning sweep at 5.7K. Solid (dotted) lines represent optomechanical theory including (excluding) a finite probe laser detuning.

Chapter 5

First measurements at mK temperatures

There is a crack in everything, that's how the light gets in.
– Leonard Cohen, *Anthem*

In a 200 mK cryogenic environment, the power of the read-out laser is varied, and the mechanical noise spectra are measured. We expect to observe a decrease of the noise floor and amplification of the mechanical motion by the read-out laser. However, an additional effect manifests itself.

5.1 Varying the probe laser power: optical absorption

After full characterization of the system at a cryostat temperature of 5.7K, the dilution refrigeration unit brings down the temperature even further, and we enter the sub-Kelvin regime. When the lowest possible stable temperature is reached, the system is ready for measurements. The final objective is: reaching a phonon occupation $\bar{n}$ or effective temperature T_{eff} as close to zero as possible, by optical cooling of the resonator, starting from a base temperature T_{mat} that is also as close to zero as possible. Since the optical cooling results from optical damping, or broadening, of the motion, one should be prepared to measure spectra that become progressively more difficult to distinguish from the noise background. The noise floor $\mathcal{N}_{\text{PDH}}$ is the accumulation of classical noise from various origins (technical noise, laser noise, intensity noise, and so on) [19, 44].

More movement, less noise

The signal to noise ratio depends on how much probe laser light is used: the

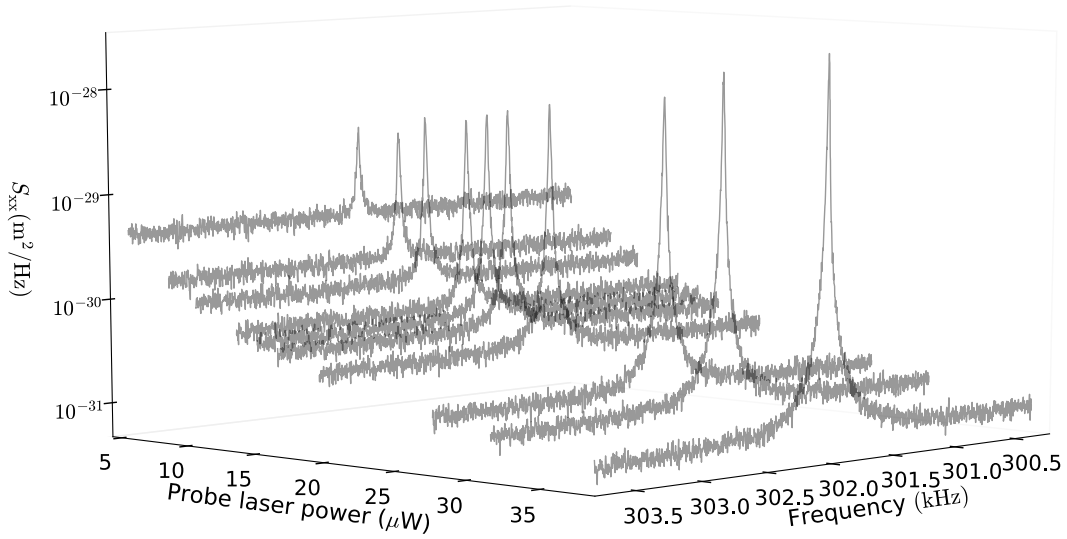

Figure 5.1: PSD's for a power sweep of the read-out laser. Measurement at $T_{\mathrm{cryo}} = 200\mathrm{mK}$.

higher P_{LI}, the lower $\mathcal{N}_{\mathrm{PDH}}$ [45]. In the previous section, we argued that deviations between experiment and theory in a pump laser detuning sweep can be explained as stemming from slight amplification of the motion by detuning of the probe laser. That means that if we increase the power of the read-out laser with all other parameters fixed, we expect to see three effects:

1. The noise floor decreases for increasing P_{LI}
2. The total damping and effective resonance frequency decrease, according to Eq. (4.5) and (4.6)
3. The effective temperature increases, according to (4.3) and (4.4) with $T_{\mathrm{mat}} = T_{\mathrm{cryo}} = 200\mathrm{mk}$

Fig. 5.1 shows the spectra measured via the PDH-read-out method while increasing the locking laser power. The noise background in Fig. 5.2 decreases according to

$$\mathcal{N}_{\mathrm{PDH}} \propto 1/P_{\mathrm{LI}}^2. \tag{5.1}$$

The left panel of Fig. 5.3 shows the measured linewidths Γ_{eff} and resonance frequencies Ω_{eff}, as well as the expected behavior given by Eq. (4.5), (4.6) with $\kappa/2\pi = 85\mathrm{kHz}$ and $C_{\mathrm{mm}} = 0.112$ (as obtained from the system characterization measurement in section 4.1), a probe laser detuning of 3kHz, and a continuous 26Hz damping of from the 5μW cooling laser. When the read-out laser power is increased, the damping decreases, or equivalently, the motion of the mirror is amplified. Theory and experiment agree; we can check the first two boxes.

The upper right panel of Fig. 5.3 shows the measured effective temperature from

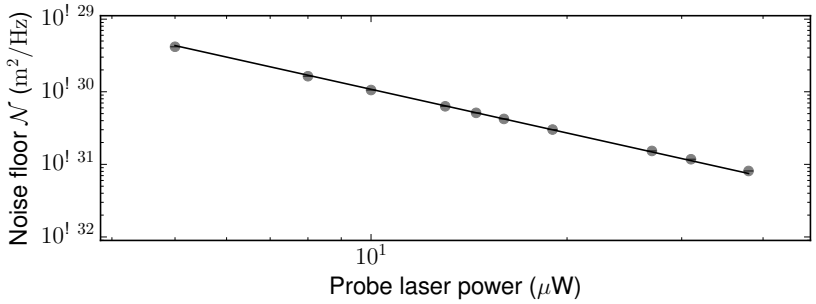

Figure 5.2: Measured noise floors for a power sweep of the read-out laser at $T_{\rm cryo} = 200$mK. Measured data and fit to $\mathcal{N}_{\rm PDH} \propto 1/P_{\rm Ll}^2$.

the rescaled area under the spectrum using Eq. (4.3) [blue points], the effective temperature as expected from the measured linewidths using Eq. (4.4) [yellow points], and the effective temperature that should result from the theory shown in the left panel [yellow line]. While the motion of the mirror is anti-damped according to theory, *the effective temperature* $T_{\rm eff}(P_{\rm Ll}) = \frac{m\Omega_m^2}{k_B}\mathcal{A}(P_{\rm Ll})$ *rises more than expected on the basis of probe laser induced antidamping* $\Gamma_{opt}^{Ll}(P_{Ll})$ *alone.* There is a discrepancy between Eq. (4.3) and (4.4):

$$\underbrace{T_{\rm eff} = \frac{m\Omega_m^2}{k_B}\mathcal{A}(P_{\rm Ll})}_{\text{[blue]}} \neq \underbrace{T_{\rm cryo}\frac{\Gamma_m}{\Gamma_{\rm eff}(P_{\rm Ll})}}_{\text{[yellow]}} \tag{5.2}$$

Optical absorption

The discrepancy is the result of optical absorption of the read-out laser light by the Ta_2O_5/SiO_2 mirror and subsequent heating of the material. Independent measurements by F.M. Buters in Ref. [35] show identical behavior, and are explained as resulting from poor heat conduction in the silicon nitrite arms that connect the resonator to the surroundings. A tiny fraction of the light leaking through the resonator is absorbed, and the heat cannot flow away: the mirror does not thermalize with the cryogenic environment ($T_{\rm mat} \neq T_{\rm cryo}$), and its temperature $T_{\rm mat}$ rises. With the physical temperature $T_{\rm mat}$, also the effective temperature of the motion $T_{\rm eff}$ increases.
The poor heat conductivity of the suspensions is characteristic for the ultra cold environment. Although the heat conductivity of Si_3N_4 is not precisely known, it is feasible that the conductivity strongly decreases with decreasing temperature in the sub-Kelvin regime. Optical cooling experiments at super-Kelvin base temperatures are therefore less prone to heating caused by optical absorption. It has been experimentally verified in Ref. [35] that for in-fiber locking laser powers up

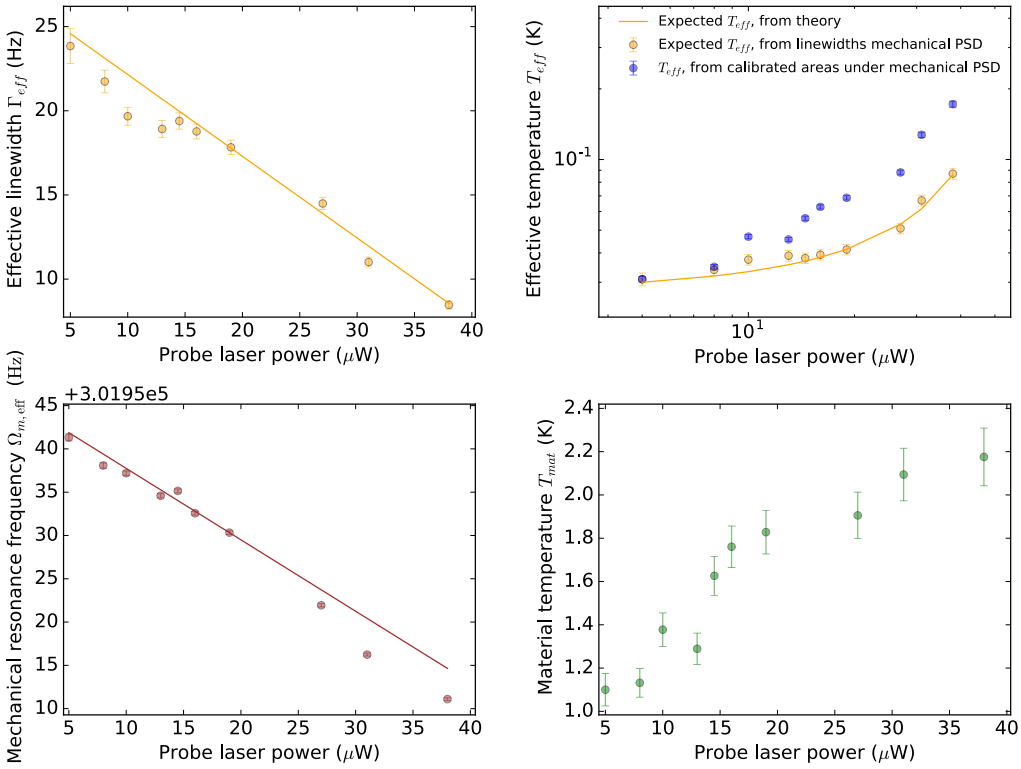

Figure 5.3: Power sweep of the read-out laser at $T_{\mathrm{cryo}} = 200\mathrm{mK}$.

to 15μW, the heating from optical absorption is negligible. The results presented in chapter 4 of this thesis were therefore unaffected.

A more elaborate description, as well as a toy model for the thermodynamics involved, can be found in Ref. [35]. So, as a result of the optical absorption, the effective temperature evolves according to:

$$T_{\mathrm{eff}} = \frac{m\Omega_m^2}{k_B}\mathcal{A}(P_{\mathrm{Ll}}) = T_{\mathrm{mat}}(P_{\mathrm{Ll}})\frac{\Gamma_m}{\Gamma_{\mathrm{eff}}(P_{\mathrm{Ll}})}. \tag{5.3}$$

The temperature of the mirror is then

$$T_{\mathrm{mat}}(P_{\mathrm{Ll}}) = \mathcal{A}(P_{\mathrm{Ll}})\Gamma_{\mathrm{eff}}(P_{\mathrm{Ll}})\frac{m\Omega_m^2}{k_B\Gamma_m}, \tag{5.4}$$

plotted in the lower right panel of Fig. 5.3. In the first measurement, when using an in-fiber probe laser power $P_{\mathrm{Ll}} = 5\mu$W, the material temperature has already increased from 0.2K to 1.1K. If the read-out laser power is further increased to 38μW, the material temperature increases to 2.2K.

5.2 What now?

The results indicate that increasing the power of the probe laser in order to suppress the noise floor of the spectrum obtained via PDH read-out of the motion is not desirable. The power absorbed should be minimized, and because the light is absorbed by the mirror itself, the transmitted power must be minimized. Ergo, *the amount of laser light circulating in the cavity must be minimized.* Retaining the PDH scheme only for the locking of the lasers to the cavity resonance and implementing an alternative read-out method, could provide a solution. We find out why, how, and what, in the next chapter.

Chapter 6

Sideband-thermometry of the mirror's motion

Two roads diverged in a yellow wood,
And sorry I could not travel both
And be one traveler, long I stood
And looked down one as far as I could.
– Robert Frost, *The Road Not Taken*

We want a noise floor as low as possible, but turning up the probe laser power comes at a price. In this section, we will demonstrate two alternatives for PDH read-out of the motion. First, we will enhance the signal from the probe laser with light that does not get absorbed by the moving mirror. Secondly, we will completely eliminate the probe laser from the read-out scheme and read out the motion with the cooling laser.

6.1 Locking laser sideband thermometry

In section 3.1.4, we described how light with frequency ω_l circulating in the cavity develops a red and blue sideband at respectively frequency $\omega_\mathrm{l} - \Omega_\mathrm{eff}$ and $\omega_\mathrm{l} + \Omega_\mathrm{eff}$. If the laser is red detuned, the blue sideband is closer to the cavity resonance than the red sideband, so the blue sideband is pumped. If the laser is blue detuned, the red sideband is closer to the cavity resonance, so the red sideband is pumped. In the first case, energy flows from the mechanical oscillator to the optical field, and vice versa for the second case. This is depicted in Fig. 3.12. If the frequency of the laser is equal to the cavity resonance frequency, the amplitude of the sidebands must be equal for $\bar{n} \gg 1$. In this section we will describe how the sidebands of the locking laser can be read out. Because the locking laser must be locked approximately to the cavity resonance, we expect the sidebands to be approximately equal.

6.1.1 Experimental implementation

In order to resolve the individual sidebands, a beating tone separated by ω_{LO} from the probe beam frequency ω_{l} must be combined with the tones reflected from the cavity. [44, 46] This was explained in section 3.1.4, and summarized in Fig. 3.8 and 3.9. In practice, part of the locking laser light is split off by a beam splitter, and shifted by an acousto-optic modulator (AOM). This is shown in Fig. 6.1. Light entering the AOM is diffracted by a sound wave generated in the crystal and frequency shifted. Depending on the angle a which the beam emerges, the frequency can be upshifted or downshifted. In our set-up, the AOM shifts the incoming laser light of frequency ω_{Ll} with $\omega_{\mathrm{LO}} = -2\pi \times 40\mathrm{MHz}$. Two beams emerge from the AOM, the original beam with frequency ω_{Ll}, and the deflected beam with frequency $\omega_{\mathrm{Ll}} - \omega_{\mathrm{LO}} = \omega_{\mathrm{Ll}} + 2\pi \times 40\mathrm{MHz}$. The original beam is blocked, and the diffracted light is coupled into a fiber. Finally, it is recombined with the rest of the probe beam, and sent to the cavity. The component at frequency $\omega_{\mathrm{Ll}} + 2\pi \times 40\mathrm{MHz}$ is promptly reflected from the cavity and does not enter it. All reflected light, containing components at $\omega_{\mathrm{Ll}}/2\pi + 40\mathrm{MHz}$ (the beating tone), ω_{Ll} (the carrier) and $\omega_{\mathrm{Ll}} \mp \Omega_{\mathrm{eff}}$ (the sidebands) are finally separated from the reflected pump laser light by a polarizing beamsplitter and detected by photodetector $\mathrm{PD}^{\mathrm{L}}_{\mathrm{refl}}$. The resulting beating signal comprises two Lorentzian features: the blue sideband at $40\mathrm{MHz} - \Omega_{\mathrm{eff}}/2\pi$, and the red sideband at $40\mathrm{MHz} + \Omega_{\mathrm{eff}}/2\pi$. Note that the profile at $40\mathrm{MHz} - \Omega_{\mathrm{eff}}/2\pi$ is an image of the $\omega_{\mathrm{Ll}} + \Omega_{\mathrm{eff}}$ sideband, and the profile at $40\mathrm{MHz} + \Omega_{\mathrm{eff}}/2\pi$ an image of the $\omega_{\mathrm{Ll}} - \Omega_{\mathrm{eff}}$ sideband, because the frequency is upshifted rather than downshifted.[1] The sidebands are displayed in Fig. 3.8 and 3.9, and the final recorded spectrum in Fig. 3.10, with $\omega_{\mathrm{l}} = \omega_{\mathrm{Ll}}$ and $\omega_{\mathrm{LO}} = -2\pi \times 40\mathrm{MHz}$.

While the sideband spectra are read out and analyzed for thermometry, the PDH lock of the probe laser to the cavity remains intact, to ensure the probe laser (carrier of the sidebands) and pump laser follow the noisy low-frequency changes in the cavity resonance. Therefore, it is still possible to read out the PDH spectrum at Ω_{eff}, simultaneous with the individual sidebands at $40\mathrm{MHz} \mp \Omega_{\mathrm{eff}}/2\pi$.

6.1.2 Does it work?

We demonstrate locking laser sideband thermometry by performing a detuning sweep of the pump laser. We recorded both sidebands, as well as the PDH spectrum for verification. In principle, measuring one sideband is enough to carry out thermometry. Because the power and detuning of the locking laser remain constant during this measurement, data analysis for the sidebands proceeds no

[1] In Fig. 3.8 and 3.9 in the theory section, we assumed the frequency of the laser light was downshifted for didactic purposes. In that case, the displayed spectra inherit the same order in frequency space as the sidebands: the red sidebands resides at the lower frequency $\omega_{\mathrm{LO}} - \Omega_{\mathrm{eff}}$, and the blue sideband at the higher frequency $\omega_{\mathrm{LO}} + \Omega_{\mathrm{eff}}$.

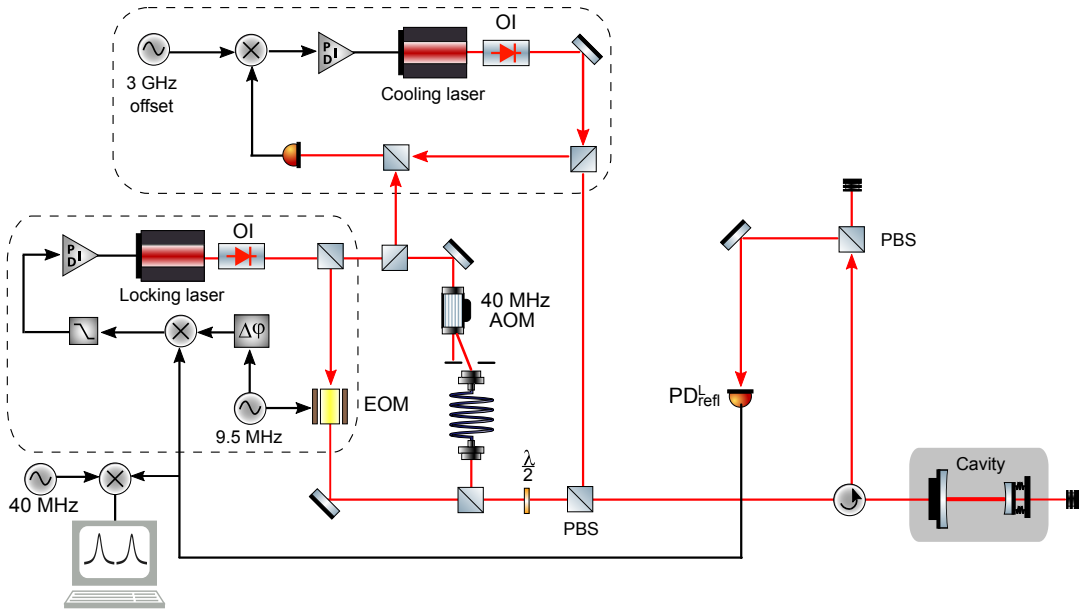

Figure 6.1: Optical set-up for locking laser sideband-thermometry. The components displayed are: $\lambda/2$: waveguide, BS: beam splitter, PBS: polarizing beam splitter, EOM: electro-optical modulator, OI: optical isolator and PI: proportional-integral feedback controller.

different than for the PDH spectrum. As seen from Eq. (3.30), the linewidths of both sidebands must be equal to that of the PDH spectrum, and therefore to the mechanical noise spectrum. The calibrated area under each spectrum $\mathcal{A}_{r,b}$ is proportional to the effective temperature $T_{\rm eff}$ of the mirror, as described in section 3.1.4 by Eq. (3.30).

Fig. 6.2 shows the data and the fit to theory of the blue sideband recorded at $40\text{MHz} - \Omega_{\rm eff}/2\pi$. The fit is strongly constrained by using the system parameters $\kappa/2\pi = 85.4 \pm 0.5\text{kHz}$ and $C_{\rm mm} = 0.12$, determined at 5.7K in section 4.2. The only free parameters are the offset for the detuning, and the optical (anti) damping and resonance shift caused by the probe laser. The measurement was performed using 27μW LO power, 11μW in-fiber cooling laser power and 10μW probe laser power. We need to take into account that a fraction of the circulating probe laser light is optically absorbed, and from the lower right panel of Fig. 5.3, we infer that the physical temperature of the mirror in the 200mK cryostat, subject to 10μW in-fiber locking laser light, is 1.38 ± 0.08K.

The fit returns values $\Gamma_{opt}^{\rm LI}/2\pi = -5.5 \pm 0.3\text{Hz}$ and $\delta\Omega_m^{\rm LI}/2\pi = -6 \pm 0.1\text{Hz}$. Data from the red sideband returns identical values: $\Gamma_{opt}^{\rm LI}/2\pi = -5.5 \pm 0.5\text{Hz}$ and $\delta\Omega_m^{\rm LI}/2\pi = -6 \pm 0.1\text{Hz}$. Excellent agreement is therefore observed between theory and experiment, and between analysis of the blue and red sideband. The insets in Fig. 6.2 show the strong damping and cooling of the mirror, by broadening

and shrinking of the sideband spectra as the detuning approaches $\Delta_{\mathrm{Cl}} = -\Omega_m$. At the point of maximal damping, the effective temperature of the mirror was $T_{\mathrm{eff}} = 10 \pm 0.7\mathrm{mK}$, corresponding to 687 ± 50 phonons.

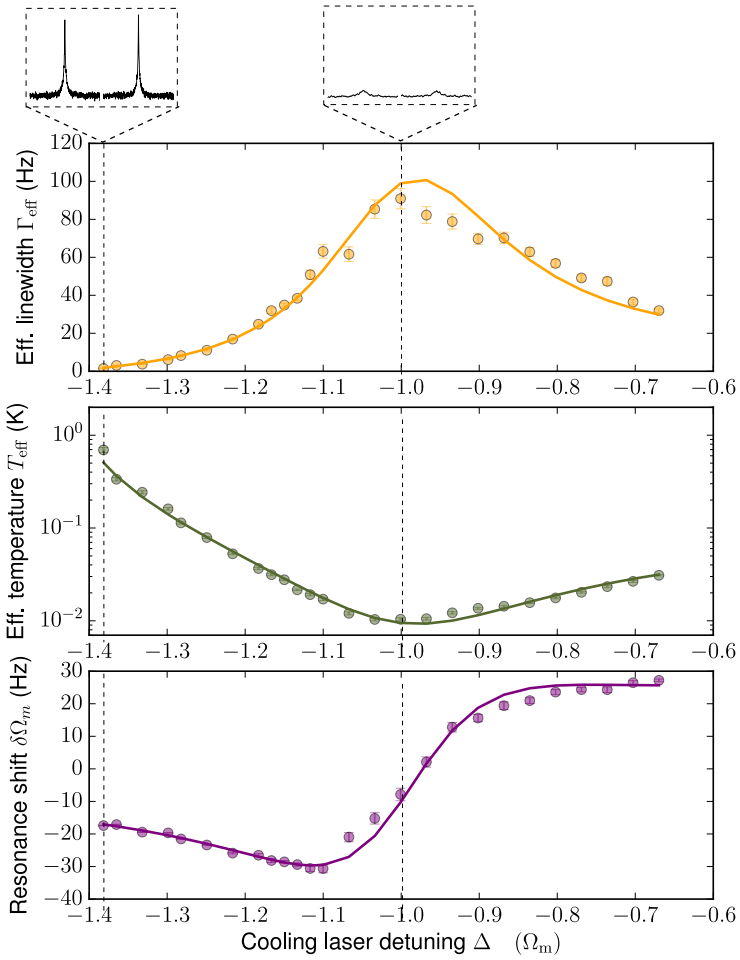

Figure 6.2: Locking laser sideband-thermometry. Measured parameters for the blue sideband, and comparison to optomechanical theory. Measured PSD show the blue sideband PSD recorded at $40\mathrm{MHz} - \omega_{\mathrm{Ll}}/2\pi$ and the red sideband PSD at $40\mathrm{MHz} + \omega_{\mathrm{Ll}}/2\pi$ for two different cooling laser frequencies.

6.1.3 Sideband asymmetry

The inset in Fig. 6.2 shows that the sidebands are almost equal, the amplitude of the red sideband recorded at $\omega_{\mathrm{LO}} + \Omega_{\mathrm{eff}}$ being slightly larger than that of the blue sideband recorded at $\omega_{\mathrm{LO}} - \Omega_{\mathrm{eff}}$. From Eq. (3.38) and (3.39) with $\Delta = \Delta_{\mathrm{Ll}}$,

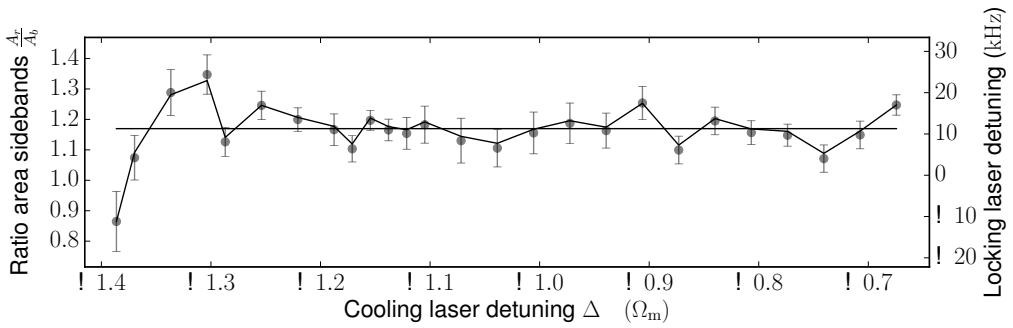

Figure 6.3: Measured asymmetry of the locking laser sidebands [datapoints] during a detuning sweep of the pump laser, and corresponding estimation of the locking laser detuning [solid]. The horizontal line gives the average asymmetry $\mathcal{A}_r/\mathcal{A}_b = 1.16$, corresponding to $\Delta_{\mathrm{Ll}}/2\pi = 12\mathrm{kHz}$.

we expect the asymmetry $\mathcal{A}_r/\mathcal{A}_b$ to be fully attributable to the detuning of the locking laser, because even at $\Delta_{\mathrm{Cl}} = -\Omega_m$ we have $\bar{n} \approx 700 \gg 1$, and thus the asymmetry from $\bar{n}/\bar{n}+1$ is negligible. If $\bar{n}$ were close to one, that is, if we were close to the ground state, we would expect a strong dependence of the asymmetry on the pump laser detuning. Thus, because Δ_{Ll} stays constant during the measurement, the asymmetry is expected to stay constant. The measured asymmetry is shown in Fig. 6.3. The sideband asymmetry fluctuates around $\mathcal{A}_r/\mathcal{A}_b = 1.16$. Appreciable deviations are observed in regions of weak damping, attributable to departure of the resonator from thermal equilibrium as mentioned in section 4.2. At high damping (around $\Delta_{\mathrm{Cl}} = -\Omega_m$), the measured asymmetry is stable, with fluctuations barely exceeding the statistical error margins. One can estimate the detuning of the probe laser by inserting the measured asymmetry in Eq. (3.38). An asymmetry $\mathcal{A}_r/\mathcal{A}_b = 1.16$ then indicates $\Delta_{\mathrm{Ll}}/2\pi = 12\mathrm{kHz}$, which is reasonable considering we estimated a detuning of approximately 10kHz in section 4.2.

6.1.4 (How) does it bring us closer to the ground state?

We have seen that in the PDH read-out method, the bath temperature of the mirror increases if the power from the locking laser is increased. Decreasing the probe laser power reduces optical absorption, but the reverse of the medal is a rise of the background noise.

Reducing the probe power: less heat, a bit more noise

In the PDH read-out, the noise floor increases with decreasing locking laser power ($\mathcal{N}_{\mathrm{PDH}} \propto 1/P_{\mathrm{Ll}}^2$). It is evident that using the sideband read-out, similar behavior must be observed, because the locking laser beam is the carrier for the

sidebands. However, the increase in background noise is much less for the sidebands than for the PDH signal. In fact, for each sideband the noise increases only with the inverse of the probe laser power:

$$\mathcal{N}_b \approx \mathcal{N}_r := \mathcal{N}_{SB} \propto 1/P_{\mathrm{Ll}} \tag{6.1}$$

This makes sense because, as we argued in section 3.1.4, the PDH signal incorporates both sidebands, folded on top of each other. The effect is shown in Fig. 6.4, where we have reduced the probe laser power from 38 to 5 μW.[2] Because less power is optically absorbed, the temperature of the mirror drops from 2.2K to 1.1K. The noise floor of the PDH signal rises with a factor 50, while the noise floor of the sideband signals only rises with a factor 7. The measurement was conducted with $P_{\mathrm{LO}} = 34\mu$W. Using this amount of local oscillator power, the signals for the sidebands and that for the PDH signal are approximately equal for 5μW of locking laser power. The question is then: "Can we re-improve the signal to noise ratio *without* adding heat?"

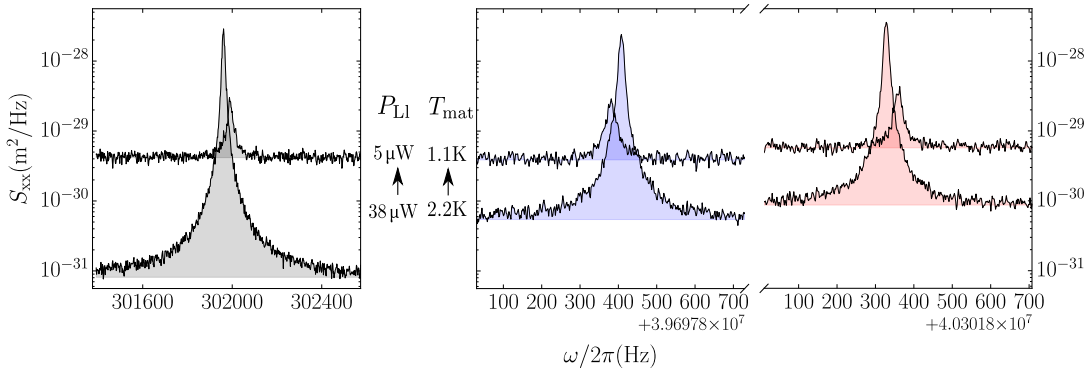

Figure 6.4: Comparison of read-out methods for decreasing locking laser power. PDH-spectrum and sideband spectra measured with 5μW of in-fiber cooling laser power at $\Delta_{\mathrm{Cl}} = -1.1\Omega_m$ and $P_{\mathrm{LO}} = 34\mu$W. If P_{Ll} is decreased from 38μW to 5μW, reduced optical absorption allows the material temperature to drop from 2.2K to 1.1K. The noise floor increases for the PDH-spectrum and the sidebands respectively with a factor 50, and 8. Reduced anti-damping by the probe laser manifests itself as a resonance frequency shift towards the intrinsic resonance $\Omega_m/2\pi = 302$kHz, and decrease of the amplitude and area of the Lorentzian profile.

Increasing the LO power: less noise, not more heat

Keeping the probe laser power at 5μW, we increased the power in the local

[2]This is the reverse of the process displayed in Fig. 5.1 and Fig. 5.3.

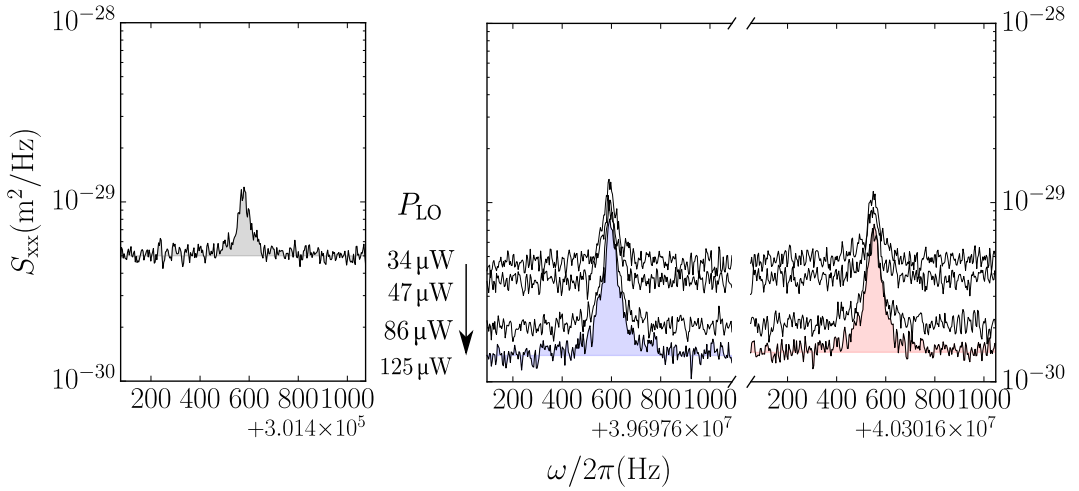

Figure 6.5: PDH-spectrum and sideband spectra for $P_{\mathrm{Ll}} = 5\mu$W, when increasing the power in the local oscillator from 34 to 125μW. A much better signal-to-noise ratio is obtained for the sideband spectra. Measured at $T_{\mathrm{cryo}} = 0.2$K, with $P_{\mathrm{Cl}} = 10\mu$W and $\Delta_{\mathrm{Cl}} = -1.1\Omega_m$. T_{mat} remains 1.1K during the measurement.

oscillator beam from 34μW to 125μW. The spectra of the PDH signal and the sidebands are depicted in Fig. 6.5. The fixed cooling laser power was 10μW, i.e. the double of that used in the spectra depicted in Fig. 6.4, hence the lower amplitude. The noise background for the PDH signal remains at 5×10^{-30}m, while the noise floor for the sideband spectra are lowered to 1×10^{-30}m for 125μW of LO power. It is immediately clear that the signal to noise ratio has improved significantly. In Fig. 6.6, the noise floors are plotted for a series of measure-

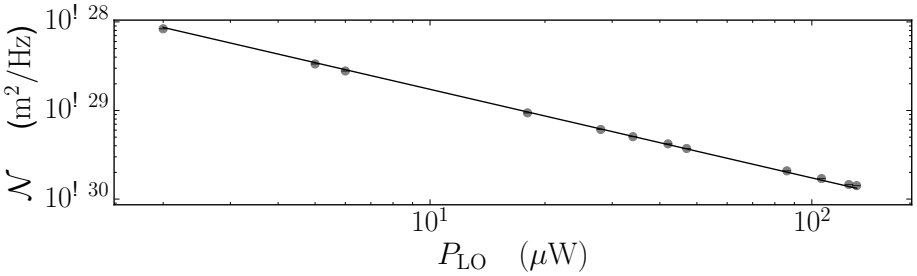

Figure 6.6: Decrease of the red sideband noise floor with increasing local oscillator power. The noise floor is drastically reduced while varying P_{LO} from 2 to 130 μW. Measurement at $T_{\mathrm{cryo}} = 200$mK, with $P_{\mathrm{Ll}} = 5\mu$W and $P_{\mathrm{Cl}} = 10\mu$W. We show measured datapoints and fit to $\mathcal{N}_r \propto 1/P_{\mathrm{LO}}$.

ments over a broader range of LO powers from 2μW to 130μW. The noise floor is observed to decrease with the inverse LO power:

$$\mathcal{N}_{SB} \propto 1/P_{\mathrm{LO}} \tag{6.2}$$

Combining this with Eq. (5.1) and Eq. (6.1), we conclude:

$$\mathcal{N}_{\mathrm{PDH}} \propto \frac{1}{P_{\mathrm{Ll}}^2} \text{ and } \mathcal{N}_{\mathrm{SB}} \propto \frac{1}{P_{\mathrm{Ll}} P_{\mathrm{LO}}}.$$

Because the power of the probe laser remained constant, and the local oscillator beam does not enter the cavity, the physical temperature of the mirror remains 1.1K. This can be seen in Fig. 6.7: all parameters that characterize the motion of the mirror merely fluctuate around constant values.[3] There are no optomechanical, nor thermodynamical changes during the measurement. As the power in the

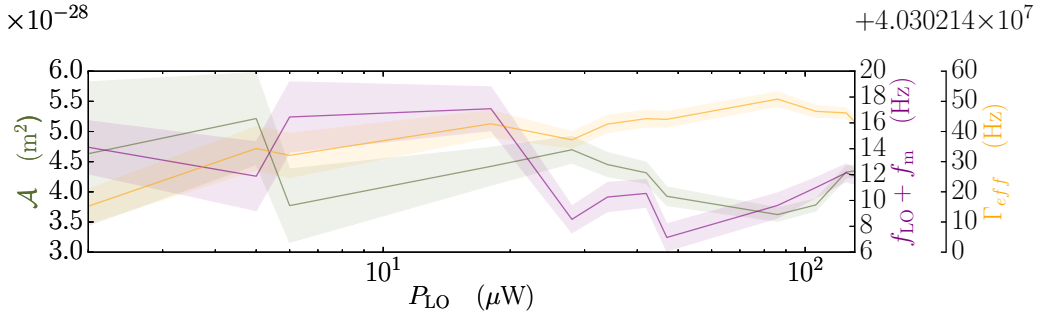

Figure 6.7: Measured parameters of the Lorentzian profile of the red sideband while varying P_{LO} from 2 to 130 μW at $T_{\mathrm{cryo}} = 200$mK, with $P_{\mathrm{Ll}} = 5\mu$W and $P_{\mathrm{Cl}} = 10\mu$W.

LO beam is turned up, the only aspect that changes is the precision: the signal to noise ratio drastically improves - well over that achieved using the PDH method - and the error margins on the spectral parameters converge. Therefore, *probe laser sideband-thermometry can be performed reliably even for strongly damped (large Γ_{eff}, low $\bar{n}$) spectra, by reducing the noise floor with increased LO power.* When the motion of the mirror is cooled so severely that the motional spectrum cannot be separated from the PDH noise floor anymore, it can still be read-out from the sidebands: we can't increase the probe laser power, but we *can* increase the LO power.

6.1.5 Sideband thermometry in the ground-state regime

In section 3.1.5, we introduced the possibility of inferring the phonon occupancy of a resonator close to the ground state from the sideband asymmetry of a zero detuned laser [44, 46]. In that case, $\mathcal{A}_r/\mathcal{A}_b = \bar{n} + 1/\bar{n}$. We reported that fixing the probe laser at exactly $\Delta_{\mathrm{Ll}} = 0$ is difficult due to instabilities, but this is not

[3] Another interesting aspect of Fig. 6.7 is that the statistical error margins apparently underestimate the true errors on the measured values. Identical measurements for the PDH signal show the same effect.

a problem if we incorporate our findings from chapter 4. At non-zero detuning, Eq. (3.38) applies:

$$\frac{\mathcal{A}_b}{\mathcal{A}_r} = \frac{\bar{n}}{\bar{n}+1}\frac{(\frac{\kappa}{2})^2 + (\Delta_{\mathrm{Ll}} - \Omega_m)^2}{(\frac{\kappa}{2})^2 + (\Delta_{\mathrm{Ll}} + \Omega_m)^2}$$

In chapter 4, we optimized the precision with which the cavity linewidth κ can be determined, and simultaneously we found a way to determine the detuning of the probe laser Δ_{Ll}. Hence, all parameters in Eq. (3.38) are known and the phonon occupation can be readily extracted, provided the areas under the sidebands can be measured reliably as well. In Fig. 6.3 we had seen that for strongly damped, low T_{eff} signals, the measured asymmetry is consistent. This is of course the region in which one would use low-occupancy-sideband-asymmetry-thermometry. From Fig. 6.7, it is clear that the precision of the measured area, and therefore the precision of the measured asymmetry, appreciably increases with increasing P_{LO} (and decreasing noise background).
In conclusion, the probe laser sideband read-out scheme is successfully implemented and demonstrated in a millikelvin environment, and in its current form it is ready to carry out sideband asymmetry thermometry in the countable phonon regime.

6.2 Cooling laser sideband thermometry

In the previous section, we explained how the amount of probe laser light necessary for thermometry of strongly damped spectra can be reduced by reading out (one of) the sidebands of the probe laser light rather than the PDH spectrum. However, a minimum of probe laser power is still necessary to generate these sidebands in the first place. Can't we completely eliminate the probe laser from the thermometry scheme? It turns out we can, and this section explains how.

6.2.1 Experimental implementation

In an optical cooling measurement, the frequency of the R&S signal generator will be set such that the cooling laser detuning is approximately $-\Omega_m$, the detuning at which maximal optical damping occurs. In that case, two important effects occur:

1. Only a tiny fraction of the pump laser light circulates in the cavity, because our system is sideband resolved ($\Omega_m \gg \kappa/2$).
2. The light that circulates, develops sidebands at frequencies $\omega_{\mathrm{cav}} - \Omega_m + \Omega_m = \omega_{\mathrm{cav}}$ and $\omega_{\mathrm{cav}} - \Omega_m - \Omega_m = \omega_{\mathrm{cav}} - 2\Omega_m$. Hence, the blue sideband at zero detuning is strongly pumped, and the red sideband at $-2\Omega_m$ from the cavity resonance is very small.

The sidebands of the pump laser can be displayed and used for thermometry if we detect the reflected pump laser light and add a beating tone to it, analogous

to the visualization of the probe laser sidebands. An extensive theoretical review of the concept can be found in Ref. [44]. Again, Fig. 3.8 and 3.9 show the necessary tones, now with $\omega_{\mathrm{l}} = \omega_{\mathrm{Cl}}$. Fig. 6.8 shows the modifications to the optical set-up. An AOM shifts part of the pump laser light, instead of the probe laser light, by a frequency $\omega_{\mathrm{LO}} = -2\pi \times 40\mathrm{MHz}$. Thus the tones incident on the cavity for the purpose of cooling and thermometry are ω_{Cl} and $\omega_{\mathrm{Cl}} + 2\pi \times 40\mathrm{MHz}$. The tones at ω_{Ll}, $\omega_{\mathrm{Ll}} - 2\pi \times 9.5\mathrm{MHz}$ and $\omega_{\mathrm{Ll}} + 2\pi \times 9.5\mathrm{MHz}$ that are part of the PDH locking scheme also remain incident on the cavity. As mentioned in section 3.2.3, they can be treated completely independent from the tones necessary for cooling and thermometry, because they are separated by a 3GHz free spectral range. The reflected components of the PDH scheme are detected by $\mathrm{PD}^{\mathrm{L}}_{\mathrm{refl}}$ and the signal is forwarded to the PID, as usual. The reflected cooling laser light, consisting of components at $\omega_{\mathrm{Cl}} + 2\pi \times 40\mathrm{MHz}$ (the beating tone), ω_{Cl} (the carrier) and $\omega_{\mathrm{Cl}} \mp \Omega_{\mathrm{eff}}$ (the sidebands) are finally separated from the reflected locking laser light by the polarizing beamsplitter and detected by photodetector $\mathrm{PD}^{\mathrm{C}}_{\mathrm{refl}}$. The resulting beating signal comprises profiles at $40\mathrm{MHz} - \Omega_{\mathrm{eff}}/2\pi$ and $40\mathrm{MHz} + \Omega_{\mathrm{eff}}/2\pi$, the first being an image of the blue sideband at $\omega_{\mathrm{Cl}} + \Omega_m$, and the latter of the red $\omega_{\mathrm{Cl}} - \Omega_m$ sideband.

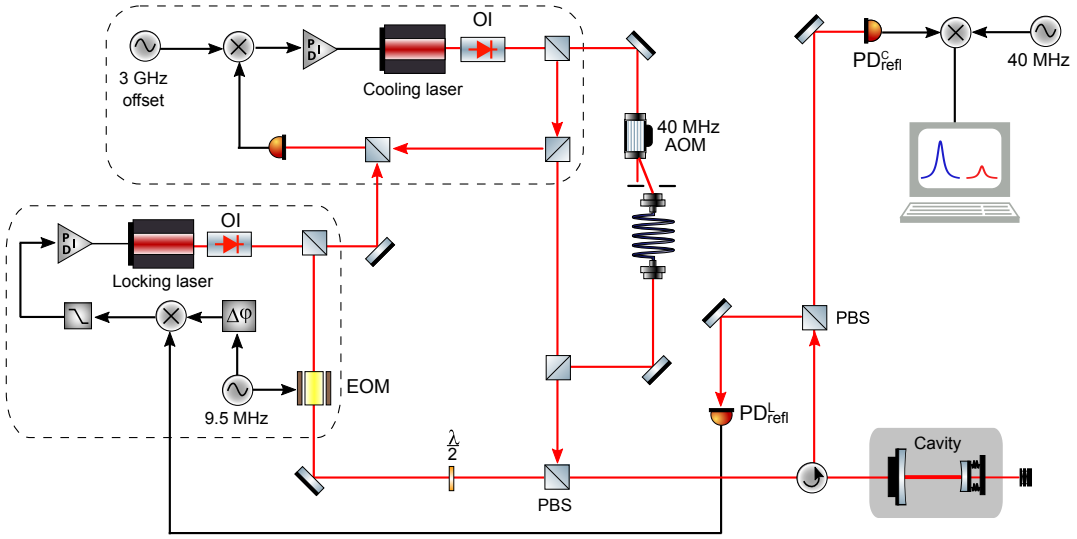

Figure 6.8: Optical set-up for cooling laser sideband-thermometry. The components displayed are: $\lambda/2$: waveguide, BS: beam splitter, PBS: polarizing beam splitter, EOM: electro-optical modulator, OI: optical isolator and PI: proportional-integral feedback controller.

6.2.2 Does it work?

We demonstrate pump laser sideband thermometry by performing a detuning sweep of the pump laser with 40μW in-fiber cooling power, 88μW in the LO

beam, and 10μW locking laser power. The results are shown in Fig. 6.9. As expected, extreme asymmetry is observed. Around $\Delta_{\rm Cl} = -\Omega_m$, the rate of anti-stokes scattering (cooling) is so high, that the red sideband is invisible. As we move towards the cavity resonance, reducing the damping and cooling, the red sideband grows and appears. This is shown in the inset of Fig. 6.9.
Thermometry of the cooling laser sidebands is slightly less straightforward than for the PDH signal or the probe laser sidebands. While the linewidths of the blue and red sideband are equal to each other and to that of the mechanical noise spectrum, the areas of the sidebands do not scale with the phonon occupancy or effective temperature of the mirror. This can be seen from Eq. (3.36) and (3.37): the sideband amplitudes depend on the detuning of the pump laser. The prefactor of the Lorentzian profile in Eq. (3.36), i.e. the amplitude or area under the spectrum, consists of three factors. The first is the effective temperature or phonon occupancy $\bar{n} + \delta_r^{r,b}$. As the frequency of the pump laser moves towards the cavity resonance in Fig. 6.9, the $T_{\rm eff}$ and $\bar{n}$ increase, so the amplitude of the mechanical noise spectrum increases, which makes the sidebands increase. The second factor is $\left[(\Delta_{\rm Cl} - \Omega_m) + (\frac{\kappa}{2})^2\right]^{-1}$ for the red, or $\left[(\Delta_{\rm Cl} + \Omega_m) + (\frac{\kappa}{2})^2\right]^{-1}$ for the blue sideband, representing respectively the Stokes and anti-stokes scattering rate proportional to $\bar{n}_{\rm cav}(\Delta_r)$ and $\bar{n}_{\rm cav}(\Delta_b)$. As the frequency of the pump laser ($\Delta_{\rm Cl} < -\Omega_m$) moves towards the cavity resonance, $\Delta_{\rm Cl}$ decreases, the rate of stoke scattering increases, and the rate of anti-stokes scattering decreases. This makes the red sideband grow and the blue sideband shrink. The third factor is $\bar{n}_{\rm cav}(\Delta_{\rm Cl})$, given by Eq. (3.4). As the pump laser frequency moves towards the cavity resonance, more light of the carrier builds up in the cavity, and therefore also more light in the sidebands circulates in the cavity. Therefore, the amplitudes of the red and blue sideband signal are enhanced.

The cumulative effect of these three aspects can be seen in the insets in Fig. 6.9. The measured linewidths and resonance frequencies are displayed, as well as the effective temperatures calculated from Eq. (3.33), with $\kappa/2\pi = 85$kHz and $P_{\rm in} = C_{\rm mm} P_{\rm Cl} = 0.12 \times 4\mu$W. The solid curves show the expectation according to optomechanical theory, using the parameters determined in the analysis of the detuning sweep using the *probe laser sideband*-thermometry depicted in Fig. 6.2. Overall, the agreement between the results from these vastly different read-out methods is satisfying. The parameters from the red sideband are displayed solely for illustrative purposes.[4] Although they cannot be used for analysis, their agreement with the values found from the blue sideband is encouraging, especially for the effective temperatures which depend on three variables now ($\mathcal{A}_{r,b}$, $\Delta_{\rm Cl}$ and $\Delta_{r,b}$), rather than one ($\mathcal{A}_{r,b}$).

[4]The data from the red sideband furthermore confirm the observation in Fig. 6.7 that for very noisy signals, the error margins underestimate the true error on the Lorentzian parameters.

6.2.3 (How) does it bring us closer to the ground state?

We have demonstrated that it is possible to perform thermometry of the resonator by reading out the strongly pumped blue sideband of the cooling laser beam. The probe laser is completely eliminated from the read-out protocol and is necessary only to keep the cooling laser locked to the desired frequency (which is, during a cooling experiment, $\Delta_{\mathrm{Cl}} = -\Omega_m$). It is feasible that the amount of probe laser power, and hence the physical temperature of the mirror T_{mat}, can be drastically reduced in this way. The drawback of this read-out scheme is that it waives the prospect of using sideband asymmetry to infer the phonon occupation close to the ground state, because the red sideband cannot be read out. Thus, *the critical factor that determines whether read-out of the probe laser or the cooling laser sidebands is most beneficial, is the amount of probe power that is necessary to generate detectable probe laser sidebands, in proportion to the probe power necessary to keep the lasers locked.* In favor of pump laser sideband-thermometry, one can point out that the cavity resonance fluctuations caused by the thermal motion of the mirror are detected and damped, while the fluctuations caused by environmental noise are detected and compensated for. Because the noisy oscillations are undamped, very little power might suffice to extract the spectral information for the PID to keep the lasers locked. However, there is only one way to conclusively find it out: that is to try it out. Therefore, we propose a follow-up experiment: "Set up the *pump laser sideband thermometry* scheme described in this section, gradually reduce the probe laser power and read out the blue pump laser sideband." Two effects are foreseen:

- First, a decrease of $\mathcal{A}_b$ is expected, attributable to a decreasing phonon occupancy, following the relations $T_{\mathrm{mat}}(P_{\mathrm{Ll}})$ and $\Gamma_{opt}^{\mathrm{Ll}}(P_{\mathrm{Ll}})$ expressed in Eq. (4.4) and (4.6), and displayed in Fig. 5.3.
- Secondly, as lower and lower P_{Ll} is used, eventually the lock will be lost. It is possible that already before that point, the cooling efficiency is gradually undermined because of deterioration of the lock. The probe power might suffice to read out the strongest noise fluctuations, but weaker signals can be lost and therefore remain uncompensated for. This might manifest itself as a decrease of Γ_{eff} and a saturation or increase of T_{eff}.

This way, one can infer the lowest required locking laser power, and by comparison to Fig. 5.1, to what bath temperature T_{mat} that corresponds.
The next step would be to use this exact amount of probe laser power for *locking laser sideband thermometry*, and directly compare the signals obtained via the two methods to infer which has the best signal-to-noise ratio. This finding would truly close this chapter, and open the door to thermometry in the ground state regime.

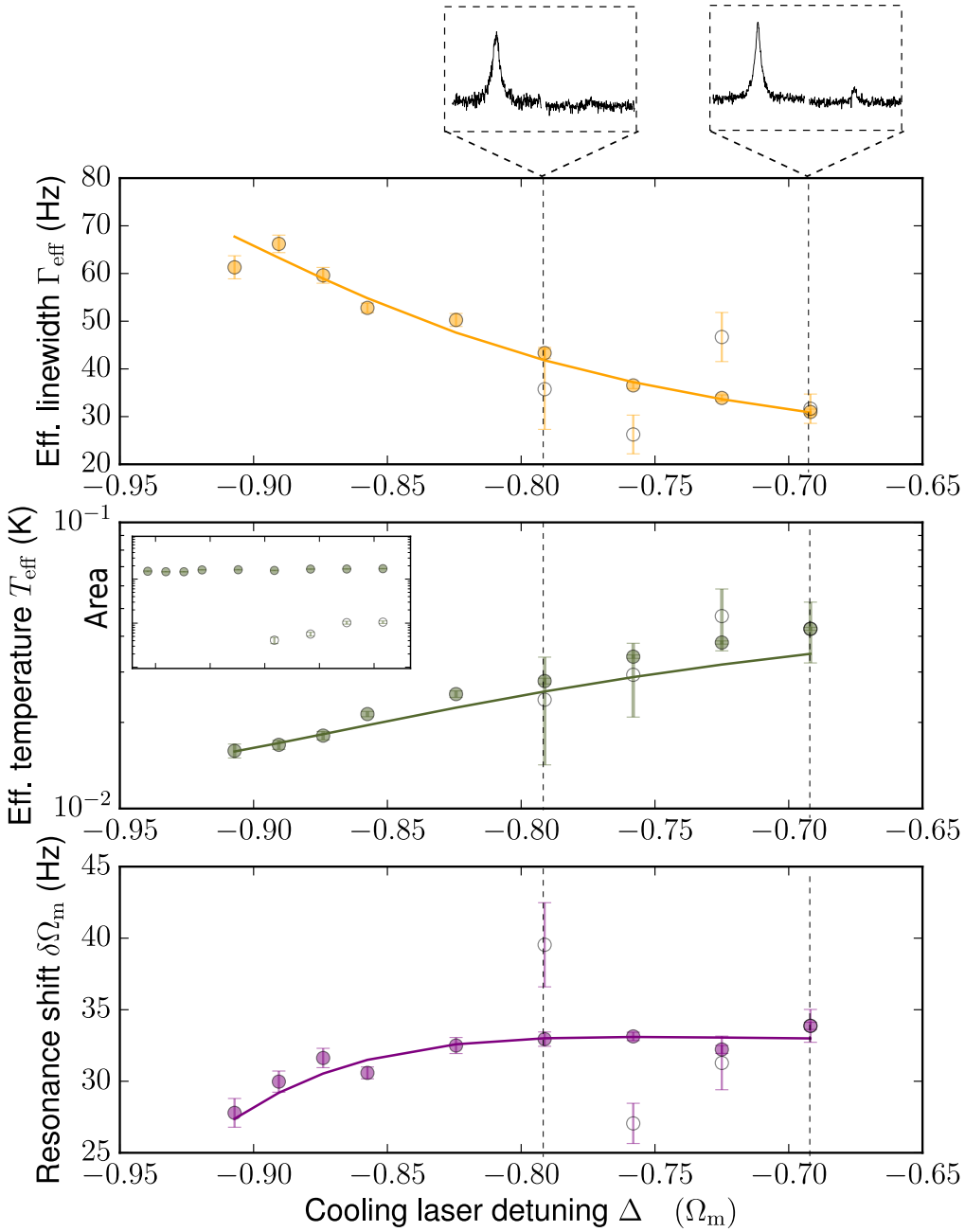

Figure 6.9: Cooling laser sideband-thermometry. Measured parameters for the blue sideband [filled] and red sideband [empty], and comparison to optomechanical theory. Measured PSD show the blue sideband PSD recorded at $40\text{MHz} - \omega_{\rm Cl}/2\pi$ and the red sideband PSD at $40\text{MHz} + \omega_{\rm Cl}/2\pi$ for two different cooling laser frequencies.

Chapter 7

Cold, colder, coldest

> *What we essentially want is to draw something unknown to us in all its shadowiness, not something we know in all its illumination.*
> – Orhan Pamuk, *My Name is Red*

Having laid out all pieces of the puzzle, we get down to the core business of cryogenic cavity-optomechanics: optical cooling of a resonator, as close to the absolute zero as possible. After presenting and analyzing the results of optical cooling in a 5.7K environment in the first part of this chapter, we will turn to the fundamental question that this thesis aims to answer: "With the accumulated knowledge, instruments, and methods, how near the ground state are we?"

7.1 Optical cooling in a cryogenic environment

In an optical cooling run, the pump laser is set at $\Delta_{\mathrm{Cl}} = -\Omega_m$ and the power of the cooling laser is increased. The measured noise spectrum is expected to steadily broaden while the effective temperature T_{eff} or $\bar{n}$ decreases, until the signal is swallowed by the noise background and thermometry becomes impossible.

7.1.1 Varying the pump laser power

Fig. 7.1 shows the data collected in an optical cooling measurement at $T_{\mathrm{cryo}} =$ 5.7K, with PDH thermometry of the mechanical motion. Anticipating the weakness of the signal at strong damping, 47μW of in-fiber locking laser power was used for the read-out while increasing the cooling laser power from 4.6μW to 364μW. As mentioned in chapter 5, the heating of the mirror due to optical absorption of probe laser light in a 5.7K environment is marginal. For 47μW of in-fiber probe laser power, $T_{\mathrm{mat}} = 6.9$K. [35]

A minimal effective temperature of 7.9$\pm$0.5mK or 545$\pm$31 phonons was reached,

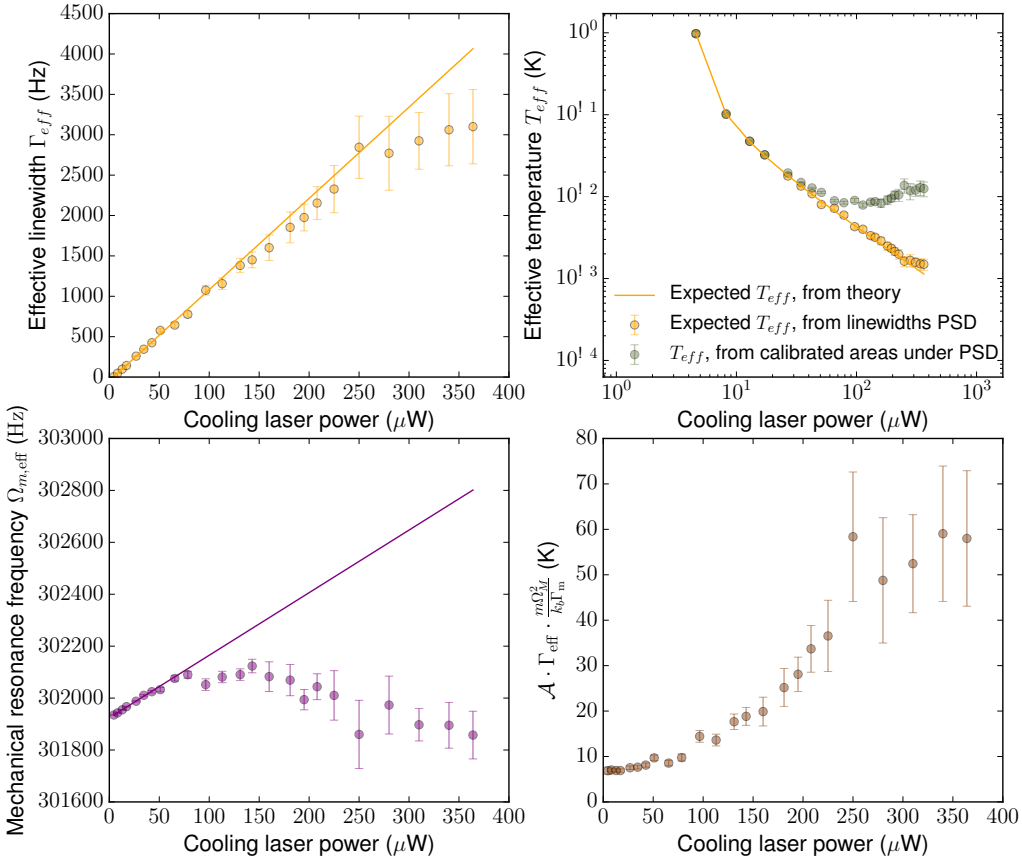

Figure 7.1: Optical cooling run at $T_{\mathrm{cryo}} = 5.7\mathrm{K}$. The power of the cooling laser is driven up, and the motion of the mirror is read out from the PDH signal, using $47\mu\mathrm{W}$ of in-fiber probe laser power. The starting temperature of the mirror was $T_{\mathrm{mat}} = 6.9\mathrm{K}$.

but this did not occur at the highest cooling laser power. As can be seen in the upper right panel in Fig. 7.1, the minimal phonon occupancy is reached at $P_{\mathrm{Cl}} = 113\mu\mathrm{W}$, after which the effective temperature starts to increase again. At first sight, this might seem another imprint of heating by optical absorption. Therefore, we use the theory applied in chapter 5. In Fig. 5.1, the material temperature was calculated as follows:

$$T_{\mathrm{mat}} = \mathcal{A}\Gamma_{\mathrm{eff}}\frac{m\Omega_m^2}{k_B\Gamma_m}$$

Using the same expression for the current measurement, one obtains the result depicted in the lower right panel of Fig. 7.1. In the cryogenic environment, the physical temperature of the mirror allegedly increases by an order of magnitude, from approximately 5.7 to 57K.
Furthermore, the effective linewidth shows deviations from theory for high cool-

ing laser power, as depicted on the upper left panel in Fig. 7.1. While these could be ascribed to the low signal to noise ratio in this region, and to the underestimation of the statistical error margins reported in sections 6.1.4 and 6.2.2, the same cannot be said about the deviations observed for the effective mechanical resonance frequencies. The lower left panel of Fig. 7.1 shows grave departure from the expected optical spring effect.

7.1.2 The intrinsic mechanical resonance

When comparing Fig. 7.1 to Fig. 5.1 showing the effects of heating caused by optical absorption of locking laser light, we spot two differences. The first is the functional form of the relationship between the material temperature and the laser power. The second is the deviation of the mechanical resonance frequency, which is only present in Fig. 7.1.

In section 3.2.4, we mentioned that the mechanical resonance frequency of the cavity strongly depends on the temperature of the environment T_{cryo} and the material T_{mat} (which are equal in thermal equilibrium). This is attributed in a large part to the temperature dependent thermal expansion coefficient of the materials. Consequentially, we do expect to see an imprint of physical heating of the mirror on its intrinsic resonance frequency, certainly if the temperature of the mirror exceeds cryogenic temperatures. If the deviation of the effective mechanical resonance observed in Fig. 7.1 is caused by a change in the intrinsic resonance frequency, we can incorporate this in the theory and extract the intrinsic mechanical resonance frequency from the data. We modify Eq. (4.5):

$$\Omega_{\mathrm{eff}} \to \Omega_m(P_{\mathrm{Cl}}) + \delta\Omega_m^{\mathrm{Cl}}(P_{\mathrm{Cl}}) + \delta\Omega_m^{\mathrm{Ll}}$$

where Ω_m depends on P_{Cl} via T_{mat}. Then

$$\Omega_m(P_{\mathrm{Cl}}) = \Omega_{\mathrm{eff}} - (\delta\Omega_m^{\mathrm{Cl}} + \delta\Omega_m^{\mathrm{Ll}})$$

The temperature dependent intrinsic mechanical resonance Ω_m calculated in this way, with Ω_{eff} measured and $\delta\Omega_m^{\mathrm{opt}} := \delta\Omega_m^{\mathrm{Cl}}(P_{\mathrm{Cl}}) + \delta\Omega_m^{\mathrm{Ll}}$ from theory, is displayed in Fig. 7.2. The decrease of the intrinsic resonance frequency is strikingly similar to the increase of $\mathcal{A}\Gamma_{\mathrm{eff}}$, depicted on the lower right panel of Fig. 7.1. The values are plotted again in Fig. 7.1 on the same horizontal axis, and suggest a linear relation between Ω_m and $\mathcal{A}\Gamma_{\mathrm{eff}}$.

The evolution of the intrinsic mechanical resonance frequency during a cryogenic cool-down and warm-up, i.e. the dependence of Ω_m on T_{cryo}, has been measured for precursors of the nested resonator by P. Sonin [47]. Fig. 7.2 indicates an intrinsic resonance frequency shift of approximately -1kHz when T_{mat} rises from 7 to 70K, or a decrease by 0.3%. P. Sonin reported an approximately

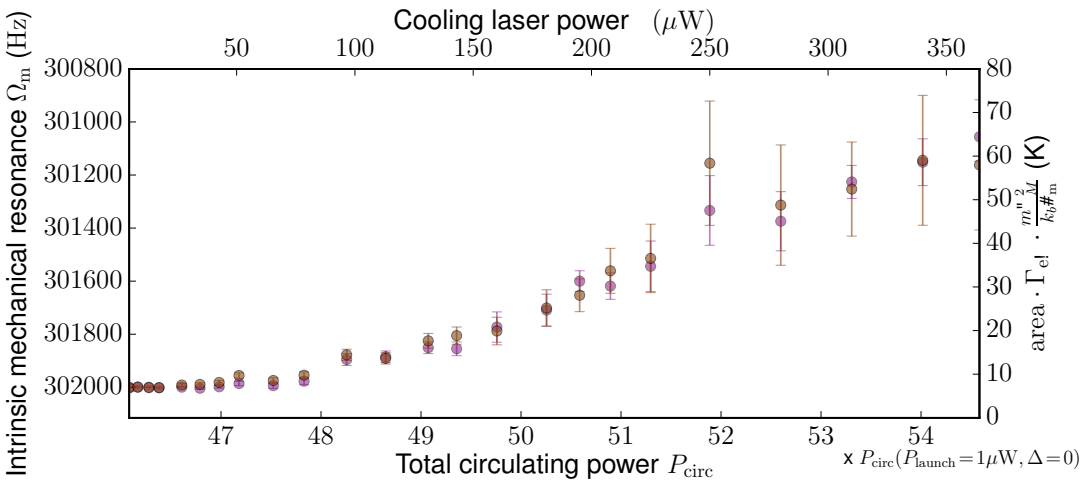

Figure 7.2: Decrease of the intrinsic resonance frequency [purple] observed in when increasing P_{Cl} from 4.6μW to 364μW. The material temperature $T_{\mathrm{mat}} = \mathcal{A}\Gamma_{\mathrm{eff}} m\Omega_m^2 k_B/\Gamma_m$ in Eq. (4.5) is plotted on the right axis [brown]. The upper horizontal axis gives the in-fiber cooling laser power P_{Cl}. The lower horizontal axis gives the total power circulating in the cavity, relative to the power that would circulate if there were 1μW of zero-detuned light in the fiber. A detuning of 6.5kHz was taken into account for the 47μW locking laser.

linear decrease of Ω_m by 0.5kHz from 137.5kHz to 137kHz, or 0.4%, when T_{cryo} is increased from 7 to 70K. [1] It must be noted here that it would be quite curious for the mechanical resonance frequency to change with the material temperature in the same way when the increase of T_{mat} is caused by optical absorption, versus when it is caused by an overall in crease in environment temperature. When warming up the cryostat, the mirror is continuously in thermal equilibrium with the environment, while in the case of optical absorption, the heating is very localized. The latter can result in complex behavior and effects, like the occurrence of local deformations in the material caused by very localized heating.

The argument presented in this section provides a context for the two discrepancies emphasized at the beginning. In summary, the mirror heats up due to absorption of a fraction of the cooling laser light. This results in a strong increase of $T_{\mathrm{mat}} = \mathcal{A}\Gamma_{\mathrm{eff}} m\Omega_m^2/k_B\Gamma_m$. The relation between T_{mat} and P_{Cl} ob-

[1] In chapter 4, we found that the intrinsic resonance of the resonator had decreased during the cryogenic cool-down from 308kHz in the $T_{\mathrm{cryo}} = 293K$ stage to 302kHz in the $T_{\mathrm{cryo}} = 5.7K$ stage. This does not contradict the current observations: P. Sonin reports in Ref. [47] that the full evolution from room temperature to the cryogenic regime comprises a sharp drop (5-10%) in Ω_m between $T_{\mathrm{cryo}} = 250$K and $T_{\mathrm{cryo}} = 150$K, followed by a slow, monotoneous increase by 1kHz between $T_{\mathrm{cryo}} = 150$K and $T_{\mathrm{cryo}} = 7$K.

served at $T_{\mathrm{cryo}} = 5.7\mathrm{K}$ differs from the relation observed between T_{mat} and P_{Ll} at $T_{\mathrm{cryo}} = 0.2\mathrm{K}$, but this might be attributable to temperature dependence of the heat conductivity of silicon nitride, which differs for super- and sub-kelvin temperatures. The relation between T_{mat} and P_{Cl} has the same functional form as the relation between the intrinsic mechanical resonance $\Omega_m = \Omega_{\mathrm{eff}} - \delta\Omega_m^{\mathrm{opt}}$ and P_{Cl}, indicating a linear relation between Ω_m and T_{mat}. The linearity of this relation, as well as the magnitudes of the frequency and temperature shifts involved, as well as the fact that the resonance frequency shift is observed only at $T_{\mathrm{cryo}} = 5.7\mathrm{K}$ and not at $T_{\mathrm{cryo}} = 200\mathrm{mK}$, are all consistent with the observed dependence of Ω_m on $T_{\mathrm{mat}} = T_{\mathrm{cryo}}$ in thermal equilibrium.

The case laid out here was built on the premise that the observed material temperature resulted from heating due to optical absorption of a fraction of the cooling laser light. This assumption imposes one insuperable issue, that we will explain in the following section.

7.1.3 Can the mirror heat up by absorbing cooling laser light?

The foundation of the statement that heating is caused by optical absorption and subsequent poor heat conduction, is that a fixed fraction of the transmitted light is absorbed by the moving mirror. Referring back to section 3.1.1, this means that a fixed fraction of the circulating light is absorbed.
The physical mechanism behind photon absorption is indifferent to whether the photon originated from the cooling laser or the locking laser, because the difference in wavelength between the lasers is negligible. Remember that both are 1064nm lasers, operating around frequencies of the order of 100THz, only a few GHz apart. From the cavity profile given in Eq. (3.4), one can readily estimate that for the same in-fiber power, the power that circulates in the cavity when the light is zero-detuned is 55 times larger than the power that would be circulating if the laser were $-\Omega_m$ detuned. This is shown on the horizontal axes in Fig. 7.2. Because a fixed fraction of the circulating power is absorbed by the mirror, we must have $T_{\mathrm{mat}}(P_{\mathrm{Cl}}) \approx T_{\mathrm{mat}}(P_{\mathrm{Ll}}/55)$. Therefore, the vast temperature rise perceived when augmenting the cooling laser power from 5 to $350\mu\mathrm{W}$ is irreconcilable with the observation that the temperature rise, perceived when augmenting the probe laser power by the same amount, is negligible. So, the answer is no. The mirror cannot significantly heat up by absorbing cooling laser light.

7.1.4 Where is the black hole?

Let us look back at Fig. 7.1. Two options remain. Either, the quantity plotted in the lower right panel *is* the temperature of the material, and the cause of the

increased temperature of the mirror is something other than optical absorption of cooling laser light by the mirror, or, the quantity plotted is *not* the actual temperature of the mirror ($\mathcal{A}\Gamma_{\text{eff}} m\Omega_m^2/k_B\Gamma_m \neq T_{\text{mat}}$).
If the first is true, that could imply that the absorption causing heating of the mirror does not only take place at the mirror upon transmission (i.e. while leaking through it). In other words, photons are disappearing someplace else. While the amount of cooling laser light transmitted through the cavity is much less than the amount of probe laser light transmitted through the cavity, equal amounts of light are incident on the stationary mirror. One could argue that absorption in the stationary mirror therefore can account for the observed heating. In order to heat up the mechanical mode, this would require the full optical bench to heat up. It is worth noting that heating of the optical bench should leave an imprint on the effective mechanical linewidths via modification of the cavity linewidth κ. Be that as it may, it is rather unlikely that the optical bench is unable to thermalize with the cryogenic environment. The concept of heating of the mirror by absorption of the probe laser light depends crucially on the assumption that the silicon nitride arms hinder the flow of heat to the environment, and there is no obvious bottleneck preventing thermalization of the optical bench as a whole. Assuming there is no additional photon sink, we must conclude that the physical quantity plotted in the lower right panel of Fig. 7.1 cannot be a true physical temperature of the mirror, and the rise of the effective temperature is caused by something else entirely.

7.1.5 Classical laser phase noise

In chapter 3, we briefly introduced the idea that the cryogenic environment, the mechanical oscillator, and the optical field, constitute three thermal baths interacting with one another, exchanging photons and phonons. A noisy laser, we explained, can be treated as a thermal bath itself, and one can ascribe an effective bath temperature T_{l} to it. Adjusting Eq. (3.34) to incorporate both the locking laser and the pump laser, we get:

$$T_{\text{eff}} = \frac{\Gamma_m T_{\text{mat}} + \Gamma_{\text{opt}} T_{\text{l}}}{\Gamma_{\text{eff}}}$$

As we saw in chapter 4, Γ_{opt}^{Ll} is of the order of a few Hz, while Γ_{opt}^{Cl} easily exceeds a kHz in an optical cooling run, as is visible in Fig. 7.1. Therefore, we can approximate

$$T_{\text{eff}} \overset{\Gamma_{opt}^{\text{Cl}} \gg \Gamma_{opt}^{\text{Ll}}}{\approx} \frac{\Gamma_m T_{\text{mat}} + \Gamma_{opt}^{\text{Cl}} T_{\text{Cl}}}{\Gamma_{\text{eff}}} \tag{7.1}$$

The extra term added to the effective temperature to the mirror depends on the cooling laser power via Γ_{opt}^{Cl}, but also via the effective bath temperature of the

cooling laser T_{Cl}. Using the result of Jayich et al. [19] that the effective bath temperature T_{Cl} is proportional to the power P_{Cl}, we set

$$T_{\mathrm{Cl}} = \alpha P_{\mathrm{Cl}}$$

with α a proportionality constant. We now have a strikingly simple mathematical model that we can fit to the data displayed in Fig. 7.1:

$$T_{\mathrm{eff}}(P_{\mathrm{Cl}}) = \frac{\Gamma_m T_{\mathrm{mat}} + \alpha \Gamma_{opt}^{\mathrm{Cl}}(P_{\mathrm{Cl}}) P_{\mathrm{Cl}}}{\Gamma_{\mathrm{eff}}(P_{\mathrm{Cl}})} \tag{7.2}$$

The result of the fit, which was strongly constrained having α as the only free parameter, is shown in Fig. 7.3. The fit returns $\alpha = 36$. Excellent agreement is observed over the full power range. We conclude that classical laser noise is very

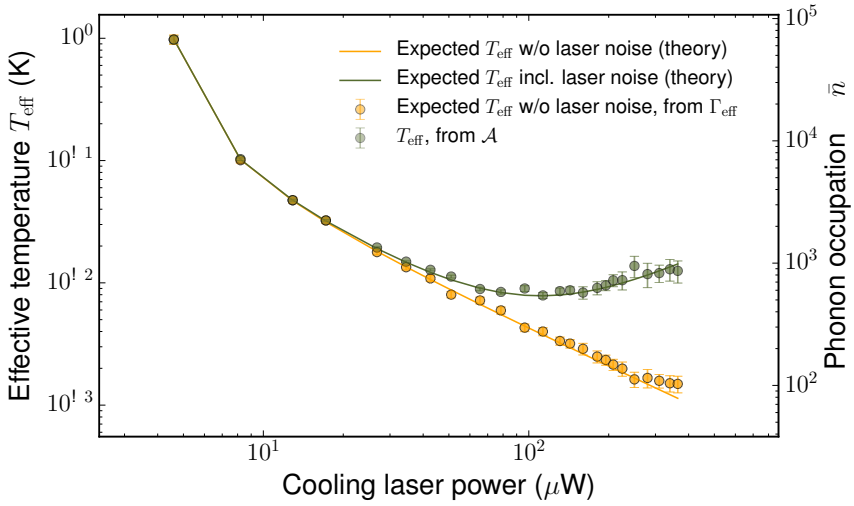

Figure 7.3: Expected and measured phonon occupancy and effective temperature while increasing the power of the cooling laser at $T_{\mathrm{cryo}} = 5.7$K, using PDH-thermometry. Depicted are measured effective temperatures, and comparison to the theory incorporating classical laser noise according to Eq. (7.2) with $\alpha = 36$.

likely the origin of the observed increase in effective temperature with cooling laser power. In other words, the classical laser noise reported and described by Jayich et al. is what limits laser cooling of the mirror at cryogenic temperatures. In Fig. 7.3, it caused the effective temperature to increase with cooling laser power in the region of strong optical damping, resulting in a final phonon occupation of approximately 1000 phonons. This stands in sharp contrast to the 100 phonons expected from the measured linewidths and the theory in the absence of laser noise.

7.2 What now?

In the sections leading up to the final verdict on the effects seen in the cooling run at 5.7K, we walked through a few other hypotheses. While we do hope that laying out these discussions carried some didactical value, we included them mostly because not all of the effects exhibited in Fig. 7.3 can be explained by laser noise. Particularly, the model for laser noise established in the previous section does not provide an explanation for the observed deviation of the (intrinsic?) mechanical resonance and linewidth. Therefore, further investigation of the subject seems worthwhile; if not to overhaul the laser noise model, then to extend it. As opposed to heating caused by optical absorption, laser noise is not a phenomenon unique for experiments at cryogenic temperatures. This section shows the effects of laser noise at room temperature, and more importantly, presents a solution to the problem.

7.2.1 Diagnostics at all temperatures

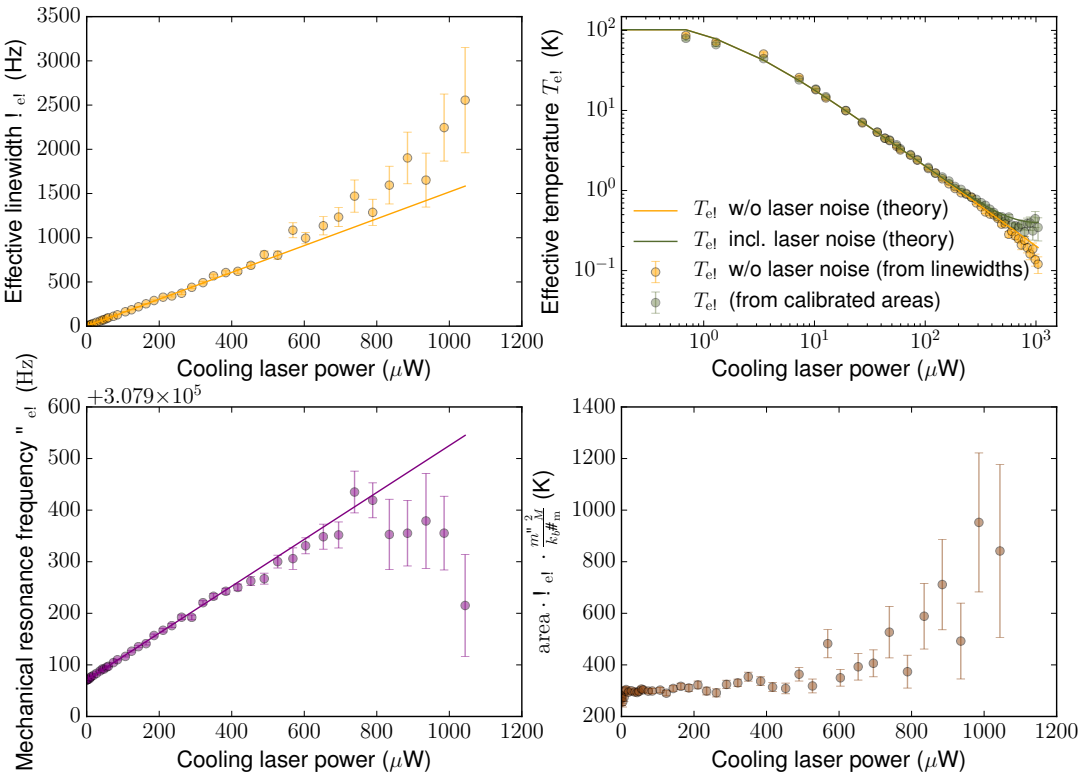

Figure 7.4: Optical cooling run at 293K.

Fig. 7.4 and 7.5 show an optical cooling run of the nested resonator at room temperature. The mechanical resonance deviates from the expected opti-

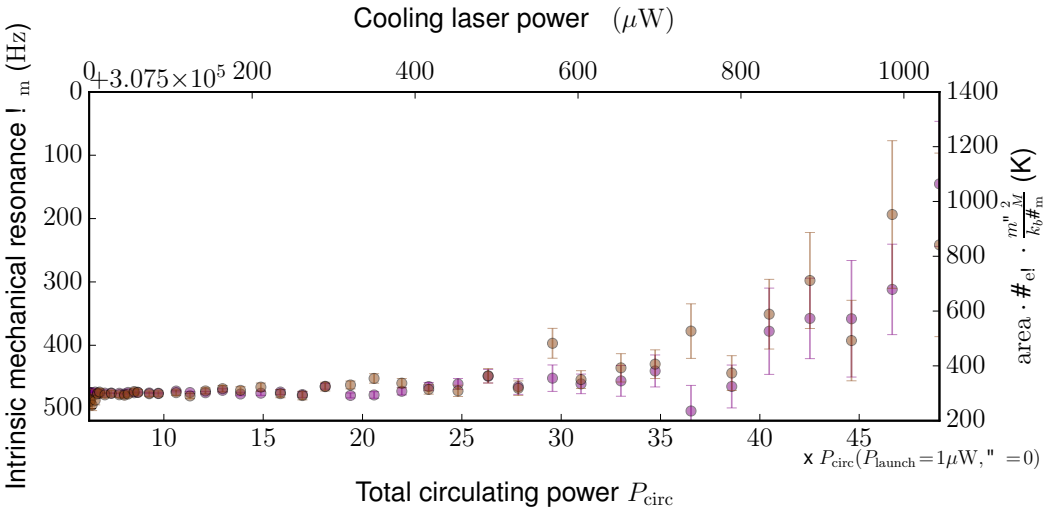

Figure 7.5: Decrease of the mechanical resonance frequency in an optical cooling run at 293K.

cal spring effect similar to the observed behavior at cryogenic temperatures. In comparison to Fig. 7.1, the deviation of the effective linewidth Γ_{eff} from theory is much more pronounced. Furthermore, the deviation is opposite to that in the measurement at $T_{\text{cryo}} = 5.7K$: the mechanical resonator is overdamped with respect to the theoretical expectation, while in Fig. 7.1 it was underdamped. The effective temperatures were fitted to Eq. (7.2), and returned $\alpha = 197$. We take this as an indication that we have not yet fully disclosed the model for the laser noise *or* the larger picture, which might comprise an interplay between a multitude of effects. (Thereby referring the reader back to the hypotheses laid out in sections 7.1.2 to 7.1.4.)

Similar measurements at millikelvin temperatures show comparable effects, and here the parameter returned by the fit was $\alpha = 30$, which is in closer agreement with the results obtained in section 7.1.1. Altogether however, the unresolved details must not obscure the central conclusion of this chapter, which condenses to the following: *The main factor preventing optical cooling of the nested trampoline resonator below* $\bar{n} = 100$ *at cryogenic temperatures is classical noise of the cooling laser.*

7.2.2 The cure for laser noise

Classical laser noise can be eliminated by adding a filter cavity, or 'mode cleaner' to the optical set-up. The filter cavity is placed in front of the cooling laser, and is PDH-locked to it. The phase noise of light transmitted through the cavity is strongly reduced with respect to the incoming (original) cooling laser light.

Jayich et al. reported a decrease in the classical noise power around Ω_m by a factor $1 + (2\Omega_m/\kappa_\mathrm{f})^2$, with κ_f the linewidth of the filter cavity, which must be substantially smaller than Ω_m. The noise can be progressively reduced by sending the light multiple times through the cavity. Results for single, double and triple passage are given in Ref. [19] as well. A detailed practical implementation scheme applicable to our set-up is given in Ref. [48].

7.3 Optical cooling at mK temperatures: the overwhelming question

We conclude this chapter with an answer to the question posed in the introduction lines of this chapter, and of this thesis: "*How close to the ground state are we?*"

The lowest effective temperature reached with the nested trampoline resonator in the millikelvin environment was 3.09 ± 0.07mK, or 213 ± 5 phonons [35]. We have identified the two factors prohibiting further cooling:

I. Optical absorption by the moving mirror of the locking laser light, causing an increase in T_mat and therefore in $T_\mathrm{eff}[P_\mathrm{Cl} = 0]$ (as verified in chapter 5)

II. Classical laser noise of the cooling laser, causing an increase in $T_\mathrm{eff}[P_\mathrm{Cl} \gg 0]$ (as identified in this chapter)

A comprehensive implementation of the methods proposed, investigated and demonstrated in this thesis is able to reduce the problems to the extent where they no longer inhibit near-ground state cooling, that is, $\bar{n} \ll 100$. The solutions are:

I. Replacement of PDH read-out of the mechanical motion by probe laser sideband thermometry (as demonstrated in chapter 6.1) or cooling laser sideband thermometry (as proposed, investigated and demonstrated in chapter 6.2)

II. Implementation of a filter cavity (as suggested in this chapter)

The claim that phonon occupancies $\bar{n} \ll 100$ are within direct reach is based on only one assumption, which is that the filter cavity eliminates the problems stemming from classical laser noise. If we re-examine the performed measurements that brought down the phonon occupation to $\bar{n} \approx 200$ at $P_\mathrm{Cl} = 60\mu$W, and we erase the increase in $\bar{n}$ caused by the noise of the cooling laser, then the lowest reached phonon occupation would have been $\bar{n} \approx 40$ at $P_\mathrm{Cl} = 200\mu$W.[2]

[2]This statement is not based on theory, but on the collected data. The phonon occupation that 'would have been' is calculated from the measured mechanical broadening Γ_eff, plotted e.g. in yellow on Fig. 6.1, Fig. 6.3 and Fig. 6.4.

This result does not take into account the solution for the first problem. F.M. Buters has conducted measurements of the sample using PDH read-out using probe laser powers as low as 2μW. Therefore, we know that implementation of cooling laser sideband-thermometry must allow reduction of the locking laser power to at least 2μW. Using 1μW of locking laser power results in a material temperature $\leq 0.7K$, further reducing $\bar{n}$ from 40 to 15. Furthermore, it must be emphasized that these measurements were halted at $P_{\mathrm{Cl}} = 200\mu$W because further increase of the cooling power was senseless: the effective temperature had long passed the minimum imposed by the cooling laser phase noise, so increasing the power further only resulted in effective heating of the mirror. This limit is of course also taken away if laser noise is eliminated. At $P_{\mathrm{Cl}} = 250\mu$W, $\bar{n}$ would drop below 10.

We conclude that the three limits impeding cooling and thermometry towards the ground state (optical absorption, phase noise, and deterioration of the signal-to-noise ratio up to the point that thermometry is no longer possible) can be drastically pushed down by exchanging PDH-thermometry with sideband-thermometry (*minimizing the necessary locking laser power* P_{Ll} and thus T_{mat}, while *maximizing the signal-to-noise ratio well above the maximum obtainable with PDH-thermometry*, because it was found that $\mathcal{N}_{\mathrm{SB}} \propto 1/P_{\mathrm{Ll}}P_{\mathrm{LO}}$, while $\mathcal{N}_{\mathrm{PDH}} \propto 1/P_{\mathrm{Ll}}^2$) and filtering the cooling beam.

How much "drastically" is, was estimated in the previous section, but can only be verified experimentally after implementation of a filtering cavity, and will depend:

- on the minimal required laser power for retaining the lock (as described in section 6.2.3)
- on the amount by which phase noise can be reduced (which determines the amount of cooling laser power that one can use before laser noise becomes dominant and $dT_{\mathrm{eff}}/dP_{\mathrm{Cl}}$ vanishes), and
- on the saturation of $\mathcal{N}_{\mathrm{SB}} \propto 1/P_{\mathrm{Ll}}P_{\mathrm{LO}}$ as $P_{\mathrm{LO}} \to \infty$, the value of which will be set by technical noise in the system that up to now has remained 'under the surface'.

Chapter 8

Conclusion & outlook

With this thesis, we have aimed to contribute to the experimental practice by optimizing the data analysis methods for system characterization (**chapter 4**), and for the control and analysis of optical cooling runs (**chapters 5** and **7**).

In **chapter 6**, two read-out methods were investigated and implemented in a 200mK cryogenic environment: monitoring of the locking laser sidebands, and of the cooling laser sidebands. We have demonstrated the feasibility of probe laser sideband-asymmetry thermometry for the countable phonon regime, once this regime is reached. Furthermore, we have disclosed the origin of the read-out noise for Pound-Drever-Hall thermometry and sideband thermometry. From this, we conclude that read-out of either the locking laser sidebands or the cooling laser sidebands allows for maximal signal-to-noise ratio while keeping the probe laser light that must be used to a minimum. In other words, one profits maximally from the light that is circulating in the cavity anyway, either the light for low-frequency vibration compensation, or that utilized for the cooling itself. One might argue that it carries a certain elegance to read-out the phonon occupancy immediately from the blue-scattered photons carrying away the energy (a benefit of cooling laser sideband thermometry), and furthermore it might seem intuitively logical that if one doesn't have to, one shouldn't send copious amounts of light onto the mirror (a benefit of both cooling laser sideband thermometry, and locking laser sideband thermometry). Indeed, we observed optomechanical amplification of the mirror's motion by locking laser light (**chapter 4**) and absorption of circulating light by the mirror (**chapter 5**). Therefore, the discussions presented in this thesis are extendable to similar cavity-optomechanicalsystems, for example systems utilizing membranes instead of a suspended trampoline mirror. Ultra high quality ($Q \sim 10^7$) silicon nitride membrane-in-the-middle setups are the subject of parallel research in our group [20], and are expected to benefit equally from the demonstrated methods.

In **chapter 7**, we disclosed the effects of laser noise, which were previously at-

tributed to absorption of cooling laser light, and we conveyed the physical model matching the observed behavior. Although they are not new or even surprising by themselves, the fact that the effects seen here are largely attributable to laser noise, and not optical absorption, is essential for the viability and the further course of the experiment. While the role of the probe laser can be minimized by the various schemes described in **chapter 6**, one cannot outsource the tasks of the cooling laser. The cooling laser and the fridge are all we have, to bring our mirror to the quantum regime, thus absorption of cooling light would have called for drastic measures, namely modification or abandonment of the trampoline resonator. Modifications to the nested resonator in the production process that can reduce the heating by optical absorption are under active investigation. Yet, even without these improvements, reaching a phonon occupation of less than 10 phonons seems feasible in the very near future, on the two conditions that we summarized in **chapter 7**. We conclude that the methods presented in this thesis pave the way for near-ground state cooling and thermometry of a cryogenically precooled nested trampoline resonator, and for similar set-ups that are foreseen to feature even higher quality factors.

Epilogue
The layman's guide to the ground state

This thesis tells the story of a mirror that can be in two places at the same time. The possibility of being in two places at once, is one of the most curious consequences of the laws of quantum mechanics. These laws describe the behavior of objects on the micro-scale, and they are vastly different from the laws that govern the world we know - that of everyday life, and that of Kepler, Newton, and Maxwell, who figured out how the earth circles around the sun, how apples fall from trees, and how light illuminates all that. The laws of quantum physics are so exotic, and come with so many fantastic names (quantum teleportation, quantum computers, and so on) that it is tempting to see them as just that: fantastic, and perhaps a good tool to describe some strange features in this world, but not necessarily *real*.

Nonetheless, they are. So before telling you how you can make a thing that's in two places at once, I will give an example of quantum physics occurring in the reality that we are familiar with, the macroscopic world.

Laboratories all over the world use scanning tunneling microscopes to make atomic-scale pictures of material surfaces [4]: real machines, printing out real images, only being able to operate because of electrons that are *in places where they cannot be*. Tunneling is a quantum mechanical phenomenon wherein objects have a finite possibility of being found in places where they cannot be in the classical sense. In the case of the microscope, the electrons belong to a metal needle. Moving electrons make up a current. If a metal needle is held a distance away from another metal surface, no current can flow in between the two. Just like attempting to charge your laptop by dangling the plug in front of the socket is very ineffective. Not so in the quantum world. There is a finite possibility of finding an electron in the void between the two. This spooky 'tunneling' through the forbidden region makes up the current on which the microscope works. Each electron of the needle, is supposed to *be in the needle*, yet it can feel the topology of the surface in front of it. The electron is smeared out all over the gap.

The problem with this example is, that electrons are not an object you can see anyway. This is where this thesis comes in. We want to make a macroscopic

object, that is, something that can be seen, and held, and touched, and put it in a quantum state. It is by no means obvious that's even possible, and it bemused the fathers of quantum mechanics themselves. In 1935 two of them, Erwin Schrödinger and Albert Einstein, exchanged letters over this. In one, Schrödinger pitched a hypothetical experiment to Einstein, wherein a cat would be locked in a box, together with a flask filled with toxic gas, and another flask, with a tiny bit of radioactive substance. Over the course of one hour, there is a fifty-fifty percent chance that one of its atoms decays. If it does, a radiation detector registers that, triggers a hammer, which smashes the glass of the poison-filled flask, thus releasing the deadly gas. Schrödinger argued that according to quantum theory, after one hour, the atom is in a quantum mechanical state of having decayed and not decayed, and therefore the cat is dead and alive in equal parts. As if being appointed this horrifying fate isn't enough, the cat in this thought experiment serves as a laughingstock, ridiculing the idea of a macroscopic superposition. A macroscopic superposition is a macroscopic object (the cat) that is simultaneously in states that mutually exclude each other in the classical sense (dead and alive). Regardless of Schrödingers intentions, the term macroscopic Schrödinger cat is now used to describe just that.

Withal, this exchange highlights the difference between a cat and an electron. Assuming you can put an electron in a superposition state, but you can't put a cat in one, what is the frontier separating them? What makes them behave so differently, even obey different laws of nature? The difference seems to be scale-related (one is macroscopic, the other microscopic), and observability-related (one can be seen, the other can't), and while the two are correlated, they immediately put the finger on two very fundamental sour spots.

First, the scale issue. An electron can be put in a superposition state. An atom, also. Cats and humans are apparently too large. This has made physicists wonder: where is the line? If there is a microscopic world, obeying the seemingly fantastic laws of quantum mechanics, and a macroscopic world, obeying the laws of Newton, Kepler and Maxwell, then what is the biggest object I can make, that still exhibits quantum effects? We believe that it is a mirror, about 70μm in diameter, encompassing about 10^{14} atoms. The mirror is shown in the center of Fig. 3.14 of this thesis. It's not big - but it's there. Our aim is to bring this mirror in a state where it's in two places at the same time. Thinking about that makes me feel itchy. An electron was one thing. But something I can hold in my hands? How can you imagine that? The answer is surprisingly simple: you can't, and you shouldn't. That brings us to the second issue. An object in a quantum state intrinsically cannot be observed. As long as it's not observed, it can be in two places at the same time. If you look, you will see it on one place, or another. The act of seeing it, dramatically changes the state of the subject.

As soon as you uncover your eyes, the object collapses[1] from a superposition state (here and there) into one of the classical states (here or there). In quantum mechanics, what's seen, very fundamentally, cannot be unseen.

Both issues come with practical challenges. Regarding the scale-issue, one might wonder: how does one put an object, like our little mirror, in such a state? In the case of the cat, it's sinister but straightforward. The quantum superposition state of the microscopic atom (decayed and not decayed) is *transferred to* the macroscopic cat (dead and alive). Instead of a cat, we use the little mirror, and instead of an atom, we use a photon. A photon is a particle of light, and like any other particle, it can exert pressure or force on an object when hitting it. This is called radiation pressure. Imagine a beam of light incident on a mirror, but instead of a ray, the beam comprises individual light particles, photons. Now imagine there is only one single photon. We mount the mirror on springs, like a trampoline. If now a laser shoots a single photon onto the mirror, the photon bounces off the mirror and moves it. In between the laser and the mirror, we place a gate. When a photon passes through, it can either be transmitted, or deflected. This is displayed in Fig. 8.1. A photon emerging from the laser has two options.

(a) The photon continues its path straightforward, passing point (a) and disappearing into the void. The mirror is unaffected.

(b) The photon is deflected, passes point (b) and hits the mirror. As a result, the mirror is displaced.

These are the two classic options. In the quantum world, however, there are three options. One can have (a), or (b), or *(a) and (b).* Bringing a photon into a superposition state of being at place (a) and (b) simultaneously is, like for an electron, not that difficult. But, if the photon is simultaneously at (a) and at (b), the mirror is simultaneously not hit, and hit. Thus, the mirror is displaced and not displaced at the same time and a spatial superposition of a macroscopic, touchable object is created. This experiment is a simplified version of an experiment designed in 2003 by William Marshall, Christoph Simon, Roger Penrose, and Dirk Bouwmeester [8].

Then, there is the observability issue: how to observe something you may not observe? This is the biggest pitfall of the experiment, and the solution to that question is non-trivial. As it turns out, it is of essential importance that the mirror has a vey, very, very low temperature. In the case of the mirror, temperature of the mirror means the same as motion of the mirror. Saying the mirror has a very low temperature, is the same as saying the mirror must stand very still, before we move it with the photon. Why is that? Atoms in any object

[1] I use this word, because this phenomenon is called 'the collapse of the ψ-function'.

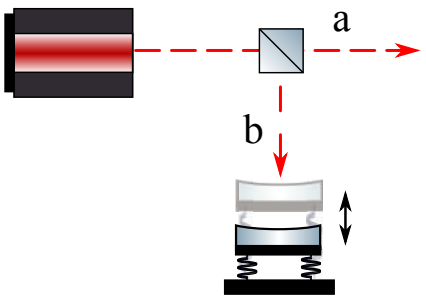

Figure 8.1: Towards quantum superpositions of a mirror. Adapted from Marshall et al. [8]

vibrate: they chaotically move around a little bit. This vibrational motion is so small, that it's unnoticeable in everyday objects. The hotter an object is, the more the atoms vibrate. We call this thermal motion. As a result, objects can in principle have infinitely high temperatures: you can always make the atoms vibrate harder. However, the opposite is not quite true. By cooling something down, you make the atoms move less and less, but at one point, it stops: when the atoms stand perfectly still, you cannot make them move less anymore. The corresponding temperature is the absolute zero. It is 0 Kelvin, or approximately $-273°$ Celcius. Physicists call this the *ground state*: you can't go any lower in temperature or energy.

The full reason that the observation of a mirror in a superposition state is so difficult, is however not entirely quantum mechanic. Because a photon is microscopic, and the mirror is macroscopic, the pressure that one photon will exert on the mirror is incredibly small. Thus, the resulting displacement is incredibly small. This has two implications. First, instead of having the photon bounce off the mirror once, we can make it bounce off multiple times. To that extent, we fix a second, stationary mirror in front of the moving mirror. This is depicted in Fig. 3.1 of this thesis. The incident photon is then transmitted through the first mirror, and subsequently gets trapped in between the two mirrors, bouncing back and forth like a ping pong ball, before it leaks out again via one of the mirrors. This set-up is called a cavity; it is a photon trap. More specific, it is called a cavity-optomechanical system, because it is a cavity, accommodating light (optics) that is interacting with a mirror on a trampoline (a mechanical element).

Secondly, as I argued above, the mirror does not perfectly stand still in the absence of any photon. If the mirror is at room temperature, its atoms vibrate so viciously that shooting a single photon at it, in order to displace it, is in vain. So, in order to measure the mirror's displacement at all, it must stand as still as possible beforehand: its thermal motion, and therefore temperature, must be brought to zero.

The cooling of the mirror is the topic of this thesis. It is done in two stages.

First, it is cooled down in the most conceivable way: by putting it in an ultra cold fridge. The fridge, a helium dilution refrigerator located in the Kamerlingh Onnes Laboratory in Leiden, is able to cool down the mirror to approximately 0.2 Kelvin. This is already very close to the absolute zero. The second stage, consists of further damping the motion of the mirror. This is done with light. In this stage, we do not use *single* photons yet. Rather large amounts of laser light are used to counteract the motion of the mirror, via radiation pressure. In order to do that properly, the motion of the mirror must be read-out as well. This is again done by sending light onto it. A second laser is used for this. The light that bounces off the mirror carries an imprint of its motion. So, by detecting that light, we can measure the movement of the mirror. This thesis deals with precisely those two issues: optical cooling (or laser cooling) and thermometry (or motion-measurement).

Currently, there are three main problems obstructing us from reaching the ground state. The first is that, the closer you get to the ground state, the less the mirror moves, and the weaker the imprint on the light is. Thus as we damp the motion of the mirror, the signal we measure becomes weaker as well, up to the point that thermometry becomes impossible because we cannot measure the signal with a high enough precision. The second problem that we encountered in this thesis is absorption of light by the material of the movable mirror. This is a problem because, as anyone who has spent a day on the beach[2] can confirm, absorbing light causes heating. Luckily we found that only the light we used for the read-out of the motion heats up the mirror, not the light from the cooling laser. Therefore, we explored methods in this thesis to outsource the task of reading out the motion, to the cooling laser. We also investigated other methods to minimize the necessary read-out laser light. However, the cooling laser imposed another challenge upon us. We found that while the light is not heating up the mirror due to absorption, the light is heating it up because of laser noise.

As said, the laser beam comprises a stream of photons. However, this stream of photons is somewhat chaotic: the photons do not all have exactly the same energy, and they do not travel in a perfectly coherent manner. Imagine that we were trying to counter the motion of the mirror by spurting a stream of water onto it. If out of our garden hose, a perfectly symmetric, controlled, straight stream of water came, all drops traveling together in a completely ordered manner, that would be terrific. Hot summer evenings with thirsty flowerbeds[3] learn however that this is not how hose pipes work in practice. The imperfectness of the light can sabotage the damping. If you send copious amounts of chaotic light onto the mirror, the mirror will start to move more viciously, instead of less. This heating caused by the noisiness of the cooling laser light is identified

[2]Or a day in a cramped office in summer - take your pick.

[3]Or sweaty summer days with filthy windows and a dust-covered car - take your pick.

as well, and a solution is proposed.

Having identified the main problems that currently obstruct ground-state cooling, we also demonstrate a practical method to directly observe quantum effects of the mirror as it approaches the ground state, transitioning from the macroscopic world into the quantum realm. Having demonstrated this, makes us prepared to effectively enter the quantum regime - provided the proposed solutions for the identified issues are successfully implemented. If not with the trampoline mirror used in this thesis, then with similar trampolines that are currently in the making as well.

Layman's abstract

Cavity Optomechanics in a Millikelvin Environment
by
Yasmine Laura Sfendla
KU Leuven

Under supervision of Prof. Dirk Bouwmeester
Leiden Institute of Physics

The possibility of being in two places at the same time, is one of the most curious consequences of the laws of quantum mechanics. These laws describe the behavior of microscopic objects, like atoms and electrons. They are vastly different from the laws that govern the everyday world, the macroscopic world. This thesis deals with the preparations of an experiment that aims to bring a macroscopic object into such a superposition state - being in two places at once. Macroscopic, means bigger than a few atoms: it must be a thing that can be seen and hand held. In practice, the object is a tiny mirror, a little over half a millimeter in diameter, mounted on springs like a trampoline. The final goal will be to bring this mirror into a quantum superposition state by shooting particles of light, photons, onto it. Like any other particle, they can exert a force, or pressure, on an object by hitting it, and even move it.

A fundamental requirement for making, and observing, an object in a quantum superposition state, is that it must be very cold. When atoms have a finite temperature, they vibrate a little bit. This is called thermal motion, and it is detrimental to the experiment. When cooling down an object, its constituent atoms move less and less until they completely stand still. That point is called the absolute zero, or the ground state. The aim of this thesis is to measure the thermal motion of the mirror, and to cool it down as close as possible to the ground state. This proceeds in two stages. First, the mirror is placed in an extremely powerful fridge. Secondly, laser light is used to damp the thermal motion even more, via the light pressure force exerted on the mirror. We lay bare two issues currently preventing ground-state cooling: heating of the mirror due to absorption of light in its surface, and amplification of the motion because of imperfections of the laser. We demonstrate two modifications to the experimental scheme that can solve these problems, and simultaneously solve another problem that is expected to show up near the ground state: as the motion becomes weaker and weaker, detecting it becomes nearly impossible. The methods demonstrated in this thesis ensure that even close to the absolute zero, the motion can be read out. In this way, we pave the path for ground state cooling of a microscopic trampoline mirror, and similar objects that are currently in development as quantum-experiment candidates.

"Men have wasted away before it, entranced by what they have seen, or been driven mad, not knowing if what it shows is real or even possible.
The Mirror will be moved to a new home tomorrow, Harry, and I ask you not to go looking for it again. If you ever do run across it, you will now be prepared. It does not do to dwell on dreams and forget to live, remember that."

– J.K. Rowling, *Harry Potter and the Sorcerer's Stone*

Bibliography

[1] H. Kragh, *Quantum Generations: A History of Physics in the Twentieth Century*. Princeton University Press, 2002.

[2] J. D. Trimmer, "The present situation in quantum mechanics: A translation of schrödinger's "cat paradox" paper," *Proceedings of the American Philosophical Society*, vol. 124, no. 5, pp. 323–338, 1980.

[3] E. Schrödinger, "Die gegenwärtige situation in der quantenmechanik," *Naturwissenschaften*, vol. 23, no. 48, pp. 807–812, 1935.

[4] J. Tersoff and D. Hamann, "Theory of the scanning tunneling microscope," *Physical Review B*, vol. 31, no. 2, p. 805, 1985.

[5] B. Pepper, *Bathed, Strained, Attenuated, Annihilated: Towards Quantum Optomechanics*. PhD thesis, University of California, Santa Barbara, 2014.

[6] M. J. Weaver, B. Pepper, F. Luna, F. M. Buters, H. J. Eerkens, G. Welker, B. Perock, K. Heeck, S. de Man, and D. Bouwmeester, "Nested trampoline resonators for optomechanics," *Applied Physics Letters*, vol. 108, no. 3, p. 033501, 2016.

[7] D. Kleckner, B. Pepper, E. Jeffrey, P. Sonin, S. M. Thon, and D. Bouwmeester, "Optomechanical trampoline resonators," *Opt. Express*, vol. 19, pp. 19708–19716, Sep 2011.

[8] W. Marshall, C. Simon, R. Penrose, and D. Bouwmeester, "Towards quantum superpositions of a mirror," *Physical Review Letters*, vol. 91, no. 13, p. 130401, 2003.

[9] P. McMahon, *Hints and Tips on (Science and Engineering) Bachelor's and Master's thesis Writing*. Stanford University, 2009.

[10] S. Aaronson, *Limits on Efficient Computation in the Physical World*. PhD thesis, University of California, Berkeley, 2005.

[11] S. G. Johnson, *Photonic Crystals: From Theory to Practice*. PhD thesis, Massachusetts Institute of Technology, 2001.

[12] D. M. Bacon, *Decoherence, control, and symmetry in quantum computers*. PhD thesis, University of California, Berkeley, 2001.

[13] "Faksimile aus den verhandlungen der deutschen physikalischen gesellschaft 2 (1900) s. 237: Zur theorie des gesetzes der energieverteilung im normalspectrum; von m. planck," *Physik Journal*, vol. 4, no. 4, pp. 146–151, 1948.

[14] A. Schliesser and T. J. Kippenberg, *Cavity Optomechanics with Whispering-Gallery-Mode Microresonators*, pp. 121–148. Berlin, Heidelberg: Springer Berlin Heidelberg, 2014.

[15] G. A. Brawley, M. R. Vanner, P. E. Larsen, S. Schmid, A. Boisen, and W. P. Bowen, "Nonlinear optomechanical measurement of mechanical motion," *Nature Communications*, vol. 7, p. 10988, 2016.

[16] J. Teufel, T. Donner, D. Li, J. Harlow, M. Allman, K. Cicak, A. Sirois, J. D. Whittaker, K. Lehnert, and R. W. Simmonds, "Sideband cooling micromechanical motion to the quantum ground state," *arXiv preprint arXiv:1103.2144*, 2011.

[17] E. Gavartin, R. Braive, I. Sagnes, O. Arcizet, A. Beveratos, T. J. Kippenberg, and I. Robert-Philip, "Optomechanical coupling in a two-dimensional photonic crystal defect cavity," *Phys. Rev. Lett.*, vol. 106, p. 203902, May 2011.

[18] T. P. Purdy, R. W. Peterson, P.-L. Yu, and C. A. Regal, "Cavity optomechanics with si 3 n 4 membranes at cryogenic temperatures," *New Journal of Physics*, vol. 14, no. 11, p. 115021, 2012.

[19] A. M. Jayich, J. C. Sankey, K. Børkje, D. Lee, C. Yang, M. Underwood, L. Childress, A. Petrenko, S. M. Girvin, and J. G. E. Harris, "Cryogenic optomechanics with a si 3 n 4 membrane and classical laser noise," *New Journal of Physics*, vol. 14, no. 11, p. 115018, 2012.

[20] M. J. Weaver, F. M. Buters, F. Luna, H. J. Eerkens, K. Heeck, S. de Man, and D. Bouwmeester, "Coherent Optomechanical State Transfer between Disparate Mechanical Resonators," *ArXiv e-prints*, Apr. 2017.

[21] A. G. Kuhn, M. Bahriz, O. Ducloux, C. Chartier, O. L. Traon, T. Briant, P.-F. Cohadon, A. Heidmann, C. Michel, L. Pinard, and R. Flaminio, "A micropillar for cavity optomechanics," *Applied Physics Letters*, vol. 99, no. 12, p. 121103, 2011.

[22] X. Lu, J. Y. Lee, P. X.-L. Feng, and Q. Lin, "Silicon carbide microdisk resonator," *Opt. Lett.*, vol. 38, pp. 1304–1306, Apr 2013.

[23] S. Stapfner, I. Favero, D. Hunger, P. Paulitschke, J. Reichel, K. Karrai, and E. M. Weig, "Cavity nano-optomechanics: a nanomechanical system in a high finesse optical cavity," *arXiv preprint arXiv:1110.6292*, 2011.

[24] X. Jiang, M. Wang, M. C. Kuzyk, T. Oo, G.-L. Long, and H. Wang, "Chip-based silica microspheres for cavity optomechanics," *Optics express*, vol. 23, no. 21, pp. 27260–27265, 2015.

[25] D. Ding, L. M. C. Pereira, J. F. Bauters, M. J. R. Heck, G. Welker, A. Vantomme, J. E. Bowers, M. J. A. de Dood, and D. Bouwmeester, "Multidimensional purcell effect in an ytterbium-doped ring resonator," *Nat Photon*, vol. 10, pp. 385–388, 06 2016.

[26] D. M. Stamper-Kurn, "Cavity optomechanics with cold atoms," in *Cavity Optomechanics*, pp. 283–325, Springer, 2014.

[27] G. I. Harris, D. L. McAuslan, E. Sheridan, Y. Sachkou, C. Baker, and W. P. Bowen, "Laser cooling and control of excitations in superfluid helium," *Nat Phys*, vol. 12, pp. 788–793, 08 2016.

[28] H. J. Eerkens, F. M. Buters, M. J. Weaver, B. Pepper, G. Welker, K. Heeck, P. Sonin, S. de Man, and D. Bouwmeester, "Optical side-band cooling of a low frequency optomechanical system," *Opt. Express*, vol. 23, pp. 8014–8020, Mar 2015.

[29] D. Kleckner, I. Pikovski, E. Jeffrey, L. Ament, E. Eliel, J. van den Brink, and D. Bouwmeester, "Creating and verifying a quantum superposition in a micro-optomechanical system," *New Journal of Physics*, vol. 10, no. 9, p. 095020, 2008.

[30] M. Aspelmeyer, T. J. Kippenberg, and F. Marquardt, "Cavity optomechanics," *Rev. Mod. Phys.*, vol. 86, pp. 1391–1452, Dec 2014.

[31] R. W. P. Drever, J. L. Hall, F. V. Kowalski, J. Hough, G. M. Ford, A. J. Munley, and H. Ward, "Laser phase and frequency stabilization using an optical resonator," *Applied Physics B*, vol. 31, pp. 97–105, Jun 1983.

[32] E. D. Black, "An introduction to pound-drever-hall laser frequency stabilization," *American Journal of Physics*, vol. 69, no. 1, pp. 79–87, 2001.

[33] F. M. Buters, H. J. Eerkens, K. Heeck, M. J. Weaver, B. Pepper, S. de Man, and D. Bouwmeester, "Experimental exploration of the optomechanical attractor diagram and its dynamics," *Phys. Rev. A*, vol. 92, p. 013811, Jul 2015.

[34] F. M. Buters, K. Heeck, H. J. Eerkens, M. J. Weaver, F. Luna, S. de Man, and D. Bouwmeester, "High-q nested resonator in an actively stabilized optomechanical cavity," *Applied Physics Letters*, vol. 110, no. 10, p. 104104, 2017.

[35] F. M. Buters, *Optical driving and cooling of trampoline resonators*. PhD thesis, Leiden University, 2017.

[36] D. Z. Anderson, J. C. Frisch, and C. S. Masser, "Mirror reflectometer based on optical cavity decay time," *Appl. Opt.*, vol. 23, pp. 1238–1245, Apr 1984.

[37] C. R. Locke, D. Stuart, E. N. Ivanov, and A. N. Luiten, "A simple technique for accurate and complete characterisation of a fabry-perot cavity," *Opt. Express*, vol. 17, pp. 21935–21943, Nov 2009.

[38] F. R. Blom, S. Bouwstra, M. Elwenspoek, and J. H. J. Fluitman, "Dependence of the quality factor of micromachined silicon beam resonators on pressure and geometry," *Journal of Vacuum Science & Technology B: Microelectronics and Nanometer Structures Processing, Measurement, and Phenomena*, vol. 10, no. 1, pp. 19–26, 1992.

[39] G. Rempe, R. Lalezari, R. J. Thompson, and H. J. Kimble, "Measurement of ultralow losses in an optical interferometer," *Opt. Lett.*, vol. 17, pp. 363–365, Mar 1992.

[40] A. M. J. den Haan, G. H. C. J. Wijts, F. Galli, O. Usenko, G. J. C. van Baarle, D. J. van der Zalm, and T. H. Oosterkamp, "Atomic resolution scanning tunneling microscopy in a cryogen free dilution refrigerator at 15 mk," *Review of Scientific Instruments*, vol. 85, no. 3, p. 035112, 2014.

[41] K. Heeck tech. rep., Leiden Institute of Physics, 2016.

[42] S. Groblacher, J. B. Hertzberg, M. R. Vanner, G. D. Cole, S. Gigan, K. C. Schwab, and M. Aspelmeyer, "Demonstration of an ultracold micro-optomechanical oscillator in a cryogenic cavity," *Nat Phys*, vol. 5, pp. 485–488, 07 2009.

[43] D. W. Stauff and D. J. Montgomery, "Effect of air damping on transverse vibrations of stretched filaments," *Journal of Applied Physics*, vol. 26, no. 5, pp. 540–544, 1955.

[44] A. H. Safavi-Naeini, J. Chan, J. T. Hill, S. Gröblacher, H. Miao, Y. Chen, M. Aspelmeyer, and O. Painter, "Laser noise in cavity-optomechanical cooling and thermometry," *New Journal of Physics*, vol. 15, no. 3, p. 035007, 2013.

[45] A. Schliesser, O. Arcizet, R. Riviere, G. Anetsberger, and T. J. Kippenberg, "Resolved-sideband cooling and position measurement of a micromechanical oscillator close to the heisenberg uncertainty limit," *Nat Phys*, vol. 5, pp. 509–514, 07 2009.

[46] M. Underwood, D. Mason, D. Lee, H. Xu, L. Jiang, A. B. Shkarin, K. Børkje, S. M. Girvin, and J. G. E. Harris, "Measurement of the motional sidebands of a nanogram-scale oscillator in the quantum regime," *Phys. Rev. A*, vol. 92, p. 061801, Dec 2015.

[47] P. Sonin, *Optomechanical experiments at low temperatures*. PhD thesis, Leiden University, 2012.

[48] C. Yang, *Progress Toward Observing Quantum Effects in an Optomechanical System in Cryogenics*. PhD thesis, Yale University, 2011.

[49] D. J. Wilson, V. Sudhir, N. Piro, R. Schilling, A. Ghadimi, and T. J. Kippenberg, "Measurement-based control of a mechanical oscillator at its thermal decoherence rate," *Nature*, vol. 524, pp. 325–329, 08 2015.

[50] R. Ghobadi, S. Kumar, B. Pepper, D. Bouwmeester, A. I. Lvovsky, and C. Simon, "Optomechanical micro-macro entanglement," *Phys. Rev. Lett.*, vol. 112, p. 080503, Feb 2014.

[51] A. H. Safavi-Naeini, J. Chan, J. T. Hill, T. P. M. Alegre, A. Krause, and O. Painter, "Observation of quantum motion of a nanomechanical resonator," *Phys. Rev. Lett.*, vol. 108, p. 033602, Jan 2012.

[52] T. P. Purdy, P.-L. Yu, N. S. Kampel, R. W. Peterson, K. Cicak, R. W. Simmonds, and C. A. Regal, "Optomechanical raman-ratio thermometry," *Phys. Rev. A*, vol. 92, p. 031802, Sep 2015.

[53] D. Kleckner, W. T. M. Irvine, S. S. R. Oemrawsingh, and D. Bouwmeester, "Diffraction-limited high-finesse optical cavities," *Phys. Rev. A*, vol. 81, p. 043814, Apr 2010.

[54] J. Chan, T. P. M. Alegre, A. H. Safavi-Naeini, J. T. Hill, A. Krause, S. Groblacher, M. Aspelmeyer, and O. Painter, "Laser cooling of a nanomechanical oscillator into its quantum ground state," *Nature*, vol. 478, pp. 89–92, 10 2011.

[55] M. Aspelmeyer, S. Gröblacher, K. Hammerer, and N. Kiesel, "Quantum optomechanics-throwing a glance," *J. Opt. Soc. Am. B*, vol. 27, pp. A189–A197, Jun 2010.

[56] S. Gröblacher, S. Gigan, H. R. Böhm, A. Zeilinger, and M. Aspelmeyer, "Radiation-pressure self-cooling of a micromirror in a cryogenic environment," *EPL (Europhysics Letters)*, vol. 81, no. 5, p. 54003, 2008.

[57] G. Li, Y. Zhang, Y. Li, X. Wang, J. Zhang, J. Wang, and T. Zhang, "Precision measurement of ultralow losses of an asymmetric optical microcavity," *Appl. Opt.*, vol. 45, pp. 7628–7631, Oct 2006.

[58] H. J. Mamin and D. Rugar, "Sub-attonewton force detection at millikelvin temperatures," *Applied Physics Letters*, vol. 79, no. 20, pp. 3358–3360, 2001.

[59] W. P. Bowen and G. J. Milburn, *Quantum Optomechanics*. CRC Press, 2015.

[60] F. M. Buters, M. J. Weaver, H. J. Eerkens, K. Heeck, S. de Man, and D. Bouwmeester, "Optomechanics with a polarization nondegenerate cavity," *Phys. Rev. A*, vol. 94, p. 063813, Dec 2016.

DEPARTEMENT OF PHYSICS AND ASTRONOMY
Celestijnenlaan 200d bus 2412
3001 HEVERLEE, BELGIË
tel. + 32 16 32 71 24
fys.kuleuven.be